Similarities of stress granules and cytosolic prions

Dissertation

zur

Erlangung des Doktorgrades (Dr. rer. nat.)

der

Mathematisch-Naturwissenschaftlichen Fakultät

der

Rheinischen Friedrich-Wilhelms-Universität Bonn

vorgelegt von

Katrin Riemschoß

aus Hennef

Bonn 2018

Angefertigt mit Genehmigung der Mathematisch-Naturwissenschaftlichen Fakultät
der Rheinischen Friedrich-Wilhelms-Universität Bonn

1. Gutachter: Prof. Dr. Ina Vorberg
2. Gutachter: Prof. Dr. Michael Pankratz

Tag der Promotion: 18.01.2019
Erscheinungsjahr: 2019

Table of contents

Summary

Eukaryotic cells contain several organelles that lack a delimiting membrane. These membrane-less organelles take over important functions within the cell and influence biological reactions by condensing nucleic acids and proteins into dense droplets. Upon environmental stress, one kind of membrane-less organelle, termed stress granules, assembles to sequester non-essential mRNA transcripts while translation is stalled. Together with RNA-binding proteins, mRNA transcripts form a network by multiple weak interactions within stress granules. Many RNA-binding proteins thereby facilitate the assembly of stress granules by their low-complexity or prion-like domains, which were identified based on their structural similarities with yeast prion domains. Several RNA-binding proteins that are part of stress granules were found aggregated in degenerative disorders. Therefore, stress granules have been proposed to contribute to the disease process by acting as nucleation sites for protein aggregates, which might evolve into pathological protein inclusions over time. In this study, we compared similarities and differences between stress granules and cytosolic prion aggregates. Specifically, we tested the hypothesis if recruitment of a protein with a prion-like domain to stress granules induces its conversion into a protein aggregate with self-perpetuating properties. To this end, we made use of the yeast prion domain NM of Sup35, expressed in mammalian cells, that can form cytosolic prions upon exposure to recombinant NM fibrils. Here we show that the interactome of NM prions significantly overlaps with that of stress granules. The presence of neither soluble nor aggregated NM altered the dynamics of stress granules, but stress granule disassembly was slightly impaired. Importantly, prolonged presence of stress granules did not induce NM aggregation, but rather led to cell death. Interestingly, chemicals that induce stress granules drastically increased NM aggregate formation upon concomitant induction with recombinant NM fibrils. However, stress granules per se were not required for the increased induction rate, as concomitant exposure to drugs or siRNA that interfere with stress granule formation did not lower the NM aggregate induction rates. We propose a model where stress that triggers a stress granule response results in a cellular environment that allows more effective protein aggregate induction by exogenous

seeds. One possible explanation for this is that the cellular quality control mechanism is overloaded under stress and thus cannot combat the additional aggregate induction by an exogenous seed. Therefore, the role of stress granules in the pathogenesis of neurodegenerative disorders might be different than so far anticipated. Still, triggers that cause stress granule formation enhance protein aggregation in the presence of exogenous seeds, thereby likely contributing to disease progression.

1. Introduction

1.1 Membrane-less organelles

Organizing complex biochemical reactions is essential for eukaryotic cells and has mainly been achieved by surrounding compartments with lipid membranes. These compartments restrict metabolic processes and signaling pathways to certain areas, thereby providing spatiotemporal control to carry out specific functions. However, cells have developed compartments that lack a separating membrane. Membrane-less organelles comprise compartments in the nucleus, such as nucleoli and nuclear speckles, and in the cytoplasm, such as stress granules (SGs) and P bodies. Consisting mainly of RNA-binding proteins (RBPs) and RNA, membrane-less organelles are also called ribonucleoprotein (RNP) granules. RNP granules fulfill numerous functions in RNA metabolism, including transport, storage and degradation of mRNAs (Buchan and Parker, 2009). Cytoplasmic RNP granules, SGs and P bodies, form from mRNAs that are not engaged in translation, thereby controlling mRNA translation and degradation (Buchan and Parker, 2009; Parker and Sheth, 2007).

1.1.1 Stress granules

SGs assemble in response to inhibition of protein synthesis due to environmental stress, such as heat, viral infection and oxidative conditions, or specific drugs (Buchan and Parker, 2009; Kedersha et al., 1999; McInerney et al., 2005). Inhibition of protein synthesis is achieved by phosphorylation of the α subunit of the translation initiation factor eIF2α at serine 51. The phosphorylation of eIF2α is mediated by four different kinases: the endoplasmic reticulum-resident protein kinase (PERK), protein kinase R (PKR), heme-regulated inhibitor (HRI) and the general control non-derepressible-2 (GCN2) (Jiang and Wek, 2005). Phospho-eIF2α restricts the availability of the eIF2-GTP-tRNAi^{Met} ternary complex, which is a key component of translation initiation (Hershey, 1991). The subsequent disassembly of polysomes leads to the active sorting of mRNAs to SGs (Kedersha et al., 2002; Kedersha et al., 1999). Along with untranslated mRNAs, SGs contain proteins involved in translation initiation (eIF4E, eIF4G, eIF4A, Papb,

eIF3 and eIF2) and RBPs that are involved in various aspects of mRNA metabolism (Anderson and Kedersha, 2006; Kedersha et al., 2002). There are also non-RNA-binding proteins that are part of SGs, including enzymes for posttranslational modifications and RNA and protein remodeling complexes, which play a role in SG assembly and disassembly (Jain et al., 2016). However, it has been shown that the composition of SGs can vary upon distinct stress stimuli (Aulas et al., 2017).

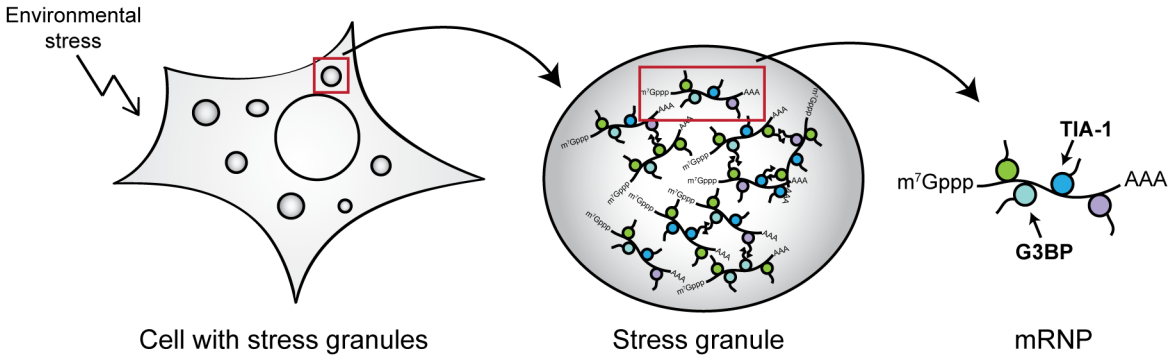

Figure 1. Schematic diagram of stress granules. Stress granules assemble in the cytoplasm of mammalian cells in response to environmental stress. They consist of translationally repressed mRNAs and proteins, mainly RBPs, that form a network by multiple weak interactions. Messenger ribonucleoproteins (mRNPs) are composed of RBPs, such as G3BP and TIA-1, and mRNA.

The first step of SG assembly is facilitated by the interaction of mRNAs and RBPs. Subsequently a dense network is formed by multivalent RNA-protein and protein-protein interactions. Overexpression of certain RBPs can lead to the assembly of SGs without any stress signaling present, indicating the importance of RBPs in the SG formation process (Gilks et al., 2004; Tourriere et al., 2003). Among these proteins is G3BP, a phosphorylation-dependent endoribonuclease, that plays a crucial role in SG assembly, as depletion of G3BP severely inhibits the formation of SGs (Matsuki et al., 2013). Furthermore, free mRNA is required for SG formation, as prevention of polysome dissociation inhibits SG assembly, whereas it is promoted upon disassembly of polysomes (Bounedjah et al., 2014; Kedersha et al., 2000). Proteins involved in SG assembly often exhibit different types of modular interaction domains to interact with other proteins or RNA (Shin and Brangwynne, 2017). Altering protein interactions by posttranslational

modifications, such as methylation, phosphorylation and glycosylation, can thereby influence SG assembly (Nott et al., 2015; Ohn et al., 2008; Tourriere et al., 2003). SG disassembly is facilitated in a chaperone-mediated manner, thereby sorting mRNAs for translation or degradation (Mateju et al., 2017; Wallace et al., 2015). Additionally, SGs can be cleared by autophagy, which is an intracellular non-selective degradation system for cytoplasmic constituents (Buchan et al., 2013; Mateju et al., 2017). The main function of SGs seems to be the translational repression, as their formation correlates with a decrease in global translation. However, specific mRNAs are excluded from SGs, shifting translation towards stress-responsive mRNAs such as heat shock proteins (Kedersha and Anderson, 2002). Furthermore, it has been suggested that the local concentration of SG components and the subsequent lower concentration of factors in the cytosol could influence biochemical reactions (Buchan and Parker, 2009). Thus, SG functions are not fully understood yet and there are many unresolved issues.

1.1.2 P bodies

Another type of RNP granule is the P body. P bodies are closely related to SGs and both share some components, such as specific proteins and mRNA. The main difference in their composition is that SGs harbor proteins involved in translation initiation whereas P bodies contain proteins of the mRNA decay machinery, for example the decapping enzymes DCP1a (decapping protein 1a) and DCP2 (Anderson and Kedersha, 2008). In contrast to SGs, P bodies are present in unstressed cells, but can be further induced in response to stress or inhibition of translation initiation (Kedersha et al., 2005). The functions of P bodies comprise mRNA degradation, translational repression and mRNA storage. During translational inhibition, P bodies dock onto SGs, indicating that these two assemblies interact with each other (Kedersha et al., 2005). Several observations suggest that there is an mRNA cycle between SGs, P bodies and polysomes. In this model mRNAs can move between these assemblies depending on their fate.

1.2 Role of phase separation in stress granule assembly

SGs are highly dynamic structures, with their components being in a constant and rapid flux with the surrounding cytosol (Kedersha et al., 2000; Kedersha et al., 2005). Recent studies suggest that SGs and other RNP granules assemble by a process known as liquid-liquid phase separation (LLPS), driven by dynamic protein-protein interactions (Hyman et al., 2014; Kroschwald et al., 2015; Patel et al., 2015). LLPS is a physical process that occurs when a mixture of molecules spontaneously separates into two distinct phases, a dilute and a dense phase. Liquid-like properties have been attributed to a number of membrane-less organelles, including P granules (RNP granules in embryos of *Caenorhabditis elegans*) and nucleoli (Brangwynne et al., 2009; Brangwynne et al., 2011). Moreover, several *in vitro* studies showed that mixtures of RNA and multi-domain proteins can phase separate into liquid droplets (Li et al., 2012; Molliex et al., 2015; Patel et al., 2015). These findings suggest that many membrane-less structures have liquid-like properties and the ability to assemble by phase separation.

Multivalent protein-protein and RNA-protein interactions are the molecular driving force underlying the assembly of membrane-less organelles. Different types of modular interaction domains and RNA-binding domains, such as RNA recognition motifs (RRMs), facilitate protein and RNA interactions (Shin and Brangwynne, 2017). Furthermore, intrinsically disordered regions (IDRs), which display low sequence complexity and conformational heterogeneity, contribute to phase separation (Oldfield and Dunker, 2014). IDRs are typically enriched in polar and charged amino acids whilst lacking hydrophobic residues (Romero et al., 2001). Many IDRs contain repetitive sequences of single amino acids or short amino acid motifs, thus they are called low-complexity domains (LCDs). Multivalent binding interactions between LCD containing proteins and RNA have been shown to drive the assembly of liquid droplets (Li et al., 2012). Hence, it is not surprising that LCD containing proteins are highly enriched in the proteome of membrane-less organelles with a significant enrichment of LCDs in RBPs (Jain et al., 2016; King et al., 2012). *In vitro* studies showed that many RBPs, such as fused in sarcoma (FUS) and hnRNPA1, can undergo LLPS in a concentration dependent manner

(Molliex et al., 2015; Patel et al., 2015). Interestingly, liquid droplets of RBPs can over time turn into more gel- or solid-like structures *in vitro*, sometimes even into fibrous aggregates (Patel et al., 2015; Xiang et al., 2015).

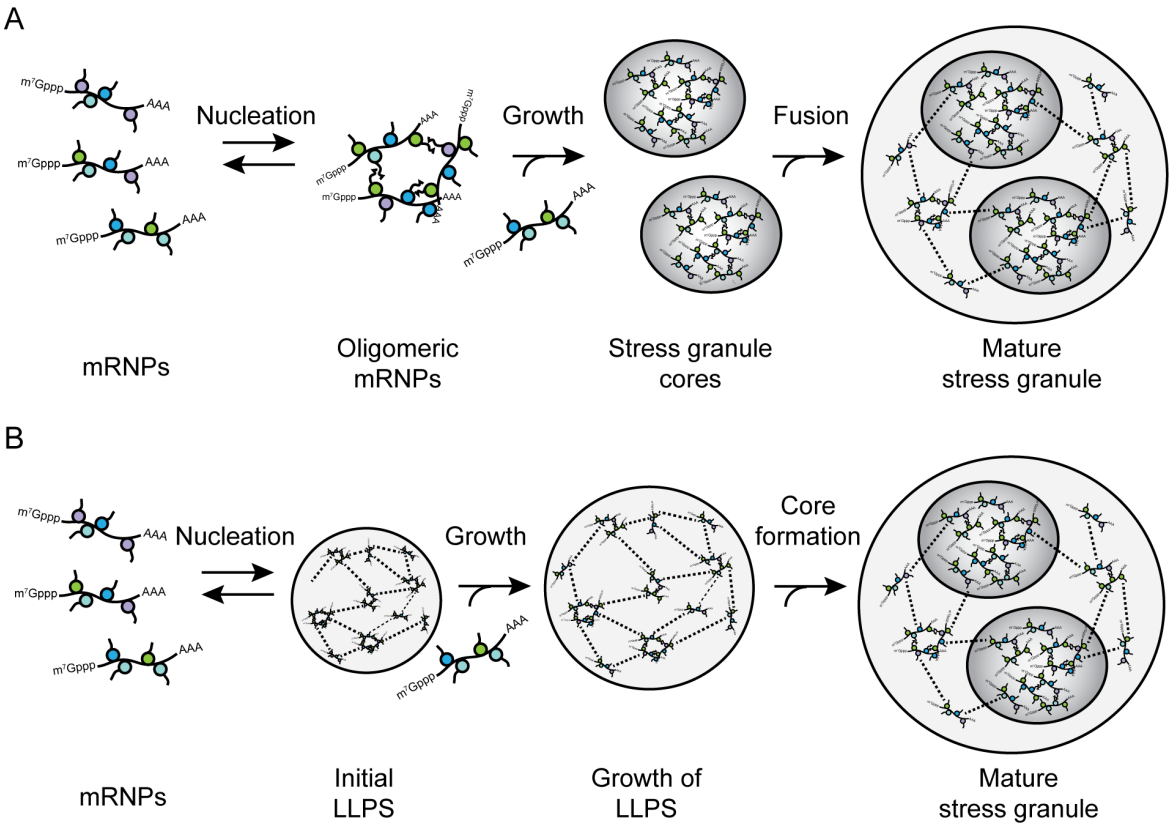

Figure 2. Two models for stress granule assembly. (A) Nucleation of translationally repressed mRNPs into oligomers occurs by specific, strong interactions. In the second step, oligomers grow by addition of mRNPs and form stable core structures. Cores fuse and a less dense shell is build by LLPS. (B) In the first step, mRNPs form small droplets by weak dynamic interactions and these phase separations grow by recruitment of mRNPs. Through the high local concentration of proteins with LCDs, stable core structures form inside the granule. (Adapted from Protter and Parker, 2016)

There are two models describing the role of LLPS in the multi-phase assembly of SGs. SGs have been shown to consist of two distinct phases: a less concentrated shell, which disassembles upon cell lysis and a more stable core structure (Jain et al., 2016). The different models for SG assembly raise the question, which phase assembles first. In one model, translationally repressed mRNPs first nucleate into oligomers by strong, specific interactions. By recruiting additional mRNPs, oligomers would grow into larger assemblies, representing the SG cores.

Afterwards, the shell structure would form by LLPS, triggered through the high concentration of LCD containing proteins within the core (Jain et al., 2016; Wheeler et al., 2016). The second model suggests that the nucleation step is facilitated by LLPS of mRNPs through weak dynamic interactions. Droplets would grow by recruitment of more mRNPs and a core would subsequently form through the high concentration of LCD containing proteins (Molliex et al., 2015; Patel et al., 2015).

1.3 RNA-binding proteins in disease

Over the last decade, several RBPs that are part of membrane-less organelles have been implicated in degenerative disorders. A common feature of these degenerative diseases is the aggregation of RBPs in the nucleus or cytoplasm. An emerging hypothesis is that the pathological RBP inclusions are related to physiological RNP granules, indicating a disturbance in RNP granule metabolism. TAR DNA-binding protein of 43 kDa (TDP-43) and FUS were the first RBPs that were found in connection with degenerative diseases (Arai et al., 2006; Neumann et al., 2009; Neumann et al., 2006). Both proteins are predominantly nuclear proteins that harbor nucleic-acid binding domains and a LCD (Iko et al., 2004; Wang et al., 2004). TDP-43 was identified to be the main constituent of inclusions found in frontotemporal lobar degeneration (FTLD) and amyotrophic lateral sclerosis (ALS) (Neumann et al., 2006). In both of these diseases, TDP-43 was found in cytoplasmic inclusions and simultaneously cleared from the nucleus (Geser et al., 2009). Interestingly, TDP-43 pathology has been found in connection with several other degenerative disorders, including inclusion body myopathy, Alzheimer's disease (AD) and Parkinson's disease (Chen-Plotkin et al., 2010). FUS has been identified in inclusions of several neurodegenerative diseases, including sporadic ALS, FTLD and Huntington's disease (Doi et al., 2010; Mackenzie et al., 2010; Woulfe et al., 2010). Furthermore, FUS mutations linked to ALS were shown to disrupt the nuclear localization and to promote accumulation of FUS in the cytoplasm (Dormann et al., 2010). This indicates that FUS and TDP-43 broadly contribute to pathology in degenerative disorders. Mutations in the RBP and stress granule protein TIA-1 are the cause of welander distal myopathy and furthermore, mutations in TIA-1 have been found in

connection with ALS and FTLD (Hackman et al., 2013; Mackenzie et al., 2017). Several observations suggest that RBP positive inclusions, seen in some degenerative disorders, are related to SGs. TDP-43 inclusions found in ALS and FTLD patients colocalized with the SG markers TIA-1 and eIF3 (Liu-Yesucevitz et al., 2010). Furthermore, AD patient samples showed colocalization of tau aggregates with TIA-1 and overexpression of TIA-1 induced the formation of tau-positive inclusions in cultured cells (Vanderweyde et al., 2012). Disease-causing mutations in RBPs (e.g. hnRNPA1, hnRNPA2, FUS) led to an increased accumulation in SGs (Bosco et al., 2010; Kim et al., 2013). Mutated SOD1 misfolded and accumulated in SGs, thereby altering the dynamic properties of SGs, leading to more stable and less dynamic SGs (Mateju et al., 2017). Supporting these observations, *in vitro* studies showed that RBPs involved in ALS could mature from a liquid into an aberrant, solid-like state (Molliex et al., 2015; Patel et al., 2015). However, direct evidence that pathological inclusions are derived from physiological SGs is still missing.

1.4 Protein misfolding disorders

Many neurodegenerative diseases are based on the underlying mechanism that a natively folded protein can adopt a different, pathological conformation. This principle also applies to a group of rare diseases known as transmissible spongiform encephalopathies (TSEs). The infectious agent of TSEs is the misfolded form of the prion protein (PrP^{Sc}). According to the prion-hypothesis the infectious agent replicates in the absence of nucleic acids and by conversion of the natively folded protein into its pathological isoform (Bolton et al., 1982; Prusiner, 1982). The conversion and replication of the pathological isoform is thought to occur through the process of seeded polymerization (Fig. 3) (Caughey et al., 1995; Come et al., 1993). This model hypothesizes an equilibrium between the monomeric protein and an unfolded, intermediate isoform. On rare events the intermediate isoform can misfold into the pathological state, causing seed formation. Seeds can recruit monomeric protein, thereby templating the conversion into the misfolded isoform and leading to aggregate formation. In secondary nucleation events, new seeds are generated, for example by

fragmentation into smaller polymers that can serve as new seeds for conversion of monomeric protein (Knowles et al., 2009; Orgel, 1996).

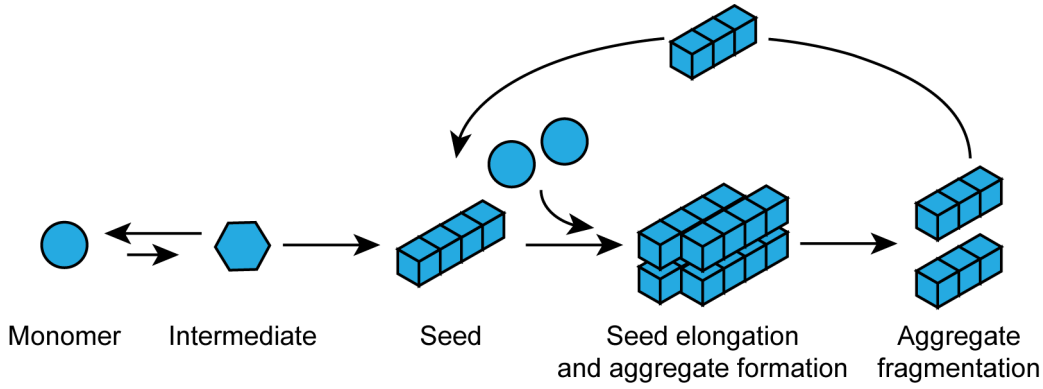

Figure 3. The seeded polymerization model. Seed formation occurs by conversion of monomeric protein into the pathological isoform via an intermediate form. The elongation of seeds and subsequent aggregate formation occurs by the recruitment and conversion of natively folded protein. Aggregates are fragmented into smaller entities that serve as new nucleation sites.

More than 20 human diseases have been identified that share the prion principle of protein misfolding. This group is collectively called protein misfolding disorders and includes diseases such as Alzheimer's disease, Parkinson's disease and type 2 diabetes (Chiti and Dobson, 2006). Many protein misfolding disorders are characterized by the accumulation of specific proteins into highly organized fibrillar aggregates. These deposits share structural characteristics as they are organized in a certain way. Aggregates arranged in a cross-β structure and with the ability to bind dyes such as Congo red and thioflavin S and T have been termed amyloid (Westermark et al., 2005). Amyloid fibrils have typically a diameter of 6-12 nm and consist of two to six protofilaments that are twisted around each other, forming supercoiled structures. Within the protofilaments the polypeptides are folded in a cross-β structure, which runs perpendicular to the fiber axis (Serpell, 2000; Serpell et al., 2000). Interestingly, proteins found in pathological aggregates do not share obvious sequence similarities (Chiti and Dobson, 2006). Amyloid formation is thought to follow the seeded polymerization mechanism, as seen for PrP^{Sc} in TSEs (Jarrett and Lansbury, 1993; O'Nuallain et al., 2004). One hallmark of prion diseases is that not only misfolded proteins can spread from cell to cell, but that the disease is transmissible between individuals.

For other protein misfolding disorders, recent studies have shown that protein aggregates are also capable of spreading from cell to cell, thereby propagating disease pathogenesis in a prion-like manner (Brundin et al., 2010). However, there are no reports of disease transmission between individuals and so far an infectious origin for these diseases cannot be confirmed.

1.5 Prions of lower eukaryotes

After detection of the mammalian prion protein, the prion principle was expanded to explain two non-Mendelian traits in *Saccharomyces cerevisiae*, [*PSI*$^+$] and [*URE3*] (Wickner, 1994). [*PSI*$^+$] and [*URE3*] are phenotypic traits that mimic a loss-of-function phenotype, yet their persistence is dependent on the expression of their associated genes, Sup35 and Ure2. Their phenotypes are explained by a prion-like mechanism, where [*PSI*$^+$] and [*URE3*] are self-propagating conformations of the host encoded proteins Sup35 and Ure2 (Wickner et al., 2001). Since the revelation that [*PSI*$^+$] and [*URE3*] are prions, several other prions in lower eukaryotes have been identified, including [*PIN*$^+$] and [*Het-s*] (Coustou et al., 1997; Sondheimer and Lindquist, 2000). Hence, multiple proteins in yeast can form prions that transmit heritable phenotypes. In contrast to the mammalian prion protein, yeast prions are rarely deleterious but sometimes are also advantageous depending on the environmental conditions (McGlinchey et al., 2011; True and Lindquist, 2000). The propagation of yeast prions occurs by seeded polymerization, similar to the mammalian prion protein. Hereby nucleus formation has been shown to be the rate-limiting step, while addition of exogenous seeds can accelerate aggregate formation *in vitro* (Serio et al., 2000). Fragmentation of prion aggregates into smaller entities is essential for maintenance and in yeast facilitated by the heat shock protein 104 (Hsp104) (Chernoff et al., 1995). Furthermore, overproduction as well as inactivation of Hsp104 can eliminate the prion phenotype (Chernoff et al., 1995). Inheritance of the prion state occurs by vertical transmission to progeny or horizontal transmission during mating (Uptain and Lindquist, 2002). Spontaneous conversion of the soluble into the prion isoform is a rare event in yeast, but once established prions faithfully propagate (Uptain and Lindquist, 2002). Verifying the protein-only hypothesis, *in vitro* fibrillized recombinant Sup35 is able to induce a self-propagating prion phenotype

in yeast (King and Diaz-Avalos, 2004). Similar to the mammalian prion protein, yeast prions can exhibit distinct prion strains/variants that differ in mitotic stability, suppressor efficiency and response to the chaperone machinery (Derkatch et al., 1996; Kushnirov et al., 2000). The distinct prion strain features are determined by differences in the conformation of the prion protein (Tanaka et al., 2004). The yeast prion behavior is encoded by prion domains (PrDs), which are enriched in uncharged, polar amino acids, mainly asparagine and glutamine, while lacking hydrophobic residues (Alberti et al., 2009; Toombs et al., 2010). Their primary sequence is of low complexity, intrinsically disordered and comprises typically at least 60 amino acids in length (Alberti et al., 2009; Toombs et al., 2010). However, the underlying features of prion formation are still not fully understood. Importantly, PrDs can be transferred to other proteins while retaining their prion propensities (Li and Lindquist, 2000).

1.6 Prion-like domains

RNP granules assemble through protein-protein interactions that are facilitated by LCDs. These domains also comprise prion-like domains (PrLDs), which were identified by an algorithm due to their compositional similarities to yeast prion domains (Alberti et al., 2009). Initially this algorithm was designed to detect prion candidates in the proteome of *Saccaromyces cerevisiae*. It is based on the prion domains of the known yeast prions Sup35p, Ure2p and Rnq1p, which are enriched for glutamine and asparagine residues (Alberti et al., 2009). Scanning the human proteome using the yeast prion based algorithm revealed that prion-like regions are more common in the human proteome than previously anticipated (Couthouis et al., 2011). Of the human protein-coding genes, ~1% were identified to harbor a PrLD. Interestingly, 12% of the proteins containing a PrLD additionally harbor a RNA recognition motif, indicating that RBPs are especially enriched for PrLDs (King et al., 2012). A different algorithm assesses compositional features of glutamine (Q) and asparagine (N) rich regions that promote prion formation (Toombs et al., 2010). Many yeast prion domains show a high Q/N content, which is not a requirement for prion formation, but provides a high propensity for it (DePace et al., 1998). Subjecting the potential prion candidates among RBPs to the Toombs algorithm further emphasizes the aggregation-prone features of this

protein class, as 17 of 29 proteins passed the test and a number of others came close (King et al., 2012). The striking over-representation of RBPs among proteins with PrLDs suggests that this distinctive class of proteins is close to the edge of pathological aggregation. Interestingly, TDP-43 and FUS ranked in the top 10 of RBPs with PrLDs, suggesting a connection between prion-like propensity and appearance in neurodegenerative disorders. Several mutations in the PrLD of TDP-43 are already linked to ALS and show accelerated aggregation *in vitro*, emphasizing the involvement of PrLDs in disease pathology (Johnson et al., 2009)

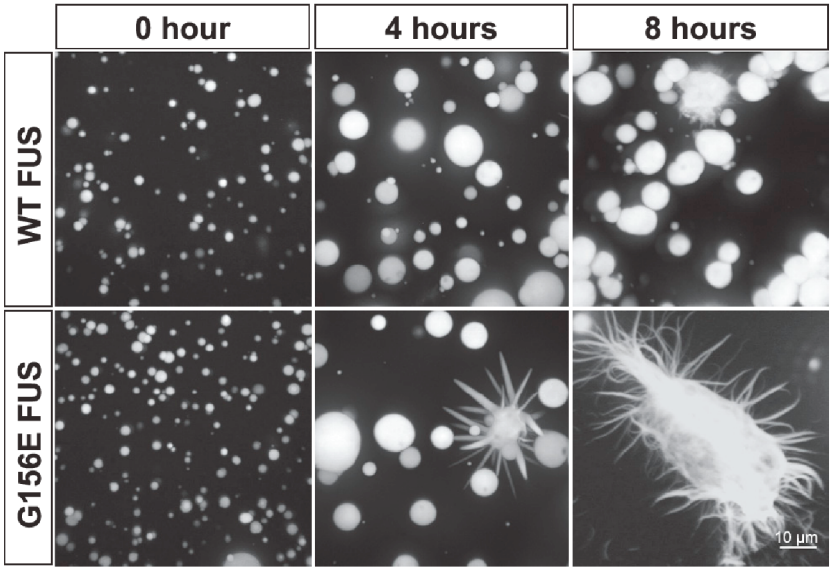

Figure 4. Conversion of mutant FUS into fibrous aggregates. *In vitro* formed liquid droplets of wild type (WT) FUS and G156E FUS fused to GFP imaged over a period of 8 hours. (Image taken from Patel et al (2015)).

SGs assemble by a regulated process of protein aggregation that is facilitated by PrLDs of RBPs. For the SG protein TIA-1 it has been shown that it contributes to SG assembly by multimerization of its PrLD (Gilks et al., 2004). This indicates that PrLDs act as generic aggregation domains that provide proteins with the ability to perform essential cellular functions. However, dysfunction of proteins harboring a PrLD might lead to aggregation. Mutations in the PrLD or enhanced environmental stress might increase the likelihood for inappropriate aggregation. In yeast, it has already been shown that a small number of mutations is sufficient

to push proteins towards aggregation or even prion formation (Paul et al., 2015). In mammalian cells, mutations in the PrLD of TIA-1, which were identified in ALS and FTLD patient samples, led to a delayed SG disassembly and accumulation of SGs that persisted for hours (Mackenzie et al., 2017). Mutations in the PrLD of other RBPs also led to a higher aggregation potential *in vitro* and increased assembly of SGs, as shown for hnRNPA1 and hnRNPA2B1 (Kim et al., 2013; Molliex et al., 2015). For recombinant FUS it has been shown that FUS liquid droplets can mature over time into fibrous aggregates and that this conversion is accelerated by patient-derived mutations in the PrLD of FUS (Fig. 4) (Patel et al., 2015). Hence, mutations in the PrLD of disease-associated RBPs might promote the formation of aggregates by accelerating the conversion of a liquid droplet into a fibrous state.

1.7 The yeast prion Sup35

Sup35 is one of the best-studied yeast prions so far. Its prion form [*PSI*$^{+}$] was first described by Brian Cox in 1965 as a non-Mendelian factor. The normal cellular function of Sup35 is translation termination, whereas [*PSI*$^{+}$] leads to the translational read-through of stop codons (Cox et al., 1988; Stansfield and Tuite, 1994). Sup35 has a length of 685 amino acids while consisting of three distinct domains (Fig. 5).

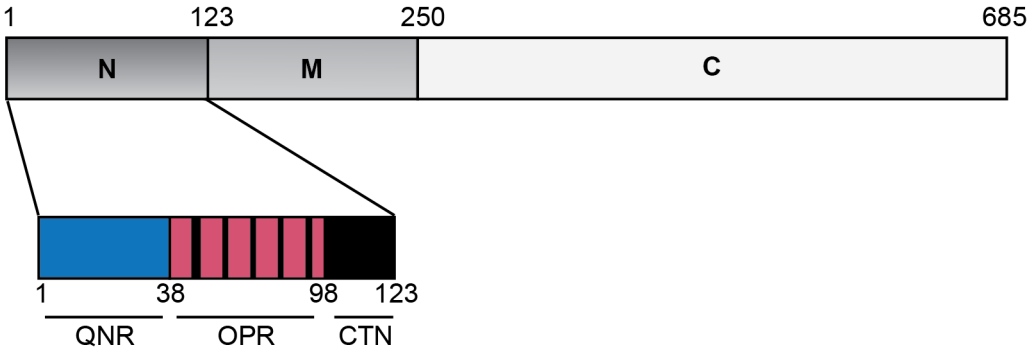

Figure 5. Primary sequence of the yeast prion Sup35. Sup35 is 685 amino acids long, comprising three domains: the aminoterminal N domain, the middle M domain and the carboxyterminal C domain. The N domain encodes the prion properties and can be further subdivided into a glutamine (Q) and asparagine (N) rich region (QNR), a region consistent of 5 1/2 oligopeptide repeats (OPR) and a carboxyterminal N domain (CTN). The highly charged M domain is important for solubility and stabilization during mitosis

and meiosis. The C domain is essential for translation termination, but dispensable for prion functions of the protein. Numbers refer to amino acids.

The aminoterminal N domain contains the prion domain and can be further subdivided into three regions: a glutamine and asparagine rich region (QNR, aa 1-39), an oligopeptide repeat region (OPR) with 5 and a half imperfect oligopeptide repeats (R1 – R6, aa 40-97) and a carboxyterminal N domain (CTN), which is also enriched in glutamine and asparagine (aa 98-123). The oligopeptide repeats found in the mammalian prion protein (PrP) are similar to the ones of Sup35 and a PrP oligopeptide repeat is able to functionally replace an oligopeptide repeat in Sup35 in supporting prion propagation (Parham et al., 2001). Furthermore, it has been shown that prion propagation is rather dependent on the amino acid composition of the prion domain than on the primary sequence (Toombs et al., 2011). Scrambling of the N domain does not disrupt prion formation, further demonstrating an independence of the primary sequence (Ross et al., 2005). The middle M domain is highly charged and facilitates stabilization of [*PSI*$^{+}$] during meiosis and mitosis, while increasing solubility (Liu et al., 2002). The carboxyterminal C domain harbors the translation termination function of Sup35, but is dispensable for the prion functions (Ter-Avanesyan et al., 1993).

1.8 Sup35NM as a model system in mammalian cells

Several recent studies suggest that proteins involved in pathological protein inclusions found in neurodegenerative diseases can spread from cell to cell in a prion-like manner (de Calignon et al., 2012; Goedert et al., 2010; Masuda-Suzukake et al., 2013). Many proteins found in such inclusions are cytosolic proteins, thus their localization differs from that of the mammalian prion protein, which is membrane-anchored. In contrast to the mammalian prion protein, yeast prions are expressed in the cytosol. Sup35 is one of the best-studied yeast prions and its aminoterminal prion domain exhibits no sequence homology to mammalian proteins, which makes it a suitable model to study prion propagation in mammalian cells without a loss-of-function phenotype. Our group has generated a cell culture model based on the prion-forming domain NM of Sup35. Therefore, NM was carboxyterminally fused to a hemagglutinin-tag (HA-tag) and

expressed in mouse neuroblastoma N2a cells by lentiviral transduction (Krammer et al., 2009). Upon expression in N2a cells, NM resides in a soluble state and spontaneous aggregation is an extremely rare event (Duernberger et al., 2018; Krammer et al., 2009). Aggregate formation can be induced by the addition of *in vitro* fibrillized recombinant NM. Thereby induced NM aggregates are faithfully propagated to progeny (Krammer et al., 2009). The successful propagation of the prion state requires fragmentation of aggregates into smaller propagons, which in yeast is facilitated by Hsp104 (Chernoff et al., 1995). Interestingly, no mammalian homolog of Hsp104 exists. Hence, the fragmentation of NM aggregates in mammalian cells is facilitated by a different, so far unknown mechanism. Limiting dilution cloning of aggregate bearing cells led to the isolation of different aggregate types with distinct morphologically and biochemically characteristics, similar to yeast prion strains (Krammer et al., 2009). Sup35NM aggregates successfully invade neighboring cells, thereby inducing a self-perpetuating prion state (Hofmann et al., 2013). These results demonstrate that Sup35NM aggregates can faithfully propagate as a prion in mammalian cells, fulfilling all criteria of the life cycle of cytosolic prions (Fig. 6).

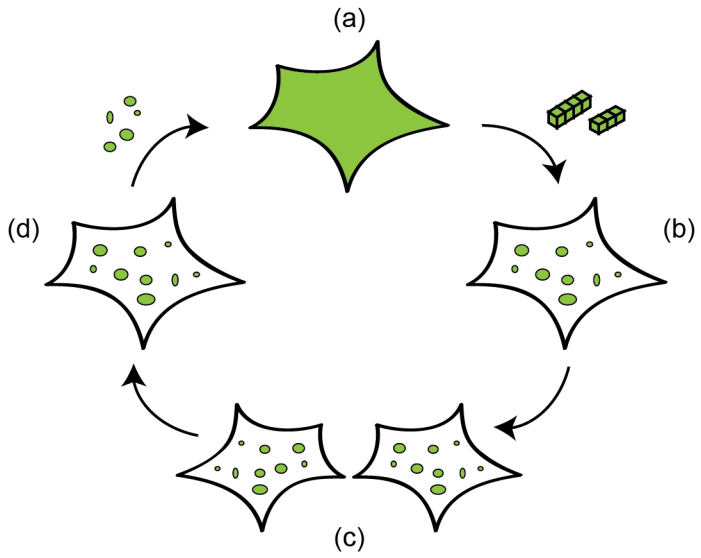

Figure 6. Cytosolic prion replication cycle. (a) The prion precursor protein resides in a soluble state, (b) upon addition of exogenous fibrils aggregation is induced, (c) fragmentation of aggregates facilitates inheritance by daughter cells, (d) neighboring cells are invaded by propagons to induce a self-perpetuating prion state.

Interestingly, the subdomains driving the different steps of prion propagation differ between yeast and mammalian cells. In yeast, prion induction and propagation is facilitated by the QNR, whereas prion maintenance is mainly driven by the OPR (DePace et al., 1998; Osherovich et al., 2004). However, in N2a cells the last 2.5 repeats of the OPR and the CTN are important for NM aggregate induction, prion formation and prion maintenance (Duernberger et al., 2018).

1.9 Objective

Membrane-less organelles are transient structures that are thought to assemble by liquid-liquid phase separation. These membrane-less organelles consist mainly of RNA and RBPs, which facilitate the assembly by forming a network of multiple weak interactions. RBPs often contain PrLDs, which were identified due to their compositional similarities to yeast prion domains and play important roles in RNP granule formation. Interestingly, several RBPs have already been implicated in a range of degenerative disorders, including FUS and TDP-43 in ALS and FTLD. Accumulating evidence points to a misregulation of membrane-less organelles and RBPs in disease, leading to the suggestion that RNP granules evolve into persistent, aberrant assemblies and at some point even into pathological aggregates (Fig. 7). However, direct evidence that physiological RNP granules can turn into disease-associated inclusions is still missing. Upon examination of the NM interactome, several SG associated proteins were identified as binding partners of NM and the interactomes of NM and SGs depicted a high degree of similarities. Aim of this study was to further investigate the correlation between SGs and protein aggregates, using NM expressed in mammalian cells as a model. The presence of prion-like domain containing proteins in SGs raised the question whether proteins harboring a prion domain, such as Sup35, are recruited to SGs and whether this recruitment could trigger the formation of a self-perpetuating protein aggregate. To this end, NM should be stably expressed in the human HeLa cell line. The recruitment of SG components to NM prions and of soluble NM protein to SGs should be assessed. The subdomain of NM required for localization to SGs should be analyzed by using NM proteins with deletions in the N domain. FRAP analysis of SGs and NM prions should give insights about the dynamics of these structures and whether the presence of NM influences SG

dynamics. Involvement of SGs in NM aggregate induction with or without an exogenous seed should be analyzed by high-throughput confocal microscopy. Combined, this research should analyze the relationship between SGs and NM prions, while answering the question whether membrane-less organelles can turn into protein aggregates.

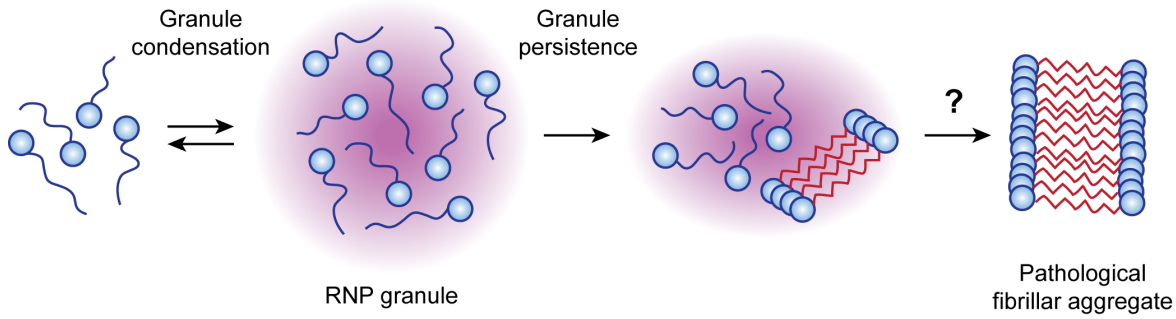

Figure 7. RNP granules may evolve into pathological aggregates. RBPs can undergo phase transition and facilitate RNP granule formation through transient interactions of their PrLDs. By bringing RBPs into close proximity in RNP granules, persistence of these granules might lead to misfolding. Eventually these persistent granules can give rise to pathological fibrillar aggregates as observed in neurodegenerative disorders. (Adapted from March et al., 2016)

2. Materials and methods

2.1 Biological safety

The work with genetically modified organisms and genetic engineering was performed under biosafety level 2 according to the German *Gentechnikgesetz* (August 31st, 2015). All contaminated materials and solutions were collected, inactivated and disposed following the official regulations.

2.2 Chemicals

All chemicals were purchased from Sigma-Aldrich (Steinheim, Germany) or Carl Roth (Karlsruhe, Germany), unless stated otherwise.

2.3 Cell culture

Cell culture was performed under sterile conditions in a laminar flow cabinet using sterile medium, glass and plastic ware. Cells were cultured in a CO_2 incubator (HERAcell 240i, Thermo Fisher Scientific, Waltham, USA) at 37°C with 5 % CO_2 in a humidified atmosphere.

2.3.1 Thawing of cells

Culture medium	Dulbecco's Modified Eagle Medium (DMEM) + GlutaMAX (Gibco, Waltham, USA) + 10 % fetal calf serum (FCS) (Biochrom, Berlin, Germany)

Cells stored in liquid nitrogen were thawed at 37°C and resuspended in culture medium. Cell suspension was centrifuged at 300 x g for 5 min at room temperature (RT) (Heraeus Multifuge X3R, Thermo Fisher Scientific, Waltham USA). The cell pellet was resuspended in culture medium and transferred to a cell culture flask.

2.3.2 Culturing of cells

Phosphate buffered saline (PBS)	Gibco, Waltham, USA
Trypsin-EDTA, 0.25 %	Gibco, Waltham, USA

Cells were grown in cell culture flasks or dishes and passaged every 2-3 days. For passaging, cells were rinsed once with PBS and detached by incubation with Trypsin-EDTA for 5 min at RT. Inactivation of Trypsin was achieved by adding at least one volume of fresh culture medium. After resuspension, cells were centrifuged at 300 x g for 5 min at RT (Heraeus Multifuge X3R, Thermo Fisher Scientific, Waltham USA). The supernatant was discarded and the pellet resuspended in culture medium. The cell suspension was plated into new flasks or dishes containing culture medium. For determination of cell numbers an automated cell counter was used (TC 20, BioRAD, Hercules, USA).

Table 1: Cell lines

Cell line	Property	Reference
N2a	Murine neuroblastoma cell line	ATCC CCL-131
HeLa	Human cervix epitheloid carcinoma cell line	93021013 ECACC
HeLa NM-HA	HeLa cells expressing NM-HA	Generated in this study
HeLa NM-HA^{agg}	HeLa cells producing NM-HA aggregates	Generated in this study
HeLa NM-GFP	HeLa cells expressing NM-GFP	Generated in this study
HeLa G3BP1-mCherry	HeLa cells expressing G3BP1-mCherry (BAC)	Kindly provided by Simon Alberti
HeLa G3BP1-mCherry NM-GFP	HeLa cells expressing G3BP1-mCherry (BAC) and NM-GFP	Generated in this study
HeLa NM-HA Δ 1-39	HeLa cells expressing NM-HA Δ 1-39	Generated in this study

HeLa NM-HA Δ 39-57	HeLa cells expressing NM-HA Δ 39-57	Generated in this study
HeLa NM-HA Δ 39-74	HeLa cells expressing NM-HA Δ 39-74	Generated in this study
HeLa NM-HA Δ 75-97	HeLa cells expressing NM-HA Δ 75-97	Generated in this study
HeLa NM-HA Δ 75-123	HeLa cells expressing NM-HA Δ 75-123	Generated in this study
HeLa NM-HA Δ 98-123	HeLa cells expressing NM-HA Δ 98-123	Generated in this study

2.3.3 Cryoconservation of cells

Freezing medium — FCS (Biochrom, Berlin, Germany) + 10 % Dimethyl sulfoxide (DMSO)

Cryoconservation of cells in liquid nitrogen was used for long-term storage of cells. Cells were detached as described (2.3.2) and pelleted at 300 x g for 5 min at 4°C (Heraeus Multifuge X3R, Thermo Fisher Scientific, Waltham, USA). Cell pellets were resuspended in freezing medium and transferred to cryogenic vials. Vials were kept at -80°C overnight and subsequently transferred to liquid nitrogen.

2.3.4 Lentiviral transduction of mammalian cells

Transduction medium — 5 % FCS (Biochrom, Berlin, Germany), 8 µg/ml Polybrene (Merck Millipore, Billerica, USA) in DMEM (Gibco, Waltham, USA)

For transduction, $2x10^4$ cells per well were plated on a 24-well plate. The next day culture medium was replaced with transduction medium and the appropriate amount of lentiviral particles was added to the cells (Table 2). Viral particles were kindly provided by Yvonne Dürnberger (Duernberger et al., 2018) .The 24-well plate was centrifuged at 800 x g for 10 min at RT (Heraeus Multifuge X3R, Thermo Fisher Scientific, Waltham, USA). After 24 h of culturing, the medium was

exchanged with fresh culture medium. Cells were expanded to generate stable cell lines and aliquots were frozen in liquid nitrogen (2.3.3).

Table 2: Expression plasmids of viral particles

Construct	Reference
pRRL.sin.PPT.CMV. NM-HA.Wpre	Duernberger et al. (2018)
pRRL.sin.PPT.CMV. NM-GFP.Wpre	Duernberger et al. (2018)
pRRL.sin.PPT.CMV. NM-HA Δ 1-39.Wpre	Duernberger et al. (2018)
pRRL.sin.PPT.CMV. NM-HA Δ 39-57.Wpre	Duernberger et al. (2018)
pRRL.sin.PPT.CMV. NM-HA Δ 39-74.Wpre	Duernberger et al. (2018)
pRRL.sin.PPT.CMV. NM-HA Δ 75-97.Wpre	Duernberger et al. (2018)
pRRL.sin.PPT.CMV. NM-HA Δ 75-123.Wpre	Duernberger et al. (2018)
pRRL.sin.PPT.CMV. NM-HA Δ 98-123.Wpre	Duernberger et al. (2018)

2.3.5 Aggregate induction by recombinant NM fibrils

Recombinant NM protein (prepared as described in 2.4.8) was rotated head-over-tail at 50 rpm for 24 h at 4°C (LD-76, Labinco, DG Breda, Netherlands) at a concentration of 100 µM (monomer concentration) to generate fibrils. To break fibrils into smaller entities, fibrils were sonicated for 3 min (5 sec on, 1 sec off) with 10 % amplitude (Sonicator Sonoplus, Bandelin, Berlin, Germany) in an ice-cold water bath. Fibrils were added to cells at a final concentration of 5 µM (monomer concentration).

2.3.6 Generation of HeLa NM-HA^{agg} cell line

To generate a cell line that stably carries NM aggregates, limiting dilution cloning was conducted using HeLa NM-HA expressing cells that were subjected to aggregate induction (2.3.5). Cells were detached and the cell number was determined as described before (2.3.2). Cells were plated on 96-well plates at a concentration of 10 cells/ml (100 µl/well). After approximately 10 days of culturing, single cell clones were selected and further expanded. Cell clones were subjected to immunofluorescence staining and microscopy analysis (2.3.14) to detect NM aggregate bearing cells. Six cell clones were selected and mixed at equal cell numbers to generate a bulk cell line (HeLa NM-HA^{agg}). Cells were expanded and aliquots were frozen in liquid nitrogen (2.3.3).

2.3.7 Live cell imaging

Cells were plated on 35 mm µ-Dishes or 4-well µ-Slides (Ibidi, Madison, USA) and cultured overnight. Time-lapse images were taken over the indicated periods of time using an widefield fluorescence microscope (Zeiss, Jena, Germany) at 37°C and 5 % CO_2. For imaging of aggregate inheritance, cells were subjected to aggregate induction (2.3.5) 48 h prior to imaging and time-lapse images were taken over a period of 16 h with a time interval of 5 min. Cells imaged for aggregate induction were incubated with 75 µM sodium arsenite for 30 min before 5 µM recombinant NM fibrils (monomer concentration) were added. Subsequently cells were imaged for 22 h with a time interval of 10 min. For stress granule (SG) assembly and disassembly, cells were treated with 500 µM (SG assembly) or 250 µM (SG disassembly) sodium arsenite and either directly subjected to imaging (60 min, 1 min interval) or incubated for 1 h, followed by two washing steps before imaging (3 h, 2 min interval).

2.3.8 Coculture analysis

HeLa NM-HA^{agg} or HeLa NM-HA^{sol} donor cells were cocultured with HeLa NM-GFP^{sol} recipient cells at a ratio of 1.5:1 on coverslips ($4x10^4$ total cells). After 48 h, cells were fixed and stained as described (2.3.14). Images were taken using a LSM 700 confocal microscope (Zeiss, Jena, Germany).

2.3.9 Stress granule induction

For stress granule induction cells were plated on coverslips and cultured overnight. To induce stress granules, cells were exposed to either 500 µM sodium arsenite for 1 h, 100 µM MG132 for 2 h, 200 mM NaCl for 1 h, heat shock at 45°C for 30 min or cells were transfected with either 300 ng high molecular weight (HMW) dsRNA (InvivoGen, San Diego, USA) or 300 ng low molecular weight (LMW) dsRNA (InvivoGen, San Diego, USA) using Lipofectamine 2000 transfection reagent (Thermo Fisher Scientific, Waltham, USA). Cells were subsequently fixed and immunofluorescence staining was performed as described (2.3.14). Images were taken using a LSM 700 confocal microscope (Zeiss, Jena, Germany).

2.3.10 Stress treatment

Microplate, 96-well, µ-clear, F-Bottom, black	Greiner Bio-One, Kremsmünster, Austria

Cells were plated on 96-well plates ($6x10^3$ cells/well) or 12-well plates ($2x10^5$ cells/well) and grown for 24 h. 30 min prior to the respective treatment the medium was replaced with fresh, pre-warmed culture medium. Compounds were added at the indicated concentrations (Table 3) or cells were subjected to heat shock at 44°C and after 1 h 5 µM recombinant NM fibrils (monomer concentration) were added or cells were left untreated. After 1 h, cells were washed once with pre-warmed culture medium and fresh culture medium was added. Cells were cultured for 16 h, subsequently fixed and stained as described (2.3.15). For SG induction control experiments, $8x10^3$ cells/well were plated on 96-well plates, fixed 2 h after addition of compounds and subjected to immunofluorescence staining (2.3.15). For detection of phosphorylated eIF2α, cells were harvested 1 h and 2 h after addition of compounds and processed as described (2.3.2 and 2.4.1).

Table 3: Stress treatment compounds

Compound	Concentration	Reference
Sodium arsenite	250 µM	Sigma-Aldrich, Steinheim, Germany
NaCl	200 mM	Carl Roth, Karlsruhe. Germany
Cycloheximide	20 µg/ml	Sigma-Aldrich, Steinheim, Germany
Puromycin	10 µg/ml	Sigma-Aldrich, Steinheim, Germany
MG132	20 µM	Merck Millipore, Billerica, USA
Tunicamycin	5 µg/ml	Sigma-Aldrich, Steinheim, Germany
Thapsigargin	0.5 µg/ml	Merck Millipore, Billerica, USA
Salubrinal	50 µM	Sigma-Aldrich, Steinheim, Germany
Rapamycin	10 µM	Merck Millipore, Billerica, USA
Wortmannin	10 µM	Selleckchem, Munich, Germany

2.3.11 siRNA Transfection

Lipofectamine RNAiMAX Transfection Reagent — Thermo Fisher Scientific, Waltham, USA

Cells were plated on 24- or 6-well plates and cultured overnight. The following day, cells were subjected to transfection according to the manufacturer's instructions. Knockdown efficiency was tested every time by western blotting (2.4.7).

2.3.12 Plasmid Transfection

Lipofectamine 2000 Transfection Reagent — Thermo Fisher Scientific, Waltham, USA

Cells were plated on 24-well plates and cultured overnight. The following day, cells were subjected to transfection according to the manufacturer's instructions. For immunofluorescence staining cells were detached after 24 h, plated on coverslips and fixed on the next day. Immunofluorescence staining was performed as described (2.3.14).

Table 4: Plasmids

Construct	Tag	Vector Backbone	Reference
VCP	EGFP	pEGFP-N1	Gift from Nico Dantuma (Addgene # 23971)
Keap1	GFP	phrGFP-N1	Gift from Qing Zhong (Addgene # 28025)
hPLIC-2	FLAG	pCMV4	Gift from Peter Howley (Addgene # 8661)

2.3.13 Fluorescent recovery after photobleaching (FRAP) analysis

FRAP analysis was performed using a LSM 710 or LSM 700 confocal microscope (Zeiss, Jena, Germany). Cells were plated on 35 mm µ-Dishes (Ibidi, Madison, USA) and grown overnight. For FRAP analysis of SGs, cells were treated with 0.5 mM sodium arsenite 30 min prior to photobleaching. A single SG was bleached with high power of the 405 nm laser and fluorescence recovery was analyzed for 60 sec. For FRAP analysis of NM prions, cells were exposed to 5 µM recombinant fibrils (monomer concentrations) 48 h prior to photobleaching. NM prions were partially bleached with high power of the 405 nm laser and fluorescence recovery was analyzed for 4 min. Data processing was carried out using Fiji analysis software. Background was determined outside the fluorescently labeled cells and subtracted. The ratio of fluorescence intensity of the photobleached region of interest (ROI) to that of a neighboring cell was calculated for each time point

[$F(t)_{ROI}/F(t)_{cell}$] to correct for photodamage. Fluorescent intensities were normalized to the prebleach intensity.

2.3.14 Immunofluorescent staining for confocal microscopy analysis

High Precision Microscope Cover Glass, No 1.5H	Marienfeld Superior, Lauda-Königshofen, Germany
Aqua Polymount	Polysciences, Warrington, USA
Superfrost Plus Microscopic Slides	Thermo Fisher Scientific, Waltham, USA
Hoechst 33342	Molecular Probes, Eugene, USA
Permeabilization solution	0.1 % Triton X-100 (Carl Roth, Karlsruhe, Germany) in PBS
Blocking solution	2 % goat serum (Dianova, Hamburg, Germany) in PBS
Blocking solution (for primary antibodies produced in goat)	2 % donkey serum (Dianova, Hamburg, Germany) in PBS

For immunofluorescence staining, cells were grown on coverslips in 24-well plates for at least 24 h. Cells were treated according to the individual experiments and subsequently fixed with 4 % paraformaldehyde (in PBS) for 10 min at RT. After rinsing the cells three times with PBS, cells were incubated with permeabilization solution for 10 min at RT. Following three washing steps with PBS, cells were incubated with blocking solution for 1 h at RT. Specific proteins were visualized by incubation with the respective primary antibodies diluted in blocking solution overnight at 4°C in a humidified chamber (Table 5). Cells were washed three times with PBS for 5 min to remove unbound antibody and were subsequently incubated with the appropriate fluorophore-coupled secondary antibodies in blocking solution for 1 h at RT (Table 6). Following three washing steps with PBS for 5 min, nuclei were stained with Hoechst 33342 (1 µg/ml in PBS) for 5 min at RT. Cells were washed four times with PBS and coverslips were dipped once in H_2O_{bidest} before they were mounted on microscopic slides using Aqua Polymount. Confocal microscopy was performed using a LSM 700 (Zeiss, Jena, Germany). For superresolution imaging, a LSM 800 with Airyscan (Zeiss, Jena, Germany) was used.

Table 5: Primary antibodies

Antibody	Origin	Specificity	Dilution	Reference
Anti-hemagglutinin F7	Mouse monoclonal	Epitope of hemagglutinin (YPYDVPDYA)	IF 1:200	Santa Cruz Biotechnology, Santa Cruz, USA
Anti-hemagglutinin 3F10	Rat monoclonal	Epitope of hemagglutinin (YPYDVPDYA)	WB 1:1000	Roche Diagnostics, Basel, Switzerland
Anti-hemagglutinin Alexa-647	Mouse monoclonal	Epitope of hemagglutinin (YPYDVPDYA)	IF 1:500	Biozol, Eching, Germany
Anti-actin C4	Mouse monoclonal	Chicken gizzard actin, all six known vertebrate isoactins	WB 1:5000	MP Biomedicals, Eschwede, Germany
Anti-G3BP	Rabbit monoclonal	Residues within Human G3BP aa 400 to the C-terminus	IF 1:500 WB 1:5000 IP 0.4 µg/ml	Abcam, Cambridge, UK
Anti-TIA-1 C-20	Goat polyclonal	Residues near the C-terminus of human TIA-1	IF 1:250 WB 1:250	Santa Cruz Biotechnology, Santa Cruz, USA
Anti-TIA-1	Rabbit monoclonal	Residues within aa 350 to the C-terminus	IP 3 µg/ml	Abcam, Cambridge, UK
Anti-TIAR	Rabbit monoclonal	Residues near the C-terminus of human TIAR	IF 1:500	Cell Signaling Technology, Danvers, USA
Anti-Dcp1a	Rabbit polyclonal	Residues within aa 300-400 of Human Dcp1a	IF 1:250	Abcam, Cambridge, UK

Anti-G3BP Alexa-568	Rabbit monoclonal	Residues within Human G3BP aa 400 to the C-terminus	IF 1:500	Abcam, Cambridge, UK
Anti-FMRP	Rabbit polyclonal	Residues 550 to the C-terminus of Human FMRP	IF 1:250	Abcam, Cambridge, UK
Anti-phospho eIF2α	Rabbit polyclonal	eIF2α phosphorylated on Serine 51	WB 1:1000	Cell Signaling Technology, Danvers, USA
Anti- eIF2α	Rabbit polyclonal	Residues in the C-terminus of eIF2α	WB 1:1000	Cell Signaling Technology, Danvers, USA
Anti-phospho EIF2S1	Rabbit monoclonal	EIF2S1 phosphorylated on Serine 51	WB 1:1000	Abcam, Cambridge, UK
Anti-EIF2S1	Mouse monoclonal	Recombinant full length protein	WB 1:1000	Abcam, Cambridge, UK
Anti-LC3A/B (D3U4C)	Rabbit monoclonal	Residues surrounding Leu44 of human LC3B protein	WB 1:1000	Cell Signaling Technology, Danvers, USA
Anti-p62	Rabbit monoclonal	Residues within Human p62 aa 400-500	IF 1:500 WB 1:5000	Abcam, Cambridge, UK
Anti-FLAG M2	Mouse monoclonal	Epitope of FLAG (DYKDDDDK)	IF 1:500	Sigma-Aldrich, Steinheim, Germany

Table 6:Secondary antibodies

Antibody	Origin	Specificity	Dilution	Reference
Horseradish peroxidase (HRP) conj. anti-rat IgG	Goat	Rat IgG	1:10.000	Dianova, Hamburg, Germany
Horseradish peroxidase (HRP) conj. anti-mouse IgG	Goat	Mouse IgG	1:10.000	Dianova, Hamburg, Germany
Horseradish peroxidase (HRP) conj. anti-rabbit IgG	Goat	Rabbit IgG	1:10.000	Dianova, Hamburg, Germany
Horseradish peroxidase (HRP) conj. anti-goat IgG	Rabbit	Goat IgG	1:10.000	Dianova, Hamburg, Germany
Alexa Fluor 488-conj. anti-mouse	Goat	Mouse IgG	1:500	Life Technologies, Darmstadt, Germany
Alexa Fluor 488-conj. anti-mouse	Donkey	Mouse IgG	1:500	Life Technologies, Darmstadt, Germany
Alexa Fluor 568-conj. anti-rabbit	Goat	Rabbit IgG	1:500	Life Technologies, Darmstadt, Germany
Alexa Fluor 568-conj. anti-mouse	Donkey	Mouse IgG	1:500	Life Technologies, Darmstadt, Germany

Alexa Fluor 568-conj. anti-goat	Donkey	Goat IgG	1:500	Life Technologies, Darmstadt, Germany
Alexa Fluor 647-conj. anti-goat	Donkey	Goat IgG	1:500	Life Technologies, Darmstadt, Germany

2.3.15 Immunofluorescence staining for automated microscopy analysis

Microplate, 96-well, µ-clear, F-Bottom, black	Greiner Bio-One, Kremsmünster, Austria
HCS CellMask Blue Stain	Molecular Probes, Eugene, USA
Hoechst 33342	Molecular Probes, Eugene, USA
Permeabilization solution	0.5 % Triton X-100 (Carl Roth, Karlsruhe, Germany) in PBS
Blocking solution	2 % goat serum (Dianova, Hamburg, Germany) in PBS

For automated microscopy analysis cells were seeded on 96-well plates and grown for at least 24 h. After the indicated treatment, cells were fixed by adding 8 % paraformaldehyde directly into the medium (final concentration: 4 %) and incubated for 15 min at RT. Cells were washed with PBS three times and permeabilization solution was added for 10 min at RT. Following three washing steps with PBS, cells were blocked with 2 % goat serum for 1 h at RT. Primary antibodies were added at the indicated dilutions and incubated for 2 h at RT (Table 5). In case of unlabeled primary antibodies, cells were washed three times for 5 min with PBS and incubated with the respective fluorophore-coupled secondary antibodies for 1 h at RT (Table 6). Nuclei and cytoplasm were stained with Hoechst 33342 (1 µg/ml) and CellMask (1:2500) for 10 min at RT. Cells were washed once with PBS and either directly analyzed or stored at 4°C until imaging. For analysis the automatic confocal microscope Cell Voyager 6000 (Yokogawa, Tokyo, Japan) was used.

2.3.16 RNA Staining

SYTO RNASelect Green fluorescent cell stain	Thermo Fisher Scientific, Waltham, USA

For staining of RNA, cells were plated on coverslips in a 24-well plate and grown for at least 24 h. Cells were either subjected to stress granule induction (2.3.9) or left untreated. SYTO RNASelect was added to the culture medium at a concentration of 1 µM and cells were incubated for 20 min at 37°C. Subsequently, cells were rinsed two times with PBS and fixed with ice-cold methanol for 10 min at -20°C. Immunofluorescence staining was performed as described (2.3.14).

2.3.17 Detection of autophagy

Cells were plated in 12-well plates and grown for 6 h. To detect induction of autophagy, the drug chloroquine was used. Chloroquine inhibits the fusion of autophagosomes with lysosomes, leading to the accumulation of autophagy markers, such as LC3-II and p62. Chloroquine and H_2O, as the respective control, were added to the cells at a final concentration of 10 µM. After 16 h cells were harvested and lysed as described (2.3.2 and 2.4.1). Samples were analyzed for autophagy markers via western blot (2.4.3 und 2.4.7).

2.4 Protein biochemical methods

2.4.1 Preparation of protein lysates from mammalian cells

Lysis buffer	150 mM NaCl 50 mM Tris/HCl, pH 7.5 1 % NP-40 in H_2O_{bidest} Protease inhibitor (complete, EDTA free, Roche Diagnostics, Basel, Switzerland)

Cells were harvested as described (2.3.2) and centrifuged at 300 x g for 5 min at 4°C (Eppendorf Centrifuge 5417R, Hamburg, Germany). Cell pellets were resuspended in PBS and centrifuged as before. Pellets were resuspended in an appropriate amount of lysis buffer and incubated on ice for 30 min. Cell debris

was spun down at 514 x g for 4 min at 4°C (Eppendorf Centrifuge 5417R, Hamburg, Germany) and supernatant was transferred to a fresh tube. Samples were either used directly or stored at -20°C.

2.4.2 Bradford protein assay

Quick Start Bradford Assay	BioRAD, Hercules, USA
Quick Start Bovine Serum Albumin Standard Set	BioRAD, Hercules, USA

The Bradford protein assay was used to determine the protein concentration of cell lysates. Lysates were diluted 1:10 in H_2O_{bidest} and 5 µl were transferred in duplicates to a clear 96-well plate. A BSA standard dilution series (62.5 - 2000 µg/ml) and a H_2O blank control were added to the plate. 250 µl Bradford reagent were added to each well and incubated for 5 min at RT. The absorbance was measured at 595 nm with a plate reader (FLUOstar Omega, BMG Labtech, Offenburg, Germany). MARS data analysis software was used to calculate protein concentrations.

2.4.3 Discontinuous sodium dodecyl sulfate - polyacrylamide gel electrophoresis (SDS-PAGE)

3x Sample buffer	90 mM Tris/HCl, pH 6.8 7 % SDS 30 % Glycerol 20 % β-Mercaptoethanol 0.01 % Bromphenol blue in H_2O_{bidest}
10x Tris/Glycine/SDS Electrophoresis buffer (BioRAD, Hercules, USA)	250 mM Tris 1.92 M Glycine 1 % SDS pH 6.8
Any kD Mini-PROTEAN TGX Precast Gels	BioRAD, Hercules, USA
Any kD CRITERION TGX Precast Gels	BioRAD, Hercules, USA

4-20 % Mini-PROTEAN TGX Precast Gels	BioRAD, Hercules, USA
PageRuler Plus Prestained Protein Ladder	Thermo Fisher Scientific, Waltham, USA
InstantBlue Protein Stain	C.B.S Scientific, San Diego, USA

SDS-PAGE is a method to separate proteins according to their size. The any kD precast gels from BioRAD were used for all experiments, except for detection of autophagy, where the 4-20% precast gels (BioRAD) were used. Protein samples were mixed with 3x sample buffer and heated for 5 min at 95°C. Samples and 4 µl of protein ladder were loaded onto the gel and run at 20 mA (Mini PROTEAN gels) or at 30 mA (CRITERION gels) for 1.5 h. Gels were further used for western blotting or stained with InstantBlue for 30 min to directly detect proteins.

2.4.4 Immunoprecipitation

Lysis Buffer	50 mM Tris/HCl, pH 7.5 150 mM NaCl 1 % NP-40 Protease inhibitor (complete, EDTA free, Roche Diagnostics, Basel, Switzerland) in H_2O_{bidest}

Cells cultured in 10 cm dishes were harvested and lysed as described (2.3.2 and 2.4.1). Protein concentration was determined via Bradford assay (2.4.2) and samples were adjusted to comparable protein concentrations. As control, protein extract samples for western blotting were prepared as described (2.4.3). Specific antibodies (Table 5) were added at the indicated concentrations and samples were incubated overnight at 4°C, on a rotating wheel. On the following day, 10 µl magnetic beads (Dynabeads, Thermo Fisher Scientific, Waltham, USA) were added and samples were rotated for 1 h at 4°C. Samples were placed in a magnetic rack (Thermo Fisher Scientific, Waltham, USA) and captured protein complexes were washed five times with lysis buffer. Beads were resuspended in 3x sample buffer and boiled for 5 min at 95°C. Using the magnetic rack, bead-free

samples were transferred to fresh tubes. Samples were either stored at -20°C or used directly for SDS-PAGE (2.4.3) and western blot analysis (2.4.7).

2.4.5 Sedimentation assay

Lysis Buffer	10 mM Tris/HCl, pH 7.5 100 mM NaCl 10 mM EDTA 0.5 % Triton X-100 0.5 % sodium deoxycholate Protease inhibitor (complete, EDTA free, Roche Diagnostics, Basel, Switzerland) in H_2O_{bidest}
TNE Buffer	50 mM Tris/HCl, pH 7.5 150 mM NaCl 5 mM EDTA in H_2O_{bidest}

Cells were plated on 6 cm dishes, grown overnight and harvested as described (2.3.2). Pellets were resuspended in lysis buffer and incubated on ice for 30 min. Cell debris was removed by centrifugation at 1000 x g for 1 min at 4°C (Eppendorf Centrifuge 5417R, Hamburg, Germany). The supernatant was transferred to a fresh tube and centrifuged at 20.000 x g for 20 min at 4°C to separate the soluble from the insoluble fraction. The pellet containing the insoluble fraction was resuspended in TNE buffer. Proteins in the soluble fraction were precipitated with four volumes of methanol overnight at -20°C. Samples were centrifuged at 2100 x g for 25 min at 4°C and pellets were resuspended in TNE buffer. Samples were prepared for SDS-PAGE and western blotting as described (2.4.3 and 2.4.7). To detect NM in the insoluble fraction, 10x more of the insoluble fraction was loaded compared to the soluble fraction.

2.4.6 Semi-denaturing detergent – agarose gel electrophoresis (SDD-AGE)

Lysis buffer	150 mM NaCl 50 mM Tris/HCl, pH 7.5 1 % NP-40 in H_2O_{bidest} Protease inhibitor (complete, EDTA free, Roche Diagnostics, Basel, Switzerland)
4x Sample Buffer	2x TAE buffer (80 mM Tris/HCl, pH7.6; 40 mM Acetic acid; 2 mM EDTA; in H_2O_{bidest}) 20 % Glycerol 8 % SDS Bromphenol blue
Running buffer	1x TAE buffer 0.1 % SDS
TBS	25 mM Tris/HCl, pH 7.6 137 mM NaCl in H_2O_{bidest}
Thick blot filter paper	BioRAD, Hercules, USA
0.2 µm Nitrocellulose membrane	GE Healthcare, Little Chalfont, UK

SDD-AGE is a technique used for the detection of amyloidogenic proteins (Kryndushkin et al., 2003). Cells were harvested as described (2.3.2) and pellets were resuspended in an appropriate amount of lysis buffer. After 30 min incubation on ice, samples were centrifuged at 514 x g for 4 min at 4°C to remove cell debris (Eppendorf Centrifuge 5417R, Hamburg, Germany). The supernatant was incubated with sample buffer for 5 min at RT and subsequently loaded on an 1.5 % agarose gel supplemented with 0.1 % SDS. The gel was run in an electrophoresis chamber (Peqlab, Erlangen, Germany) at 15 V overnight at 4°C. On the next day, ten thick blot filter paper, eight whatman paper, a nitrocellulose membrane and a long whatman paper, to be used as a wick, were prepared. Four whatman paper, the long whatman paper and the membrane were submerged in TBS and the agarose gel was briefly washed with water to remove excess running

buffer. The blotting setup was stacked in a dry electrophoreses chamber in the following order: ten thick blot filter paper, four dry whatman paper, one pre-wetted whatman paper, the membrane, the agarose gel, three pre-wetted whatman paper. The wick was placed on top with both ends submerged in TBS. A weight was placed on top and the capillary transfer proceeded overnight at RT. The following day, the stack was disassembled and the membrane was further processed as specified for western blot analysis (2.4.7).

2.4.7 Immunochemical detection of proteins via Western blot

1x Blotting Buffer	25 mM Tris 192 mM Glycine 0.01 % SDS 20 % Methanol in H_2O_{bidest}
10x TBST	250 mM Tris/HCl, pH 7.6 1.37 M NaCl 0.05 % TWEEN-20 in H_2O_{bidest}
0.2 µm Nitrocellulose membrane	GE Healthcare, Little Chalfont, UK
0.22 µm PVDF membrane	GE Healthcare, Little Chalfont, UK
Pierce ECL solution	Thermo Fisher Scientific, Waltham, USA
Amersham ECL Prime Western Blotting Detection Reagent	GE Healthcare, Little Chalfont, UK
10x ReBlot Plus Strong Antibody Stripping Solution	Merck Millipore, Billerica, USA

Western blotting was performed to transfer proteins, separated by SDS-PAGE (2.4.3), onto a membrane for the detection of proteins via antibodies. In this study, western blotting was conducted using the wet blot method. Nitrocellulose membrane was used for all experiments except for the detection of phosphorylated eIF2α, where a PVDF membrane was used. Membrane and whatman paper in size of the gel were pre-equilibrated in blotting buffer. Gel, membrane, whatman paper and pre-wetted sponge pads were packed in perforated plastic plates and placed into the wet blot tank (PerfectBlue, Tank-

Electroblotter Web, Peqlab, Erlangen, Germany). The transfer was performed at 300 mA (small tank) or 800 mA for 65 min (large tank) at RT. Afterwards the membrane was blocked with 5 % milk powder in TBST for 1 h at RT and incubated with the primary antibody diluted in blocking buffer overnight at 4°C (Table 5). On the following day, the membrane was washed five times for 6 min with 1x TBST and incubated with the appropriate HRP-coupled secondary antibody diluted in blocking buffer for 1 h at RT (Table 6). The membrane was washed five times for 6 min with 1x TBST and incubated with ECL solution according to the manufacturer's instructions. The light signal of the luminescence reaction was detected using the Stella imaging system (Raytest, Straubenhardt, Germany). For detection of additional proteins, the membrane was incubated with a stripping buffer (ReBlot Plus Strong Antibody Stripping Solution) for 20 min at RT to remove bound antibodies. The membrane was washed once with 1x TBST, blocked for 1 h with 5 % milk powder in TBST and stained with antibodies as described.

2.4.8 Production and purification of recombinant NM protein

Protein Purification Buffer A	10 mM Tris/HCl, pH 7.2 8 M Urea in H_2O_{bidest}
Protein Purification Buffer B	10 mM Tris/HCl, pH 7.2 8 M Urea 1 M NaCl in H_2O_{bidest}
Protein Purification Buffer C	5 mM KPhos, pH 7.2 8 M Urea in H_2O_{bidest}
Protein Purification Buffer D	500 mM KPhos, pH 7.2 8 M Urea in H_2O_{bidest}

For the production of recombinant NM, BL21 *Escherichia coli* (*E.coli*) were transformed with the pNOTAG-NM plasmid as described (2.5.2). A single bacteria colony was picked and used to inoculate 5 ml of LB medium supplemented with

100 µg/ml Ampicillin and grown overnight at 37°C and 180 rpm (LT-X Lab-Therm, Kuhner Shaker, Aachen, Germany). On the following day, the bacteria were transferred to 3 l of LB medium supplemented with 100 µg/ml Ampicillin and shaken at 180 rpm and 37°C until an OD_{600} of 0.6 was reached. Gene expression was induced by addition of 1 mM IPTG and bacteria were shaken at 180 rpm and 30°C for 3 - 4 h. Bacteria were pelleted at 3488 x g for 15 min at RT (Heraeus Multifuge X3R, Thermo Fisher Scientific, Waltham, USA) and either used directly or stored at -80°C until further use. The bacteria pellet was resuspended in 150 ml of buffer A and incubated for at least 30 min at 37°C and 180 rpm. Subsequently the cell suspension was centrifuged at 30.000 x g for 20 min at 25°C to remove insoluble material. The supernatant was applied to a pre-equilibrated Q sepharose Fast Flow column (GE Healthcare, Little Chalfont, UK) and washed with 5 volumes of buffer A. The protein was eluted with a gradient of buffer A and B (Table 6). The eluted material was collected in 5 ml fractions and analyzed via SDS-PAGE and InstantBlue staining as described (2.4.3). The fractions containing the highest amount of NM protein were pooled and loaded on a pre-equilibrated Macro Prep Ceramic Hydroxyapatite Type I (40 µm) (CHA) column (BioRAD, Hercules, USA). The column was washed with two volumes of buffer C and the protein was eluted with a gradient of buffer C and D (Table 7). The eluate was collected in fractions, which were analyzed by SDS-PAGE and InstantBlue staining. Fractions containing the NM protein were pooled and dialyzed twice against 5 l of PBS at 4°C. Protein concentration was determined and aliquots of 100 µM (monomer concentration) were stored at -80°C.

Table 6: Gradient for Q sepharose column

Time	% of buffer B
0 min	0
30 min	10
90 min	70
105 min	99
120 min	100

Table 7: Gradient for CHA column

Time	% of buffer D
0 min	0
30 min	10
90 min	50
105 min	99
120 min	100

2.5 Molecular biological methods

2.5.1 Generation of chemically competent *E.coli*

LB Medium	2 % LB Broth-agar in H_2O_{bidest}

A liquid culture of 2 ml LB medium was inoculated with BL21 *E.coli* and incubated in a shaker at 220 rpm overnight at 37°C (LT-X Lab-Therm, Kuhner Shaker, Aachen, Germany). On the following day, 100 ml of LB medium were inoculated with 500 µl of the overnight culture. Bacteria were shaken at 220 rpm and 37°C until an OD_{600} of 0.3 was reached. All following steps were performed on ice. The bacteria were cooled for 10 min and subsequently centrifuged at 1500 x g for 10 min at 4°C (Heraeus Multifuge X3R, Thermo Fisher Scientific, Waltham, USA). The supernatant was discarded and the bacteria were resuspended in 10 ml 0.1 M $MgCl_2$. The bacteria were centrifuged at 1500 x g for 10 min at 4°C and the pellet was resuspended in 20 ml 0.1 M $CaCl_2$. After an incubation of 20 min, bacteria were centrifuged as before and the pellet was resuspended in 1 ml 0.1 M $CaCl_2$ supplemented with 15 % glycerol. Aliquots of 50 µl were snap frozen and stored at -80°C.

2.5.2 Transformation of chemically competent *E.coli*

pNOTAG-NM	Provided by Jens Tyedmers

BL21 *E.coli* were thawed on ice and 10 - 100 ng of DNA was added. After an incubation of 30 min on ice, bacteria were subjected to a heat shock at 42°C for 42 sec and subsequently cooled on ice. 500 µl of LB medium was added and the

bacteria were incubated at 300 rpm for 30 - 90 min at 37°C (Thermomixer Compact, Eppendorf, Hamburg, Germany). Bacteria were spun down at 514 x g for 3 min at RT (Eppendorf Centrifuge 5417R, Hamburg, Germany) and most of the supernatant was discarded. Bacteria were resuspended in the residual medium and plated onto LB agar plates supplemented with 100 µg/ml Ampicillin. Plates were incubated overnight at 37°C and afterwards stored at 4°C.

2.6 Image data analysis and statistics

2.6.1 Image editing

Confocal images captured with the LSM 700, the widefield fluorescent microscope or the LSM 710 (Zeiss, Jena, Germany) were processed using Zen 2010 (black edition) or Zen 2012 (blue edition) software (Zeiss, Jena, Germany). Images captured with the LSM 800 Ariyscan were subjected to deconvolution to obtain superresolution images using the Zen 2012 (blue edition) software.

2.6.2 Image data analysis using Cell Profiler

Images obtained using the Cell Voyager 6000 (Yokogawa, Tokyo, Japan) were analyzed with Cell Profiler 2.1 image analysis software (Carpenter et al., 2006). Image analysis routines were developed for identification of stress granules and NM aggregates. In brief, nuclei and cytoplasm were identified based on morphology and intensity of Hoechst and CellMask staining. Stress granules were detected by intensity of the respective staining and size. Cells were classified as stress granule positive when three or more stress granules were identified in the cytoplasm. To identify NM aggregates, the Ilastik segmentation tool was used for pixel classification. The number of NM expressing cells as well as aggregate bearing cells was determined by using the pixel classifier and intensity levels of NM.

2.6.3 Image data analysis of time-lapse experiments

Images obtained from time-lapse experiments were subjected to an in-house deep learning approach to detect nuclei and cytoplasm. This approach is based on the software U-Net architecture for convolutional neural networks and Theano (performed by Manuel Schölling (IDAF, DZNE)). Using Cell Profiler an image analysis routine was developed to measure the fluorescence intensities for each

cell over time. The pixel classifier generated by the deep learning approach was used to detect nuclei and cytoplasm. The standard deviation of the fluorescence signal of the SG marker protein (G3BP1-mCherry) was taken as a measure of SG assembly or disassembly. The fluorescence signal of the SG marker protein is evenly distributed in the cytoplasm with a low standard deviation when no SGs are present. Upon SG formation the standard deviation becomes larger, or smaller upon SG disassembly and therefore the change in standard deviation was taken as a measure.

2.6.4 Statistical analysis

For statistically analyzed data, at least three biological replicates were analyzed. Statistical analysis was performed using Graph Pad Prism 6 (Graph Pad Software, La Jolla, USA) and data was analyzed using the unpaired two-tailed Student´s t-test for single comparisons or one-way ANOVA with Dunnett's multiple comparisons test. Statistical analysis of time-lapse experiments and high-throughput image analysis was performed by Manuel Schölling (IDAF, DZNE). For analysis of time-lapse data, a mixed linear model was used to analyze the slopes of the measured standard deviation of the fluorescence over time. Increase of local fluorescence was analyzed using a generalized linear model with corrections for experiment-dependent effects. All other analysis of high-throughput data was performed using a logistic regression model to analyze whether the ratio of positive to negative cells is significantly different with corrections for experiment-dependent effects. A p-value less than 0.05 was considered as statistically significant (*$p \leq 0.05$, **$p \leq 0.01$, ***$p \leq 0.001$, ****$p \leq 0.0001$).

3. Results

Several proteins that form insoluble inclusions in neurodegenerative diseases have been shown to sequester proteins that are part of ribonucleoprotein (RNP) granules, comprising mainly RBPs (Gunawardana et al., 2015; Lee et al., 2016). RBPs itself have been implicated in a range of neurodegenerative diseases (Li et al., 2013; Ramaswami et al., 2013). A hallmark of many RBPs is the presence of low complexity domains, which are often similar to yeast prion domains and are also referred to as prion-like domains (PrLDs). Under physiological conditions, PrLDs drive transient phase separation such as assembly of stress granules. The fact that PrLD-containing proteins are involved in RNP formation and aberrant protein inclusions argues that the two processes might be somehow interrelated. To identify putative PrLDs, algorithms were designed based on the characteristics of prion domains found in yeast proteins, such as Sup35 of *Saccharomyces cerevisiae* (Alberti et al., 2009). Sup35 has been extensively studied and its prion domain (PrD) has been shown to propagate as a prion in mammalian cells (Hofmann et al., 2013; Krammer et al., 2009). Using the PrD of Sup35 (NM) as a model of cytosolic prion aggregation, a previous study from our lab examined the interaction partners of soluble and aggregated NM. When HA-tagged NM is expressed in N2a neuroblastoma cells it remains soluble (Fig. 8A), but aggregation can be induced by exposure to recombinant NM fibrils. Single cell clones that propagate morphologically distinct NM prions have been previously isolated and characterized (Krammer et al., 2009) (Fig. 8A). To identify interaction partners of morphologically diverse NM prions, LC-MS/MS analysis of soluble and aggregated NM-HA had previously been performed by a former coworker (Verena Arndt), using N2a wildtype cells, N2a cells expressing soluble NM-HA (N2a NM-HA^{sol}) and N2a cell clones carrying NM-HA prion aggregates (N2a NM-HA^{agg}) (Fig. 8B, C). As all three NM-HA^{agg} clones exhibited comparable interactor lists, interactomes were pooled for analysis. Gene Ontology analysis revealed that the NM-HA^{sol} and NM-HA^{agg} interactomes were highly enriched for proteins involved in RNA metabolism (Fig. 8D), similar to the proteome of SGs (Jain et al., 2016). Examining the physicochemical features of the NM-HA interactomes, using the cleverMachine algorithm, revealed that compared to a random sample of the

mouse proteome, the interactomes of soluble and aggregated NM-HA were enriched in intrinsic disorder and nucleic acid binding ability (Fig. 8E, F) (Klus et al., 2014). Both features were also enriched in the proteome of SGs (Fig. 8G).

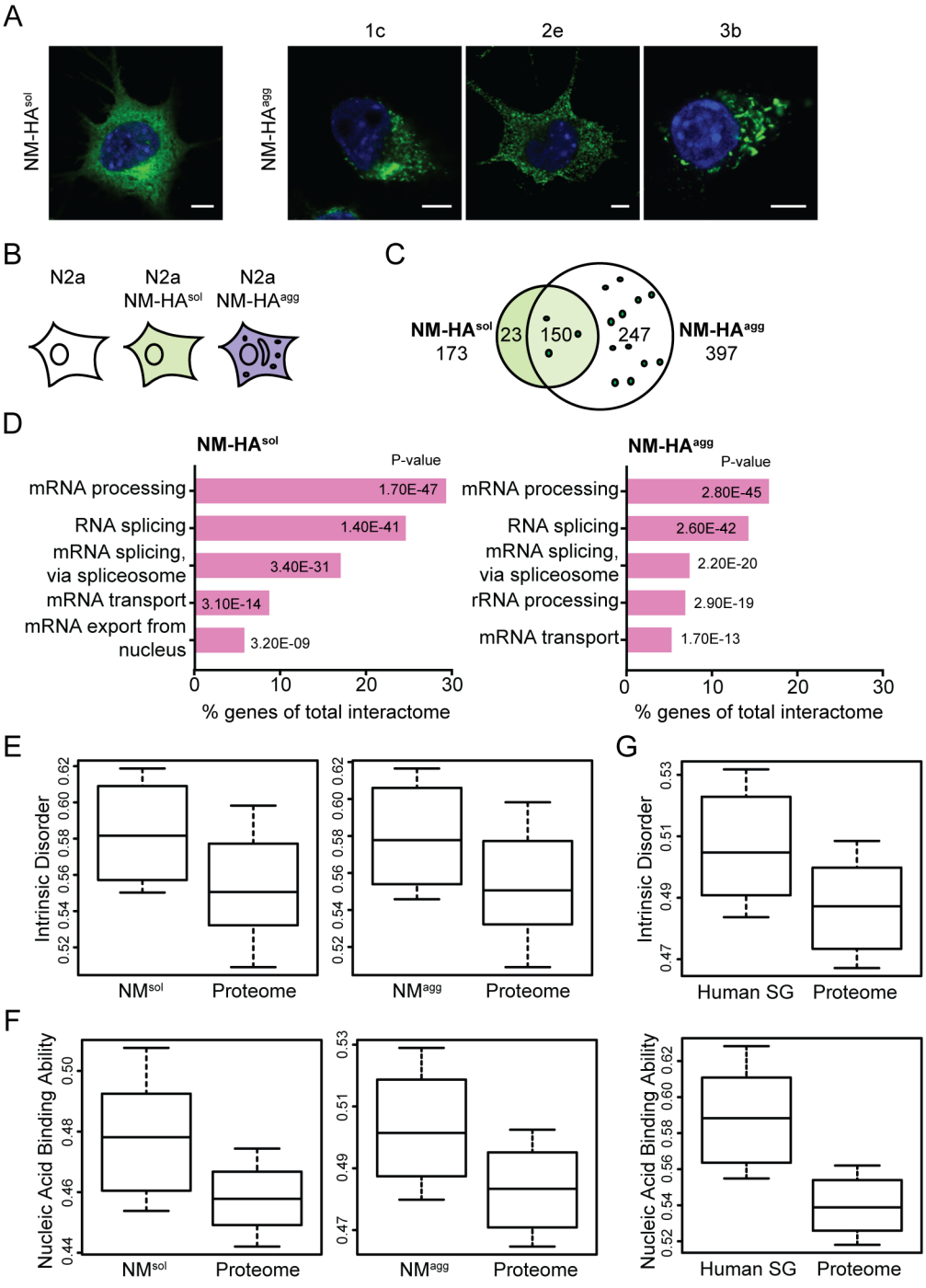

Figure 8. The NM interactome is enriched for proteins with intrinsic disorder. (A) Immunofluorescence staining of N2a cells stably expressing soluble yeast NM-HA and N2a subclones 1c, 2e and 3b persistently producing NM-HA prion aggregates. NM was

detected using mAb anti-HA (green) and nuclei were stained with Hoechst (blue). Scale bar: 5 µm (Images: Verena Arndt) (B) Biological triplicates of N2a wildtype cells, N2a cells expressing soluble NM-HA (N2a NM-HA^{sol}) and N2a cells stably carrying NM-HA prion aggregates (N2a subclones 1c, 2e and 3b combined as N2a NM-HA^{agg}) were subjected to LC-MS/MS analysis (performed by Verena Arndt). (C) Number of proteins found as interactors of soluble and aggregated NM-HA from cell clones 1c, 2e and 3b combined. (D) Gene Ontology enrichment analysis of NM-HA^{sol} and NM-HA^{agg} interactomes. Shown are the top five Gene Ontology biological process annotations. Benjamini p-value is shown. (E) Box-plots show intrinsic protein disorder of interactors calculated using DisProt (Cox et al., 2014). Intrinsic disorder of interactors was compared to that of a random subset of the mouse proteome. P-values are 1.7×10^{-8} and 3.48×10^{-9}, respectively. Statistics were performed using the Kolmogorov-Smirnov test. (F) Box-plots display the nucleic acid binding ability of interactors calculated using the scale of nonClassical RBD compared to that of a random subset of the mouse proteome (Castello et al., 2012). P-values are 3.30×10^{-13} and 3.46×10^{-11}, respectively (Kolmogorov-Smirnov test). (G) Box-plots show intrinsic protein disorder (upper panel) calculated using DisProt (Cox et al., 2014) and nucleic acid binding ability (lower panel) calculated using the Castello scale (Castello et al., 2012) for SG components compared to a random subset of the human proteome (Intrinsic disorder and nucleic acid binding ability analysis were performed by Benedetta Bolognesi).

The interactomes of soluble and aggregated NM-HA appear very similar, although twice as many proteins were found to bind to aggregated NM as compared to soluble NM. Mass spectrometry analysis revealed that aggregated NM also interacted with proteins of the degradation machinery. Interaction of key hits with NM prions was validated by immunofluorescence staining (Fig. 9). Mammalian cells degrade misfolded proteins via autophagy, which is a non-selective degradation system for cytoplasmic constituents. Valosin-containing protein (VCP) and p62 play roles in the clearance of ubiquitinated proteins via autophagy and were both identified as putative NM prion interactors. Immunofluorescence staining of NM-HA^{agg} cells confirmed a colocalization of VCP and p62 with NM prions (Fig. 9). The interactome of aggregated NM further identified Ubiquilin-2, which is a regulator of protein degradation via the proteasome and autophagy, and Keap1, which is involved in the proteasome degradation pathway. Colocalization of Ubiquilin-2 and Keap1 with NM prions demonstrated that both proteins are associated with NM prion aggregates (Fig. 9). These results suggest that cells respond to NM prions by subjecting them to degradation by autophagy. Due to the striking similarities of the NM-HA interactomes and the SG proteome we further investigated the relationship between SGs and NM prion aggregates.

In this study we used the PrD of Sup35 to assess similarities and differences of SGs and cytosolic prion aggregates and analyzed whether these two assemblies influence each other.

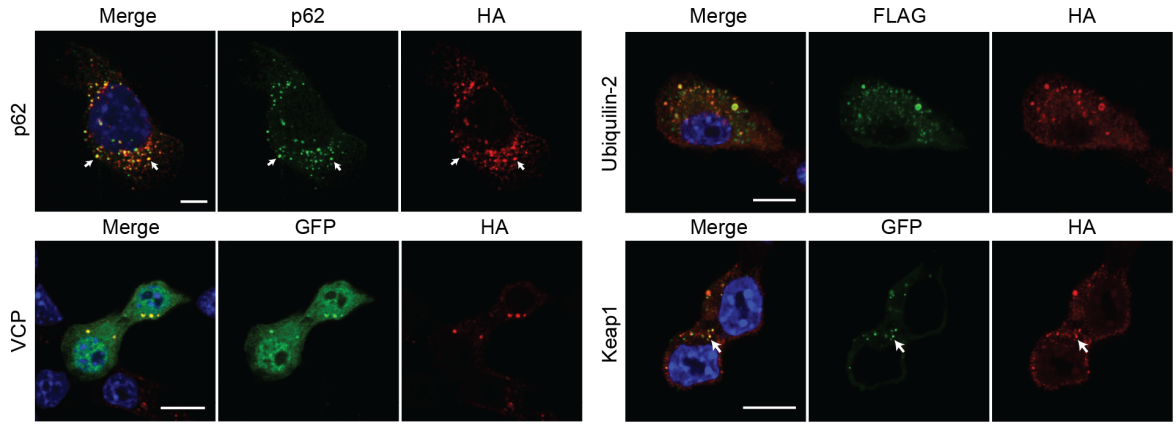

Figure 9. NM prions recruit proteins of the degradation machinery. Immunofluorescence staining of N2a NM-HA^{agg} cells was performed using mAb anti-HA (red) and mAb anti-p62 or mAb anti-FLAG (green). Nuclei were visualized using Hoechst (blue). Scale bar: 5 µm.

3.1 NM acts as a cytosolic prion in HeLa cells

In previous studies, N2a cells were used to express and investigate NM. As N2a cells do not mount a good SG response, a different cell line was chosen for the examination of SGs together with NM. HeLa cells are often used as a model to study SGs in different experimental setups, hence this cell line was chosen for further investigations (Kedersha et al., 2005; Kroschwald et al., 2015). To verify that NM could act as a prion in HeLa cells, stable HeLa cell lines expressing HA-tagged and GFP-tagged NM were generated by lentiviral transduction. When expressed in HeLa cells, NM remained in a soluble state, but readily aggregated upon exposure to recombinant NM fibrils (Fig. 10B). Phenotypically distinct aggregate types were detectable after exposure to NM fibrils, which might represent NM-HA variants as seen previously in N2a cells (Krammer et al., 2009). A sedimentation assay confirmed that NM was enriched in the insoluble fraction when exposed to NM fibrils, but was otherwise detected in the soluble fraction (Fig. 10C).

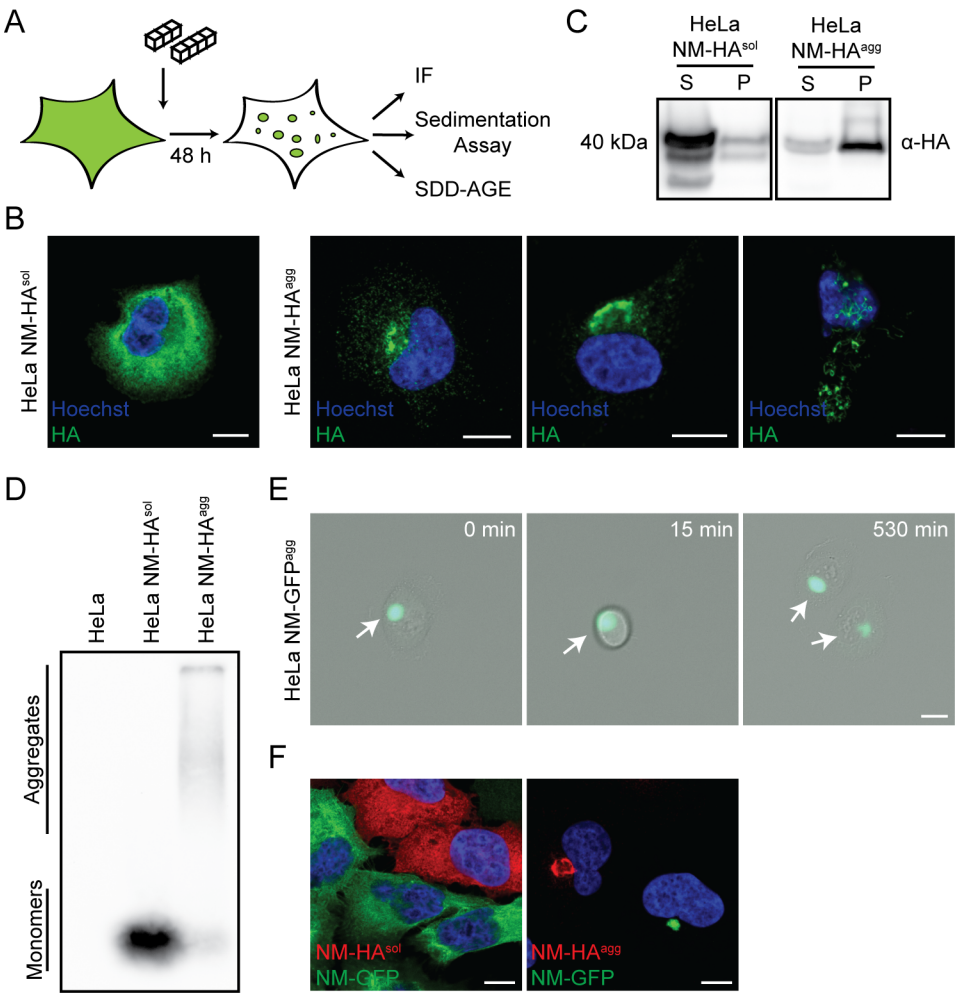

Figure 10. NM replicates as a prion in HeLa cells. (A) Schematic diagram of the experiments. (B) Confocal microscopy analysis of cellular distribution of soluble (HeLa NM-HA^{sol}) or aggregated (HeLa NM-HA^{agg}) NM-HA in HeLa cells. HeLa cells expressing soluble HA-tagged NM were exposed to 5 µM recombinant fibrillar NM (monomer concentration) to induce aggregation. NM-HA was detected using mAb anti-HA (green). Nuclei were stained with Hoechst (blue). Scale bar: 10 µm. (C) A sedimentation assay was performed with HeLa cells harboring either soluble or aggregated NM-HA. NM-HA was detected using mAb anti-HA. 10x more of the pellet fraction was loaded. S: Supernatant, P: Pellet. (D) Cell lysates of HeLa, HeLa NM-HA^{sol} and HeLa NM-HA^{agg} cells were separated by semi-denaturing detergent - agarose gel electrophoresis (SDD-AGE). NM-HA was detected using mAb anti-HA. (E) HeLa cells expressing soluble NM-GFP were exposed to 5 µm recombinant fibrillar NM (monomer concentration) for 48 h and subsequently subjected to live cell imaging for 16 h. Arrows mark cells undergoing cell division and transmitting induced aggregates to their progeny. Scale bar: 20 µm. (F) Donor HeLa cells expressing soluble NM-HA or HeLa NM-HA^{agg} cells were cocultured with recipient HeLa cells expressing soluble NM-GFP for 48 h. Cells were stained for NM-HA using mAb anti-HA (red) and nuclei were stained with Hoechst (blue). Scale bar: 10 µm.

The amyloid nature of the NM-HA aggregates was shown by performing a semi-denaturing detergent – agarose gel electrophoresis (SDD-AGE) (Kryndushkin et al., 2003) (Fig. 10D). Wildtype HeLa cells, HeLa cells expressing soluble NM-HA (HeLa NM-HA^{sol}) and HeLa cells persistently propagating NM-HA aggregates (HeLa NM-HA^{agg}) were analyzed. For HeLa NM-HA^{sol} cells, only one band could be detected, representing the monomeric protein. HeLa NM-HA^{agg} cells on the other hand showed a large SDS resistant smear, representing the aggregated, amyloidogenic NM-HA. One important feature of prions is the propagation of the prion phenotype to daughter cells. To assess the mitotic stability of NM aggregates, HeLa NM-GFP cells were incubated with recombinant NM fibrils to induce aggregation and were subsequently subjected to live cell imaging (Fig. 10E). Induced NM-GFP aggregates were evenly distributed to both daughter cells during cell division, showing that NM aggregates can be propagated to their progeny in HeLa cells. Furthermore, prion replication depends on the formation of infectious particles, which are able to infect neighboring cells and induce a self-perpetuating prion state. By coculturing HeLa NM-HA^{agg} cells together with HeLa NM-GFP^{sol} cells the infectivity to bystander cells was tested (Fig. 10F). NM-HA aggregates successfully induced the aggregation of NM-GFP in neighboring cells, whilst soluble NM-HA was unable to. Taken together, these results show that NM acts as a prion when expressed in HeLa cells.

3.2 Stress granules and NM prions share similar marker proteins

The interactome study of NM prions identified several RBPs that are also part of the proteome of SGs. Among the identified proteins, G3BP and TIA-1 are known marker proteins for SGs. Both proteins are RBPs that play crucial roles in the assembly of SGs (Gilks et al., 2004; Tourriere et al., 2003). To validate the interactome findings, we tested for the colocalization of NM prions and G3BP and TIA-1 (Fig. 11). Immunofluorescence staining of HeLa NM-HA^{agg} cells showed the sequestration of TIA-1 and G3BP by NM prions (Fig. 11A). For NM-HA almost no signal was detectable outside of the prion aggregate, whereas G3BP and TIA-1 showed only a weak sequestration by the prion with most of the protein still being located in the cytoplasm and/or nucleus. To further validate the interaction, immunoprecipitation of endogenous G3BP and TIA-1 was performed in HeLa NM-

HA^{sol} and HeLa NM-HA^{agg} cells. In the pull-down experiment, NM-HA was only detected in prion bearing cells (Fig. 11B). Hence, the interaction of the SG marker proteins seems to be prion specific. These results led us to the suggestion that NM-HA might also be recruited into SGs.

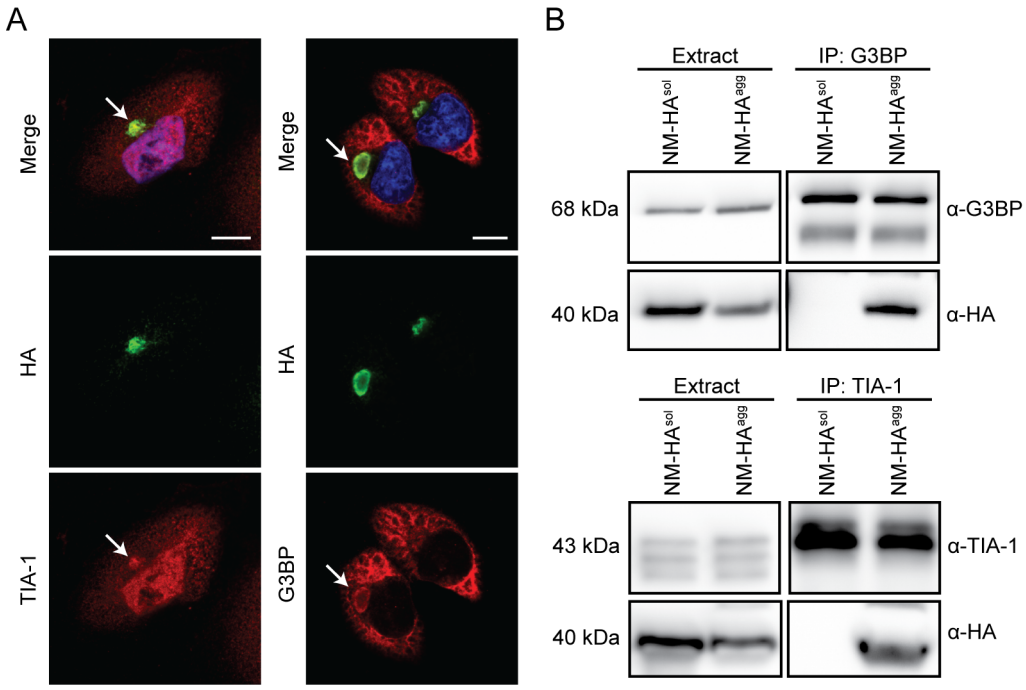

Figure 11. Stress granule marker colocalize with NM prions. (A) HeLa cells expressing soluble NM-HA were exposed to 5 µm recombinant fibrillar NM (monomer concentration) for 48 h and cells were subsequently fixed. Immunofluorescence staining was performed using mAb anti-HA (green) and pAb anti-TIA-1 or mAb anti-G3BP (red). Nuclei were stained with Hoechst (blue). Scale bar: 10 µm. (B) G3BP and TIA-1 were immunoprecipitated (IP) from cell lysates of HeLa NM-HA^{sol} or HeLa NM-HA^{agg} cells. Immune complexes were separated by SDS-PAGE and examined by western blot for the presence of G3BP or TIA-1 and NM-HA.

To test our hypotheses, we treated HeLa cells expressing soluble NM-HA with the SG inducing drug sodium arsenite, which triggers oxidative stress in cells. Treatment with sodium arsenite resulted in a robust induction of SGs, well-defined cytoplasmic foci (Fig. 12). Immunofluorescence staining using G3BP and TIA-1 as SG markers revealed that soluble NM-HA was indeed sequestered into SGs. Upon arsenite treatment, G3BP and TIA-1 accumulated in SGs with only a faint staining in the residual cytoplasm and nucleus. In contrast to the strong

recruitment of G3BP and TIA-1 to SGs, NM-HA was recruited to SGs, but still exhibited a strong signal in the remaining cytosol.

SGs can be induced by a variety of treatments leading to SGs with distinct compositions (Aulas et al., 2017). To test whether NM-HA is also part of SGs when induced by different stresses, we treated HeLa NM-HA^{sol} cells with a range of known SG inducers.

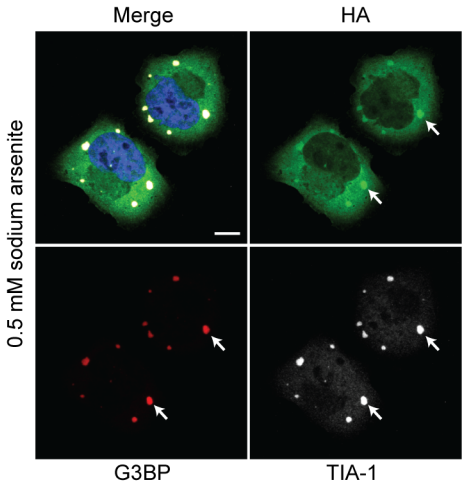

Figure 12. Soluble NM localizes to stress granules. HeLa cells expressing soluble NM-HA were exposed to 0.5 mM sodium arsenite for 1 h and cells were subsequently fixed. Immunofluorescence staining was performed using mAb anti-HA (green), mAb anti-G3BP (red) and pAb anti-TIA-1 (white). Nuclei were stained with Hoechst (blue). Scale bar: 10 µm.

We tested five different SG inducing stimuli and performed an immunofluorescence staining to assess colocalization of NM-HA and the SG marker TIAR (Fig. 13). MG132 inhibits the proteasome, leading to the appearance of SGs for a few hours during treatment (Mazroui et al., 2007), whilst the treatment with dsRNA mimics a viral infection, thereby inducing SGs as part of the immune response (Scadden, 2007; Zhang et al., 2014). Both stresses induce SGs by phosphorylation of eIF2α, as it is also the case for heat shock treatment (Clemens, 2001). In contrast, SG assembly induced by treatment with sodium chloride (NaCl) is independent of eIF2α phosphorylation and SG assembly is regulated by macromolecular crowding (Bevilacqua et al., 2010; Bounedjah et al., 2012). Note that SGs induced by NaCl have a distinct appearance compared to SGs induced by the other stresses, but are considered bona fide SGs (Kedersha

et al., 2016). Nevertheless, all of the different stresses induced SGs that sequestered soluble NM-HA (Fig. 13). NM-HA being part of different subtypes of SGs made it a good model to further study the relationship between SGs and cytosolic prion aggregates.

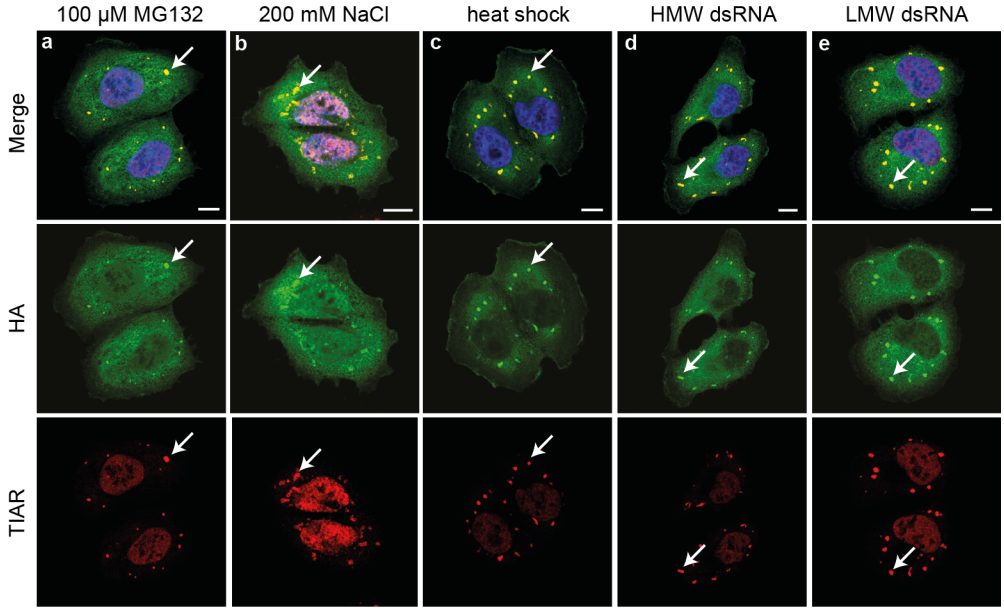

Figure 13. NM containing stress granules can be induced by diverse stimuli. HeLa cells expressing soluble NM-HA were exposed to (a) 100 µM MG132 for 2 h, (b) 200 mM NaCl for 1 h, (c) heat shock at 45°C for 30 min or were transfected with either (d) 300 ng HMW dsRNA or (e) 300 ng LMW dsRNA. Cells were subsequently fixed and immunofluorescence staining was performed using mAb anti-HA (green) and mAb anti-TIAR (red). Nuclei were stained with Hoechst (blue). Arrows mark SGs containing NM. Scale bar: 10 µm.

Next we asked which part of NM is important for the sequestration of NM into SGs. A previous study of our lab defined which regions within NM are important in mammalian cells for the three sequential steps of prion replication: *de novo* induction of prions, fragmentation of NM prions and transmission of infectious particles to daughter cells (Duernberger et al., 2018). Surprisingly, all three steps were facilitated by one region within NM: the last three repeats of the OPR and the CTN. To investigate which subdomain of NM is important for the localization to SGs, we made use of the NM deletion mutants that were generated in the previous study (Fig. 14A) (Duernberger et al., 2018). We transduced HeLa cells with six different NM mutants, carboxyterminally tagged with HA: NM Δ 1-39,

lacking the QNR; NM Δ 39-57, lacking OPR repeat 1 and partially repeat 2; NM Δ 39-74, with a deletion of OPR repeats 1 – 3; NM Δ 75-97, lacking OPR repeats 4 – 6; NM Δ 75-123, with a deletion of OPR repeats 4 – 6 and the CTN, and NM Δ 98-123 lacking the CTN (Fig 14A). HeLa cells expressing full-length NM or mutant NM were treated with 500 µM sodium arsenite for 1 h to induce SGs and an automated immunofluorescence analysis was performed (Fig. 14B-D). In all cell lines SGs could be induced, as shown by staining with the SG marker TIAR (Fig. 14C). However, the level of NM-HA being sequestered into SGs varied upon the different mutants. To analyze for each cell line how much NM-HA was located in SGs, an image analysis was performed (Fig. 14D). As NM-HA is evenly distributed in the cytoplasm with a locally increased signal in SGs, we measured the increase of fluorescence in SGs compared to the cytoplasm. Full-length NM showed the strongest recruitment to SGs, whereas NM mutants lacking the CTN (NM Δ 75-123) or the first three repeats of the OPR (NM Δ 39-74) were the least sequestered into SGs. Interestingly, NM with a deletion of repeat 4 – 6 of the OPR (NM Δ 75-97) showed a better recruitment to SGs than when additionally the CTN was lacking (NM Δ 75-123). This indicated that the size of the deletion seemed to be important for the binding of NM to SGs. Furthermore, NM lacking repeat 1 – 3 of the OPR (NM Δ 39-74) was less sequestered into SGs than NM lacking only repeat 1 and partially repeat 2 (NM Δ 39-57), emphasizing that larger regions are needed for recruitment to SGs. Deletion of the QNR (NM Δ 1-39) had only a slight effect on the recruitment of NM-HA to SGs. This demonstrates that the last part of the N domain, comprising the CTN and the OPR, plays an important role in the recruitment of NM to SGs. However, binding of NM to SGs seems to be facilitated by rather large regions as smaller deletions had a minor effect on recruitment compared to larger deletions. This leads to the suggestion that interaction of NM with SGs requires rather multiple interactions then one defined subdomain.

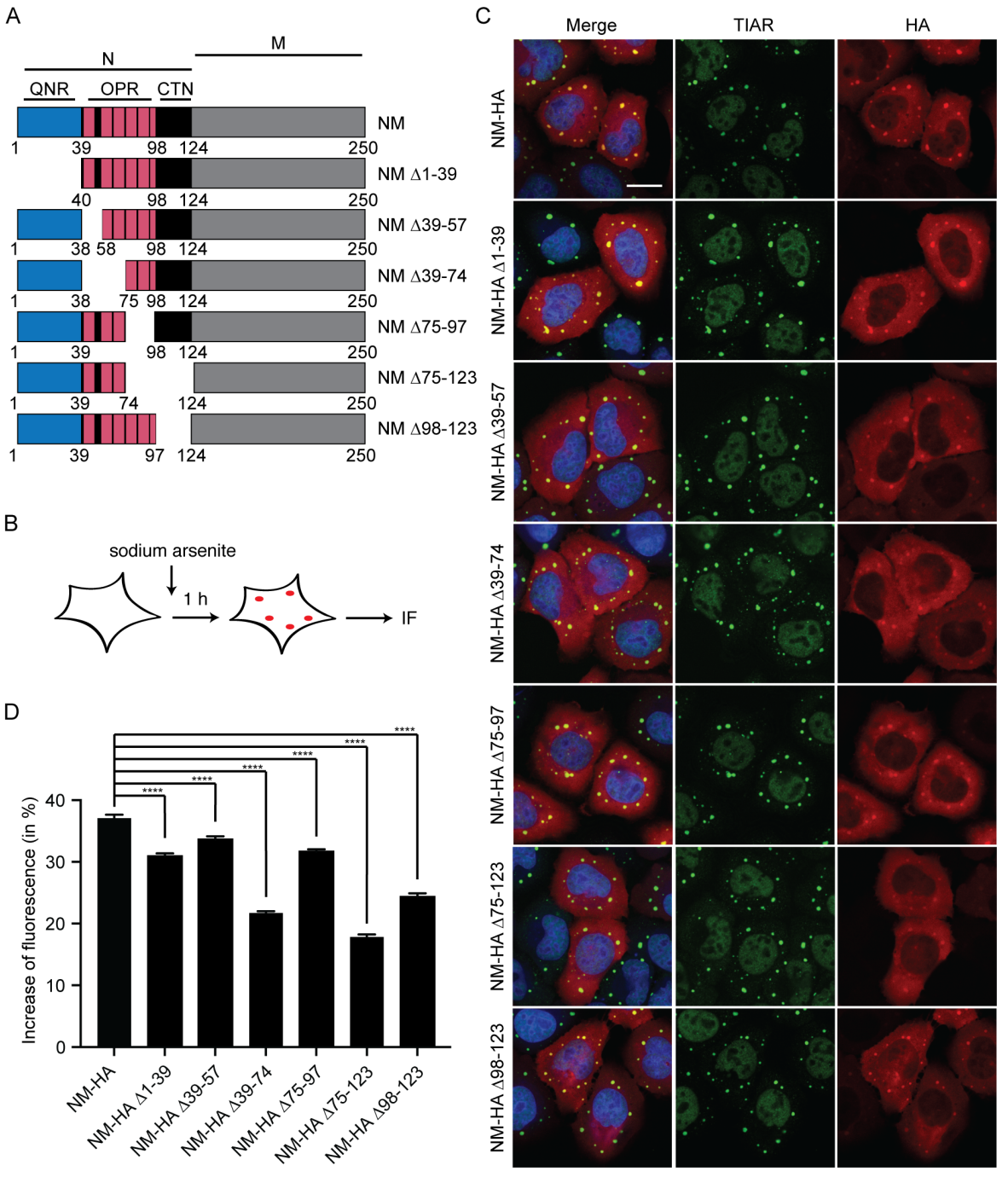

Figure 14. The OPR and the CTN are most important for recruitment to SGs. (A) Scheme of full-length NM and the six deletion mutant constructs used in this study. QNR: aa 1-39, OPR: aa 41-97, CTN: aa 98-123. NM Δ 1-39, with a deletion of the QNR; NM Δ 39-57, with a deletion of repeat 1 and part of repeat 2; NM Δ 39-74, with a deletion of repeat 1 – 3; NM Δ 75-97, with a deletion of repeats 4 – 6; NM Δ 75-123, with a deletion of repeats 4 – 6 and the CTN and NM Δ 98-123 with a deletion of the CTN. Numbers refer to amino acids. (B) Schematic diagram of the experiment. HeLa NM-HA^{sol} cells were treated with 0.5 mM sodium arsenite for 1 h and subsequently fixed. Images for analysis were taken using the automatic confocal microscope Cell Voyager 6000 (C) Immunofluorescence staining was performed using mAb anti-HA (red) and mAb anti-

TIAR (green). Nuclei were stained with Hoechst (blue). Scale bar: 10 µm (D) Analysis of sequestration of NM-HA mutants into SGs. Shown is the increase of fluorescence compared to the fluorescence signal of the cytoplasm. Bars represent mean values ± SEM (n=3). The experiment was performed three times in triplicates. At least 1500 cells were analyzed. Statistical analysis was performed using a generalized linear model (****p ≤ 0.0001).

3.3 NM prions and SGs are distinct assemblies

In the previous experiments we could show that SG marker proteins colocalize with NM prions and that soluble NM is a part of SGs. Hence, there are some similarities in the interactome of these two assemblies. To further analyze the shared interactome of SGs and NM prions, we checked for the recruitment of RNA to NM prions. RNA is one of the most crucial components of SGs, as the main function of SGs is to sequester mRNAs for translational repression (Kedersha et al., 1999).

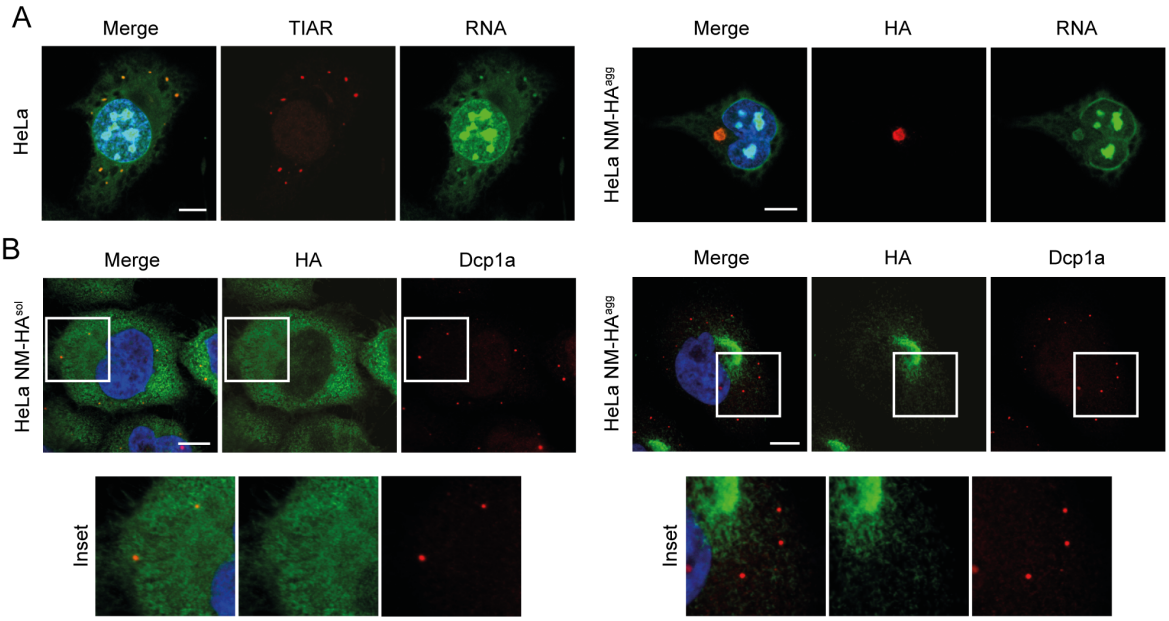

Figure 15. NM prions show colocalization with RNA but not with P body marker Dcp1a. (A) HeLa cells were treated with 0.5 mM sodium arsenite for 1 h to induce SGs and HeLa NM-HA^{agg} cells were left untreated. RNA was stained using SYTO RNASelect (green) and cells were subsequently fixed. Immunofluorescence staining was performed using mAb anti-TIAR or mAb anti-HA (red). Nuclei were stained with Hoechst (blue). Scale bar: 10 µm. (B) Immunofluorescence staining of HeLa NM-HA^{sol} and HeLa NM-HA^{agg} cells was performed using mAb anti-HA (green) and mAb anti-Dcp1a (red). Nuclei were stained with Hoechst (blue). High magnification views of the indicated regions are shown in the lower panel. Scale bar: 10 µm.

We stained for total RNA using a nucleic acid dye that exhibits bright green fluorescence upon binding to RNA (SYTO RNASelect). Immunofluorescence staining of HeLa cells treated with sodium arsenite to induce SGs showed a strong signal for RNA in the nucleus and a weak signal in the cytoplasm (Fig. 15A). Co-staining with the SG marker TIAR showed a colocalization of RNA and SGs. In HeLa NM-HA^{agg} cells, RNA was detectable in NM prions (Fig. 15A). Hence, both assemblies share RNA as a component. Translationally repressed mRNAs do not only accumulate in SGs, but also in other cytoplasmic foci, as for example in P bodies. P bodies contain the mRNA decay machinery and are present in unstressed cells, but can be further induced in response to stress (Kedersha and Anderson, 2007). SGs and P bodies are closely related RNP granules that share some components. Furthermore, SGs and P bodies physically interact during stress and mRNAs can cycle between them (Kedersha et al., 2005). Therefore, we wondered whether NM prions and P bodies share components. Immunofluorescence staining of the P body marker Dcp1a in unstressed HeLa NM-HA^{sol} cells showed no colocalization of soluble NM-HA in P bodies (Fig. 15B). Moreover, there was no recruitment of Dcp1a to NM prions as seen by an immunofluorescence staining of HeLa NM-HA^{agg} cells (Fig. 15B). Although SGs and P bodies are both RNP granules, NM shows no interaction with P bodies. Hence, the similarities between SGs and NM prions are specific.

The phosphorylation of eIF2α is an important step in SG assembly. Upon most SG inducing treatments, eIF2α gets phosphorylated at serine 51 and leads to a translational arrest by preventing the assembly of the 43S preinitiation complex (Kedersha et al., 1999). To analyze whether induction of NM aggregation by exogenous fibrils has an effect on the phosphorylation of eIF2α, wildtype HeLa cells or HeLa cells expressing soluble NM-HA were treated either with arsenite or recombinant NM fibrils and harvested at different time points for western blot analysis (Fig. 16).

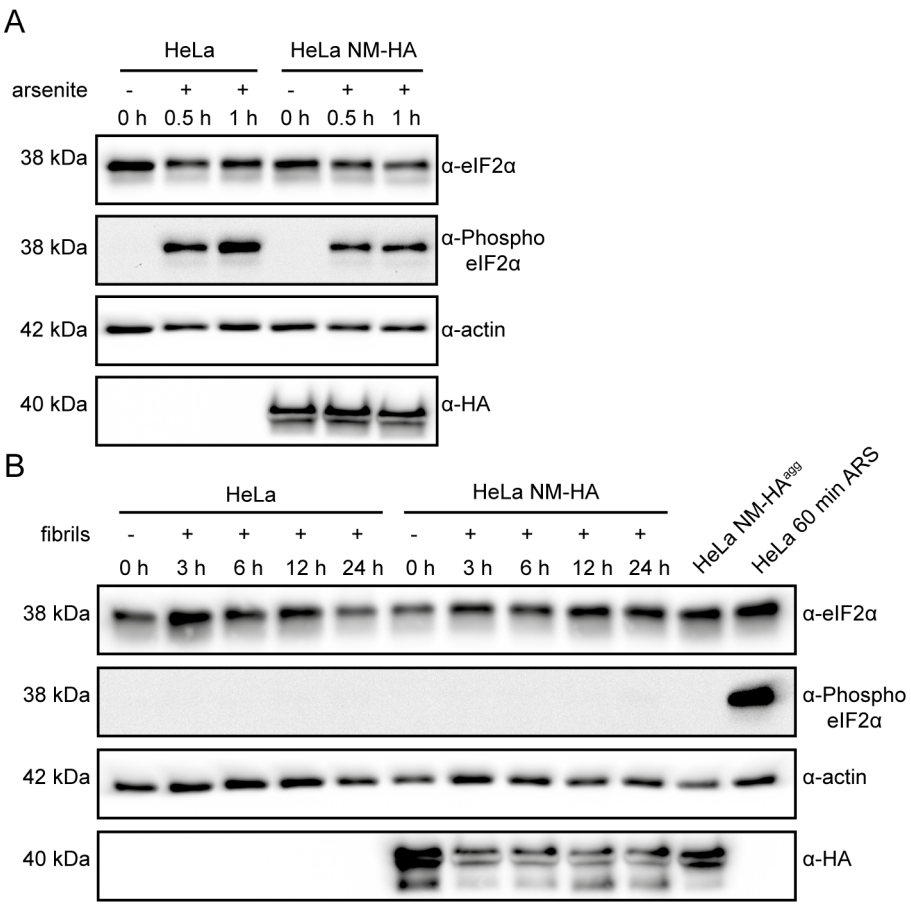

Figure 16. NM fibrils do not trigger phosphorylation of eIF2α. (A) HeLa cells with or without soluble NM-HA were exposed to 0.5 mM sodium arsenite for 30 min, 60 min or left untreated. Western blotting was performed using pAb anti-eIF2α, pAb anti-phospho-eIF2α and mAb anti-HA. Actin served as loading control. (B) HeLa cells with or without soluble NM-HA were exposed to 5 µM recombinant fibrillar NM, harvested after the indicated time points and subjected to western blotting. HeLa cells carrying stable NM prion aggregates (HeLa NM-HA^{agg}) were loaded as control and HeLa cells treated with 0.5 mM sodium arsenite (ARS) for 60 min served as positive control. Western blotting was performed using pAb anti-eIF2α, pAb anti-phospho-eIF2α and mAb anti-HA. Actin served as loading control.

The treatment of HeLa and HeLa NM-HA^{sol} cells with sodium arsenite led to the phosphorylation of eIF2α, as expected (Fig. 16A). Thus, the presence of soluble NM-HA has no effect on the phosphorylation. In contrast, incubation of HeLa cells with recombinant NM fibrils did not lead to any phosphorylation of eIF2α (Fig. 16B). Additionally, HeLa cells carrying stable NM prions showed no phosphorylation of eIF2α. We conclude that NM prions and SGs do not share the same pathway of activation.

SGs are highly dynamic structures, which assemble within minutes after exposure to stress. Fluorescence recovery after photobleaching (FRAP) studies have shown that different SG components, including G3BP and TIA-1, have a rapid turnover in SGs (Kedersha et al., 2000; Kedersha et al., 2005). Moreover, it has been suggested that stress granules have liquid-like properties (Kroschwald et al., 2015). To compare the dynamics of SGs to our NM prions we used FRAP analysis (Fig. 17).

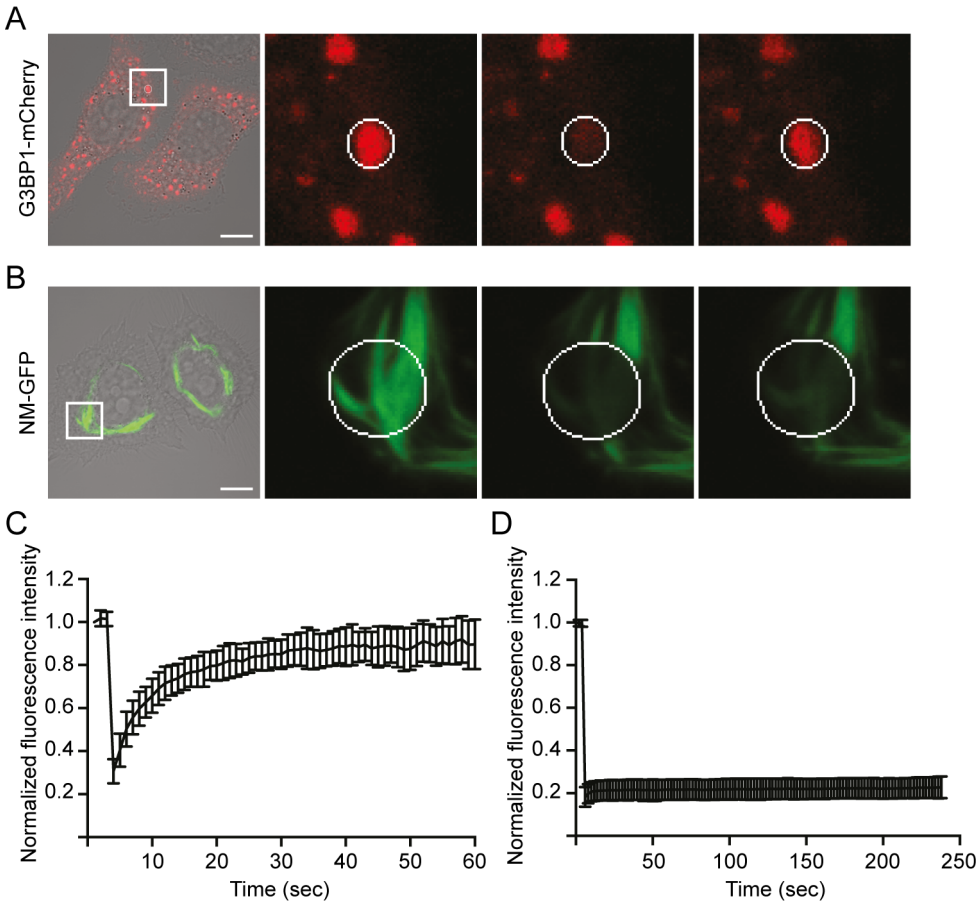

Figure 17. NM prions are not dynamic as stress granules (A-B) HeLa cells expressing either G3BP1-mCherry (A) or NM-GFP (B) were used for FRAP analysis. NM-GFP expressing cells were exposed to 5 µM recombinant fibrillar NM (monomer concentration) for 48 h and G3BP1-mCherry expressing cells were exposed to 0.5 mM sodium arsenite 30 min prior to photobleaching. High magnification views of the indicated regions are shown before, immediately after and 1 min (A) or 4 min (B) after photobleaching. Circles represent bleached areas. Scale bar: 10 µm. (C-D) Plots show the normalized fluorescence intensity of bleached stress granules (C) and bleached NM-GFP prions (D). (G3BP1-mCherry n=14; NM-GFP n=14).

We used HeLa cells expressing fluorescently tagged G3BP1 from bacterial artificial chromosomes (BAC) to detect SGs while performing live cell imaging (Mateju et al., 2017; Poser et al., 2008). Cells were treated with 0.5 mM arsenite to induce SGs and were subjected to FRAP analysis 30 min later. As expected, G3BP sowed a rapid and almost complete recovery with a half time of ~10 sec (Fig. 17A, C). To detect NM prions in living cells, we used HeLa cells expressing NM-GFP. Cells were exposed to recombinant NM fibrils 48 h prior to imaging to induce aggregation. After bleaching part of the NM prion, imaging was continued for 4 min without any recovery being measured (Fig. 17B, D). Prolonged imaging was difficult as cells got photodamaged and/or moved. Hence, in contrast to SGs, NM prions are not dynamic assemblies. In conclusion, the data demonstrates that SGs and NM prions share several components, but apart from that are different assemblies regarding their induction and dynamics.

3.4 NM has only a minor effect on SG dynamics

So far we analyzed similarities and differences of SGs and NM prions. Both assemblies share several components but show different dynamics. This led us to question whether NM prions might influence SG dynamics. First we tested whether SGs can still assemble in the presence of NM prions. HeLa NM-HA^{sol} cells were incubated with NM fibrils for 48 h to induce aggregation and were afterwards incubated with arsenite to induce SGs (Fig. 18A, B). Using the SG marker TIAR, SGs could be detected in cells harboring NM prions (Fig. 18B). Furthermore, TIAR could be detected colocalizing with the NM prions, indicating that SGs cannot only form in the presence of NM prions but also that sequestration of SG components into NM prion aggregates has no effect on the induction of SGs. To assess if the presence of SGs has an effect on the induction of NM prions, HeLa NM-HA^{sol} cells were first treated with a low dose of arsenite to induce SGs and then NM fibrils were added to induce aggregation of NM (Fig. 18C, D). As treating cells with arsenite for a long period of time is toxic to the cells, a medium exchange was performed after six hours. 24 h post fibril induction, cells were stained and imaging revealed that cells were able to assemble NM prions even in the presence of SGs (Fig. 18D).

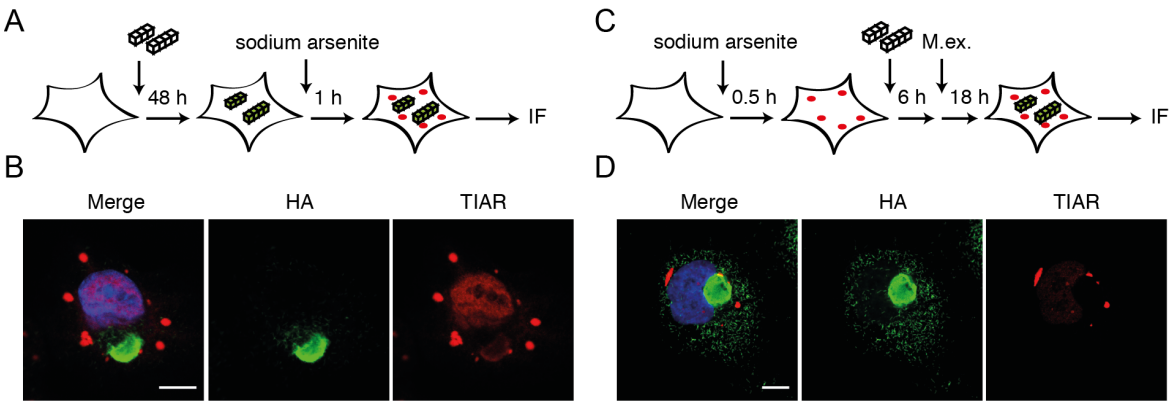

Figure 18. Stress granules and NM prions can form in the presence of each other. (A) Schematic diagram of the experiment. (B) HeLa NM-HA^{sol} cells were exposed to 5 µM recombinant fibrillar NM (monomer concentration) for 48 h before 0.5 mM sodium arsenite was added for 1 h. Cells were subsequently fixed and subjected to immunofluorescence staining. NM was stained using mAb anti-HA (green) and SGs were stained using mAb anti-TIAR (red). Nuclei were stained with Hoechst (blue). Scale bar: 10 µm. (C) Schematic diagram of the experiment. M.ex.: medium exchange (D) HeLa NM-HA^{sol} cells were exposed to 100 µM sodium arsenite and after 30 min 5 µM recombinant fibrillar NM (monomer concentration) was added. The medium was exchanged after 6 h and cells were further cultivated for 18 h. Afterwards cells were fixed and immunofluorescence staining was performed using mAb anti-HA (green) and mAb anti-TIAR (red). Nuclei were stained with Hoechst (blue). Scale bar: 10 µm.

Surprisingly, no TIAR was sequestered into the newly formed NM prion aggregates. SGs could still be detected in many cells, although arsenite was removed 18 h before fixation. As under normal conditions SGs disassemble within a few hours after the stress has been released, SG disassembly seems to be impaired during induction of NM prion aggregates. We conclude that SGs and NM prions can form in the presence of each other.

To investigate the effect of soluble and aggregated NM on SG dynamics, assembly and disassembly, we conducted live cell imaging of these events. We used HeLa cells expressing the G3BP1-mCherry BAC construct and transduced them with a construct encoding for NM-GFP. To induce aggregation of NM-GFP, cells were incubated with recombinant NM fibrils 48 h prior to the experiment. First, the effect of NM on SG dynamics was analyzed by performing FRAP analysis on SGs. HeLa G3BP1-mCherry, HeLa G3BP1-mCherry NM-GFP^{sol} and HeLa G3BP1-mCherry NM-GFP^{agg} cells were treated with 0.5 mM arsenite 30 min

prior to bleaching and cells were subsequently subjected to FRAP analysis (Fig. 19A, B). As seen before, in HeLa cells expressing only G3BP1-mCherry, G3BP showed a rapid and almost complete recovery (Fig. 19B). Surprisingly, G3BP showed the same rapid recovery in HeLa cells expressing either soluble or aggregated NM-GFP (Fig. 19B). There was no difference in recovery rate or ratio of mobile and immobile fraction detectable. This led us to the conclusion that neither aggregated nor soluble NM has an effect on SG dynamics. Next, we wanted to assess whether there is an effect of NM on the assembly of SGs. Arsenite was added to cells and imaging was started directly afterwards for 60 min (Fig. 19A, C). For analysis of images, the standard deviation of G3BP1-mCherry fluorescence was measured for each cell over time as a measure of SG assembly. Before SGs assembled, the fluorescence signal was evenly distributed throughout the cytoplasm with a relatively small standard deviation. Upon stress treatment, G3BP accumulated in cytoplasmic foci, thereby increasing the standard deviation of the fluorescence signal. Analyzing the slopes of the increase in standard deviation of the fluorescence signal showed that SG assembly is slightly impaired in HeLa cells carrying NM-GFP prions (Fig. 19D). Assembly rates were slower when NM prions were present, but after 60 min incubation with arsenite, all cell lines showed a similar SG pattern. For analysis of SG disassembly, cells were incubated with arsenite for 1 h, followed by a medium exchange and subsequent imaging for 3 h (Fig. 19A, E). Imaging was started 15 min after the medium was exchanged, as imaging positions needed to be verified. Analysis was performed in the same way as for SG assembly. The slopes of SG disassembly showed that for the first 2 h there was no difference between the different cell lines (Fig. 19F). During the last hour of imaging, SGs in HeLa G3BP1-mCherry cells almost completely dissolved, however in HeLa cells expressing soluble or aggregated NM-GFP some SGs seemed to be more persistent. In conclusion, these findings show that SGs can form in the presence NM prions, but show a slight impairment in assembly und disassembly.

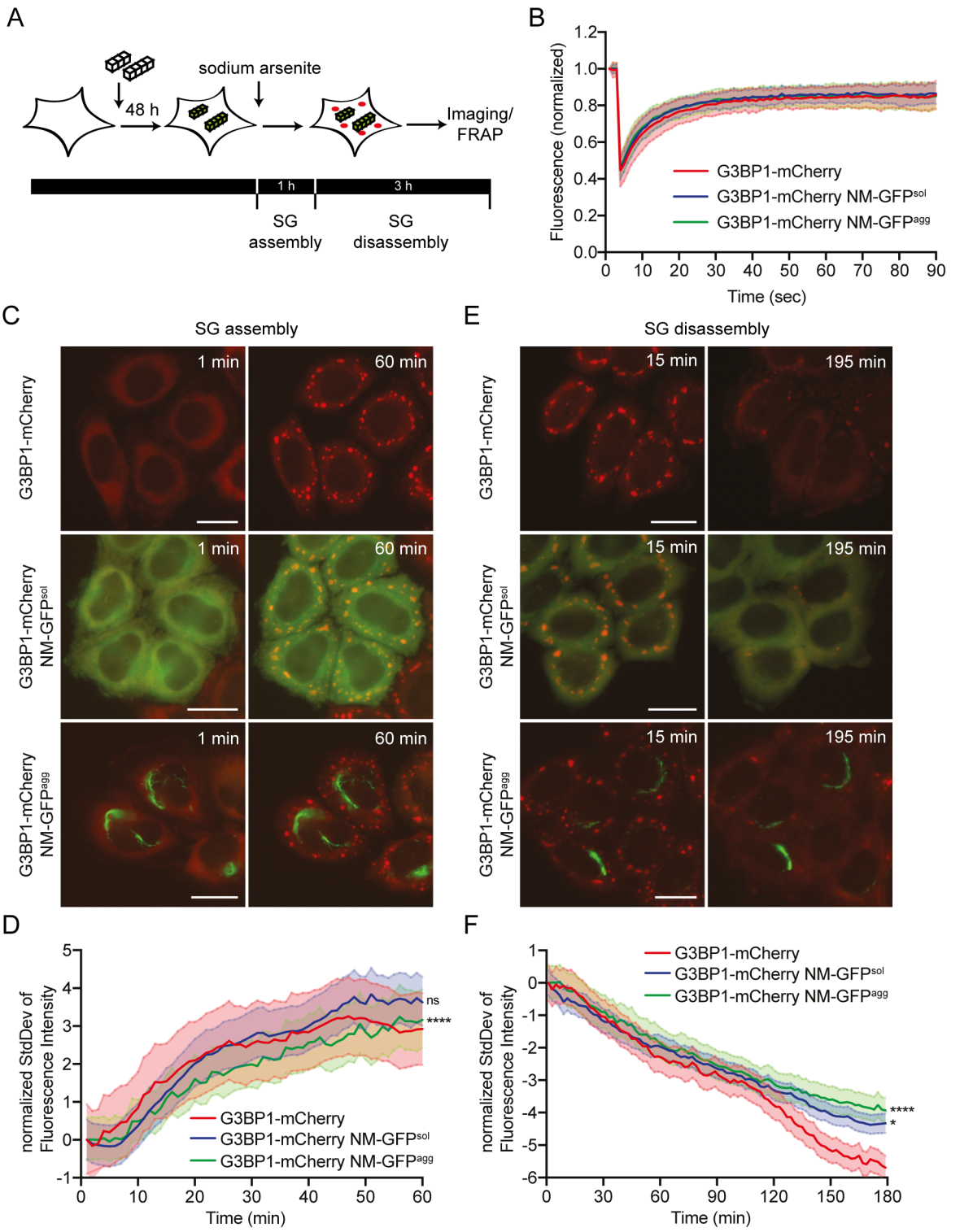

Figure 19. NM does not influence stress granule dynamics. (A) Schematic diagram of the experiment. (B) HeLa G3BP1-mCherry, G3BP1-mCherry NM-GFP^{sol} and G3BP1-mCherry NM-GFP^{agg} cells were used for FRAP analysis. Cells were exposed to 0.5 mM sodium arsenite to induce stress granules, 30 min prior to photobleaching. (G3BP1-mCherry n=39; G3BP1-mCherry NM-GFP^{sol} n=44; G3BP1-mCherry NM-GFP^{agg} n=36) (C-D) HeLa G3BP1-mCherry, G3BP1-mCherry NM-GFP^{sol} and G3BP1-mCherry NM-GFP^{agg} were subjected to live cell imaging to monitor SG assembly. Cells were treated with 0.5

mM sodium arsenite and imaged for 60 min. (C) Images taken directly (1 min) and 60 min after addition of sodium arsenite. (D) Movies were analyzed for SG assembly by using the standard deviation (StdDev) of the fluorescence intensity of each cell over time. At least 240 cells were imaged per cell population (n=3). Slopes were analyzed compared to G3BP1-mCherry and statistical analysis was performed using a mixed linear regression model (ns = not significant; ****p ≤ 0.0001). (E-F) HeLa G3BP1-mCherry, G3BP1-mCherry NM-GFP^{sol} and G3BP1-mCherry NM-GFP^{agg} cells were subjected to live cell imaging to monitor SG disassembly. Cells were treated with 250 µM sodium arsenite for 1 h, followed by a medium exchange and subsequent imaging for 3 h. (E) Images taken directly (15 min) and 195 min after medium exchange. (F) Movies were analyzed for SG disassembly by using the standard deviation (StdDev) of the fluorescence intensity of each cell over time. At least 330 cells were imaged per cell population (n=3). Slopes were analyzed compared to G3BP1-mCherry and statistical analysis was performed using a mixed linear regression model (ns = not significant; *p ≤ 0.05; ****p ≤ 0.0001).

3.5 Treatments that induce SGs also increase induction of NM aggregates by recombinant NM fibrils

It is now emerging that RBPs harboring a LC domain can form pathological inclusions, leading to the hypothesis that these inclusions are derived from SGs (Aulas and Vande Velde, 2015; Wolozin, 2012). Several *in vitro* studies showed that SG components, such as FUS and hnRNPA1, can phase separate into liquid droplets and convert into a more solid state over time (Molliex et al., 2015; Patel et al., 2015). Furthermore, it was shown that proteins with disease-linked mutations accumulate and aggregate in SGs, thereby altering SG dynamics (Mackenzie et al., 2017; Mateju et al., 2017). As the presence of soluble NM slightly impaired SG disassembly, we wondered whether the prolonged presence of SGs could induce NM prion aggregates. We used HeLa NM-GFP cells and treated them with a range of drugs, including some that are known SG inducers. Cells were treated with the compounds for 2 h, followed by a medium exchange and further cultivation for 22 h (Fig. 20A). Aggregated NM is now termed NM aggregate and not prion, as cells were analyzed 24 h after treatment and it cannot be ruled out that induced NM aggregates are not of prionogenic nature in this experimental setup. Further cultivation of cells treated with SG inducing compounds and recombinant fibrils showed that aggregates are passed on to daughter cells (data not shown), but as cell death might have falsified results after prolonged cultivation, cells were analyzed 24 h after treatment. High-throughput imaging was conducted using an automatic confocal microscope (Cell Voyager

6000). Analysis showed that only very few cells exhibited aggregates. Further inspection of potential NM prion containing cells revealed that the image analysis software detected false positives (Fig. 20B). As a positive control, cells were treated with 5 µM NM fibrils for 1 h to induce aggregation. The comparison of compound treated cells with cells incubated with NM fibrils was used to distinguish manually between positive and false positive cells (Fig. 20C).

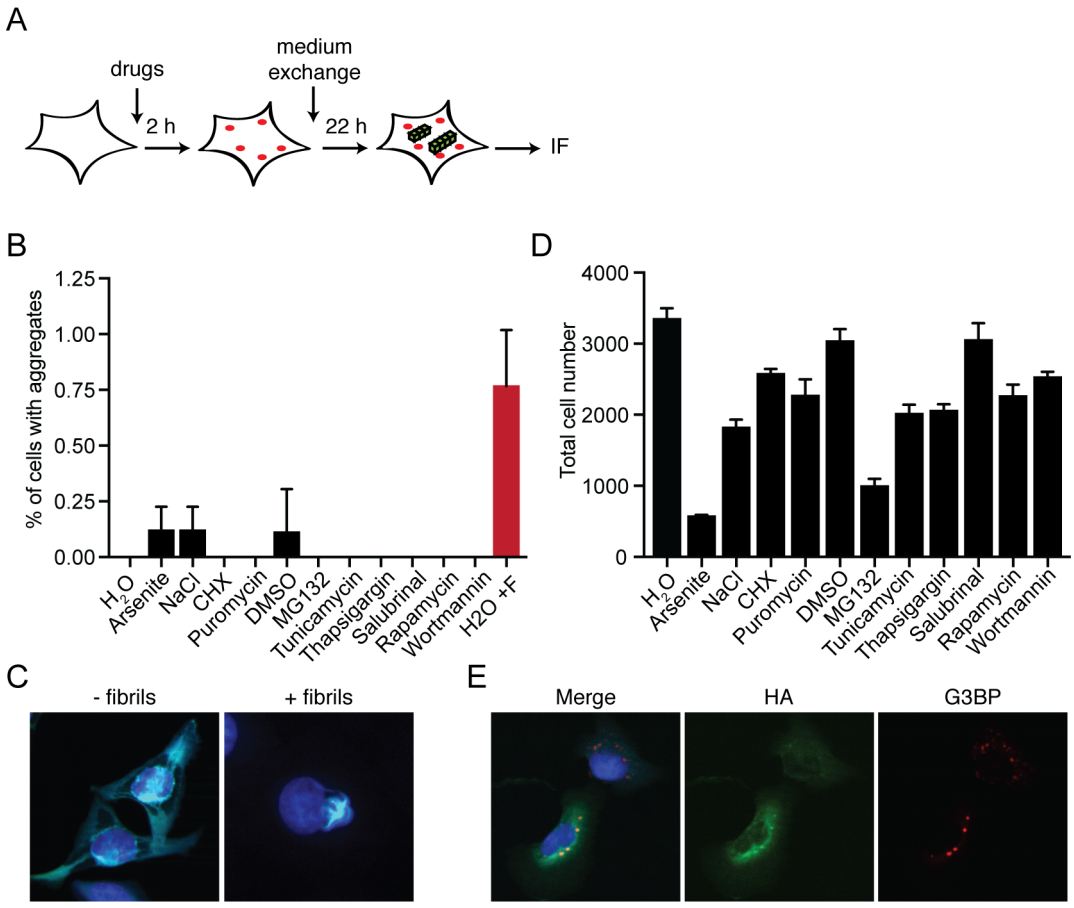

Figure 20. NM aggregates cannot be induced by severe stress treatment. (A) Schematic diagram of the experiment. HeLa NM-GFP cells were incubated with compounds for 2 h, followed by a medium exchange and cultivation for 22 h. Cells were subsequently fixed and stained. Images were taken using an automatic confocal microscope (Cell Voyager 6000). (B) Analysis of cells with aggregates. HeLa NM-GFP cells treated with recombinant NM fibrils are shown as control (red). CHX: Cycloheximide. (C) Images of HeLa NM-GFP cells treated with 250 µM arsenite for 2 h (- fibrils) or incubated with 5 µM recombinant NM fibrils (+ fibrils), followed by a recovery for 22 h. Nuclei were stained with Hoechst and cytoplasm was visualized using CellMask (blue). Note that NM-GFP aggregates also brightly stained with Hoechst dye. (D) Analysis of total cell number upon different drug treatments (E) Images of HeLa NM-GFP cells treated with 250 µM arsenite for 2 h, followed by a recovery for 22 h. SGs were stained

with mAb anti-G3BP (red). Nuclei were visualized using Hoechst and cytoplasm was stained using CellMask (blue).

Cells treated with SG inducing compounds were severely stressed and underwent morphological changes, leading to the condensation of NM-GFP in the cell (Fig. 20C). The decrease in total cell number further confirmed toxicity of compounds (Fig. 20D). Staining of the SG Marker G3BP revealed that some SGs were still present after SG induction with arsenite, indicating that our stress treatment led to the prolonged presence of SGs (Fig. 20E). Hence, treatment of cells with SG inducing compounds led to more persistent SGs, but it did not induce the aggregation of NM-GFP. As this experimental setup was already quite toxic to the cells, more severe stress, such as longer incubation periods with compounds or longer cultivation periods, was not possible. Thus, we conclude that at least in the time frame we have tested, NM recruited to SGs cannot turn into an NM prion state.

As induction of SGs itself could not lead to the aggregation of NM, we wondered whether their presence might influence NM aggregate induction by an exogenous seed. HeLa NM-GFP cells were treated with the same compounds as before and NM fibrils were added after 1 h treatment, followed by a medium exchange and further cultivation (Fig. 21A). To check for SG induction by the used compounds, cells were treated for 2 h and subsequently fixed and stained. Analysis showed that arsenite and heat shock were the most potent SG inducers (Fig. 21B). This was expected as arsenite and heat shock are commonly used to trigger SGs. The treatment with MG132 and NaCl led to a good SG response with 40 – 50 % of cells harboring SGs. Furthermore, puromycin induced SGs in ~10 % of cells. Interestingly, treatment with ER stress inducer thapsigargin did not show induction of SGs, although there have been studies in different human cell lines using thapsigargin as a SG inducing agent (Arimoto-Matsuzaki et al., 2016; Wheeler et al., 2016). Cycloheximide (CHX), salubrinal, rapamycin, wortmannin, and tunicamycin did not induce SGs, but were included as controls. CHX and salubrinal influence SG assembly positively (salubrinal) or negatively (CHX), while tunicamycin induces ER stress without inducing SGs. Rapamycin and wortmannin have opposite effects on autophagy, which is a major player in many

neurodegenerative diseases and has been shown to play a role in SG clearance (Buchan et al., 2013; Mateju et al., 2017). Treatment of HeLa NM-GFP cells with the selected compounds and NM fibrils led to increased aggregate induction especially in cells treated with SG inducing drugs, compared to the respective control (Fig. 21C).

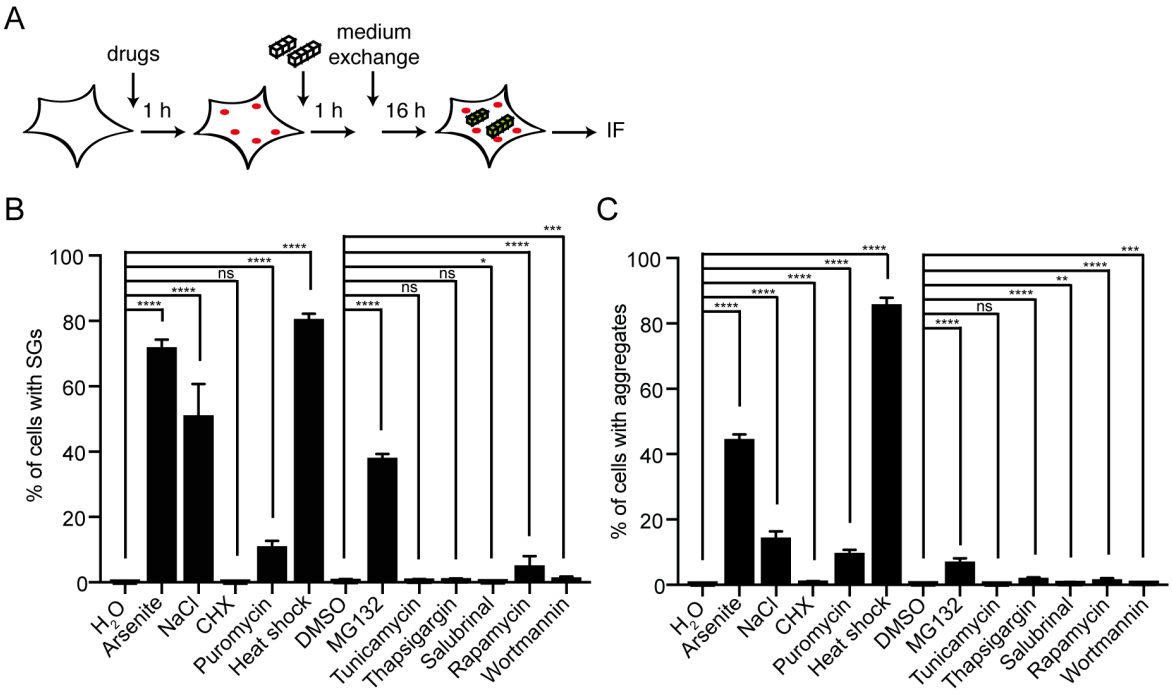

Figure 21. Presence of stress granules increases aggregate induction. (A) Schematic diagram of the experiment. HeLa NM-GFP cells were treated with stress inducing compounds for 2 h and 5 µM recombinant fibrillar NM (monomer concentration) was added after 1 h of compound treatment. A medium exchange was performed and after 16 h cells were fixed and an immunofluorescence staining was conducted. For a SG induction control, cells were fixed directly after the 2 h compound treatment. Images were taken using the automatic confocal microscope Cell Voyager 6000. (B) Percentage of cells with SGs after 2 h treatment with compounds. Bars represent mean values ± SD (n = 3). At least 1200 cells were analyzed. Statistical analysis was performed using a logistic regression model (ns = not significant; *p ≤ 0.05; ***p ≤ 0.001; ****p ≤ 0.0001). (C) Percentage of cells bearing aggregates after treatment with compounds and NM fibrils. Bars represent mean values ± SEM (n = 3). Experiment was performed three times in triplicates. At least 900 cells were analyzed. Statistical analysis was performed using a logistic regression model (ns = not significant; **p ≤ 0.01; ***p ≤ 0.001; ****p ≤ 0.0001).

Cells treated with arsenite showed an induction rate of 40 – 50 % and heat shock treatment even led to 80 % of cells harboring aggregates. Treatment with NaCl, puromycin, and MG132 led to an aggregate induction in 10 – 15 % of NM-GFP

expressing cells. In contrast, control treated cells showed only an induction rate of ~0.5 – 2 %. The aggregate induction in water and DMSO treated cells was rather low, most likely because cells were incubated with fibrils for only 1 h. Additionally, we have seen before that aggregate induction is not as efficient with GFP as a tag. Interestingly, efficiency of aggregate induction correlated with the amount of SG positive cells (Fig. 21B, C). Hence, the presence of SGs seems to have a positive effect on NM aggregate induction by exogenous fibrils.

Next, we investigated if SGs positively affect aggregation of NM by functioning as the nucleation site. As the concentration of soluble NM is increased inside of SGs, the high local concentration could contribute to aggregate induction (Patel et al., 2015). We performed live cell imaging using HeLa cells expressing mCherry tagged G3BP1 and soluble NM-GFP. Cells were treated with arsenite to induce SGs and recombinant NM fibrils were added 30 min later (Fig. 22A). Imaging was performed for 20 h. Already 1 h post fibril exposure, small NM-GFP aggregates were visible, mostly one per cell (Fig. 22B). Surprisingly, the aggregates appeared close to but not within SGs (Fig. 22B, inset). As the spatial resolution of a widefield fluorescence microscope is limited, we could not rule out that the aggregate originated from a SG. To increase resolution and confirm our live cell imaging results, we used a confocal microscope equipped with the Airyscan technology (Zeiss). The Airyscan technology increases the resolution to 120 nm, making it possible to obtain superresolution images with a confocal microscope. We used HeLa cells expressing soluble NM-HA, treated them with arsenite to induce SGs and added NM fibrils for induction of aggregation. Cells were fixed at different time points post fibril exposure to capture the moment of aggregate appearance. 5 h after exposure to NM fibrils, numerous small aggregates were distributed throughout the cytoplasm (Fig. 22C). However, there was no colocalization of NM aggregates with SGs (Fig. 22C, inset). In conclusion, these findings show that there is no evidence for SGs acting as nucleation sites for NM aggregate formation, neither without nor with an exogenous seed. However, treatments that induce SGs, also indirectly affect NM aggregate induction.

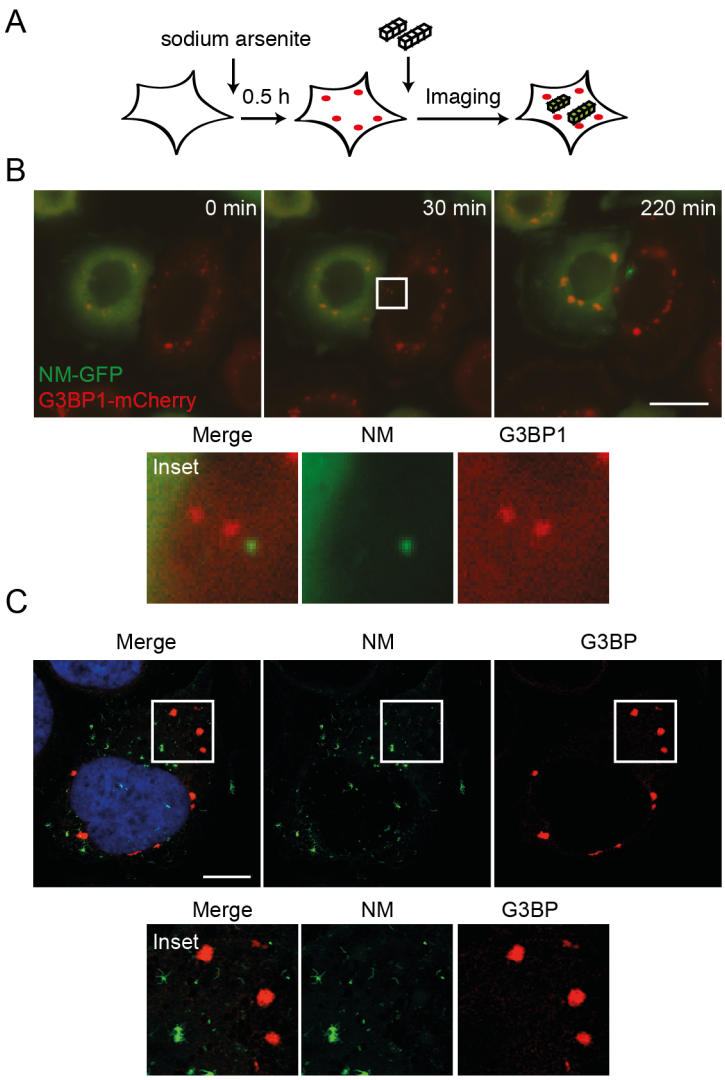

Figure 22. NM aggregates do not evolve from stress granules. (A) Schematic diagram of the experiment. (B) Live cell imaging of HeLa G3BP1-mCherry NM-GFP cells. Cells were treated with 50 µM sodium arsenite, followed by addition of 5 µM recombinant fibrillar NM (monomer concentration) after 30 min. Imaging was started 30 min after fibril exposure and was performed for 20 h. Scale bar: 20 µm (C) HeLa NM-HA^{sol} cells were treated with 250 µM sodium arsenite to induce stress granules. After 1 h, 5 µM recombinant fibrillar NM (monomer concentration) was added for 1 h, followed by a medium exchange. Cells were fixed 5 h post fibril induction and immunofluorescence staining was performed using mAb anti-HA (green) and mAb anti-G3BP (red). Nuclei were stained with Hoechst (blue). Scale bar: 10 µm. Images were captured using the LSM 800 equipped with an Airyscan.

3.6 The physical appearance of SGs is not important for an increased induction rate of NM aggregation

The foregoing experiments demonstrated that treatments that induce SGs also increase induction of NM aggregates, despite the fact that we did not observe seeding of NM aggregates by SGs. To further investigate the role of SGs in the induction of aggregates with NM fibrils, we inhibited SG assembly. So far SG inhibition has mainly been achieved by the depletion of SG nucleating factors (Bley et al., 2015; Matsuki et al., 2013). The combined knockdown of TIA-1, TIAR, and G3BP most efficiently reduces the number of visible SGs without affecting stress signaling (Bley et al., 2015). Hence, we transfected HeLa cells with a siRNA mix targeting TIA-1, TIAR and G3BP and analyzed the SG induction rate (Fig. 23A, B). The concomitant knockdown of TIA-1, TIAR, and G3BP severely impaired the formation of SGs and reduced the number of SG-positive cells to ~20 %.

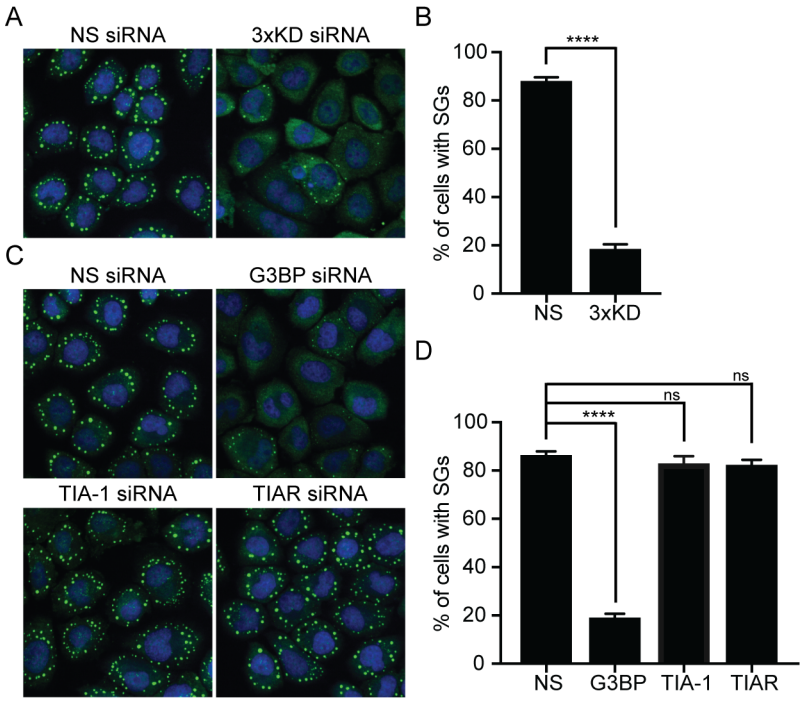

Figure 23. Knockdown of G3BP efficiently inhibits SG formation. (A) HeLa cells were transfected with either non-silencing siRNA (NS) or a siRNA mix targeting TIA-1, TIAR and G3BP (3xKD). 72 h post transfection, cells were treated with 0.5 mM arsenite for 1 h, subsequently fixed and immunofluorescence staining was performed using pAb anti-FMRP (green). Nuclei were stained using Hoechst (blue). Images were obtained using the automatic confocal microscope Cell Voyager 6000. (B) Analysis of cells harboring

SGs 72 h post siRNA transfection. Bars represent mean values ± SD (n = 3). Statistical analysis was performed using unpaired two-tailed Student's t-test (****p ≤ 0.0001). (C) HeLa cells were transfected with siRNA targeting G3BP, TIA-1, or TIAR. Non-silencing (NS) siRNA was used as control. 72 h post transfection, cells were treated with 0.5 mM arsenite for 1 h, subsequently fixed and immunofluorescence staining was performed using pAb anti-FMRP (green). Nuclei were stained using Hoechst (blue). Images were obtained using the automatic confocal microscope Cell Voyager 6000. (D) Analysis of cells harboring SGs 72 h post siRNA transfection. Bars represent mean values ± SD (n = 3). Statistical analysis was performed using one-way ANOVA with Dunnett's multiple comparisons test (ns = not significant; ****p ≤ 0.0001).

Cells showed almost no toxicity after the triple knockdown. However, the SG inducing treatment we wanted to conduct was already quite toxic to cells without siRNA transfection (Fig. 20C, D). Therefore, we wanted to test if the knockdown of a single SG factor would give a similar reduction in SG positive cells. HeLa cells were transfected with siRNA targeting TIA-1, TIAR, or G3BP alone and 72 h post transfection, cells were analyzed for SG induction after treatment with arsenite. Surprisingly, the knockdown of G3BP already led to a reduction of SG positive cells to ~20 %, comparable to the triple knockdown (Fig. 23C, D). No significant impairment of SG formation could be detected upon knockdown of TIA-1 and TIAR. Thus, depletion of G3BP substantially impaired the formation of visible SGs and was used for further experiments.

To investigate the effect of SG inhibition on aggregate formation induced by exogenous NM fibrils, HeLa NM-GFP cells were transfected with siRNA targeting G3BP. 72 h post transfection, cells were incubated with compounds and after 1 h NM fibrils were added for 1 h (Fig. 24A). The medium was exchanged for further cultivation and cells were analyzed the next day for aggregate induction. Knockdown efficiency was confirmed by immunofluorescence and western blot analysis (Fig. 24B, C). The effect of G3BP knockdown on SG assembly was assessed for all compounds by immunofluorescence staining 2 h after drug treatment (Fig. 24D). SG formation was significantly decreased in arsenite, puromycin, heat shock, and MG132 treated cells after depletion of G3BP. Interestingly, there was almost no effect on SG formation in NaCl treated cells. It has been shown that macromolecular crowding regulates the assembly of SGs upon osmotic stress (Bounedjah et al., 2012). Hence, knockdown of G3BP does

not seem to play a role in this pathway of SG assembly. For most cells, treated with drugs that do not induce SGs, a significant difference between non-silencing (NS) and knockdown of G3BP (KD) was detectable even though the total numbers of SG-positive cells were very low and varied only slightly between NS and KD conditions. This is a result from the high amount of cells used for analysis and is not relevant for our study. Hence, SG formation was efficiently inhibited for most SG inducing compounds.

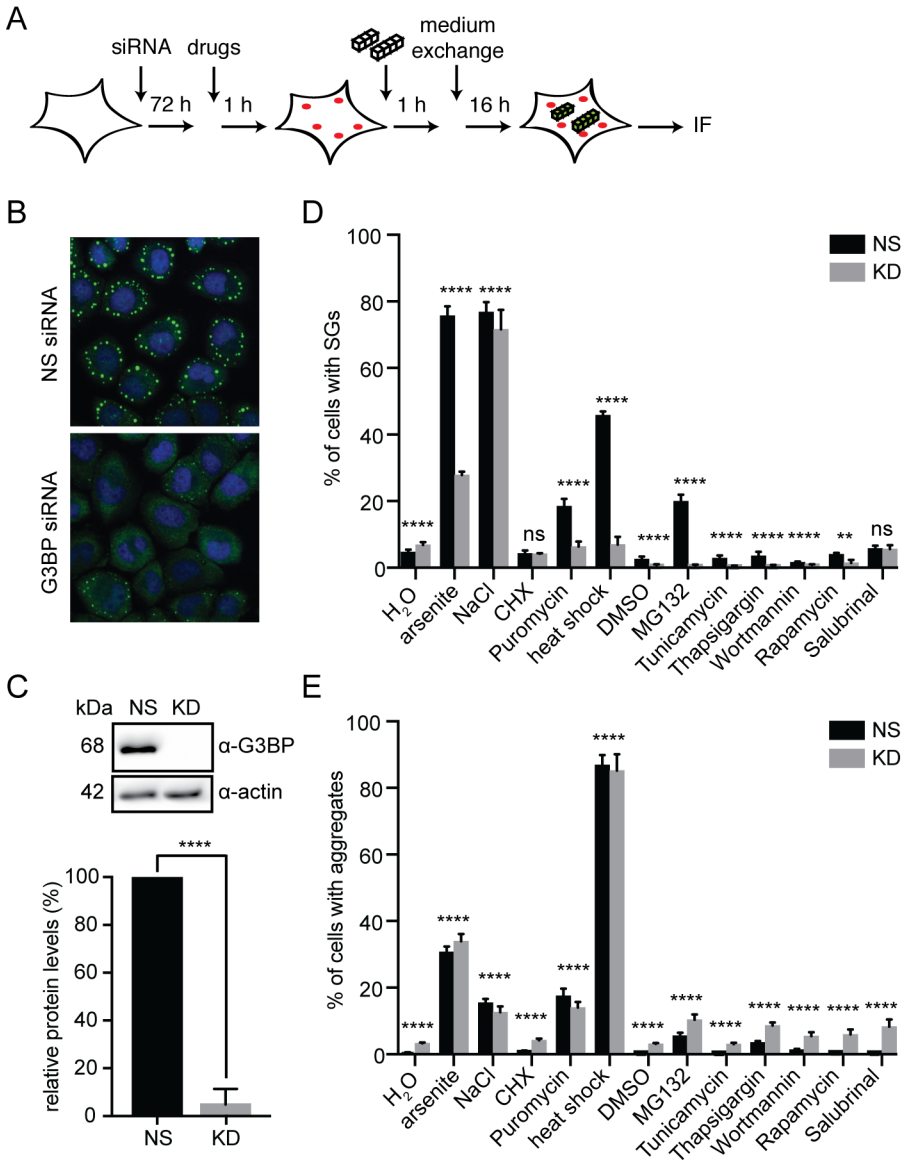

Figure 24. Inhibition of stress granule assembly by siRNA has no effect on aggregate induction. (A) Schematic diagram of the experiment. HeLa NM-GFP cells were transfected with siRNA against G3BP (KD) or non-silencing (NS) siRNA for 72 h before treatment. Stress inducing compounds were added and after 1 h cells were

exposed to 5 µM recombinant fibrillar NM (monomer concentration). The medium was exchanged after 1 h and cells were either fixed directly, to serve as the SG induction control, or further cultivated for 16 h. (B) Immunofluorescence staining was performed after 2 h treatment with 250 µM sodium arsenite using pAb anti-FMRP (green). Nuclei were stained with Hoechst (blue). (C) Analysis of KD efficiency was performed via western blot 72 h post transfection. G3BP was detected by mAb anti-G3BP, actin was detected using mAb anti-actin. The experiment was performed in triplicates. NS signal was set to 100 %. Bars represent mean values ± SD. Statistical analysis was performed using unpaired two-tailed Student's t-test (****p ≤ 0.0001). (D) Percentage of cells with SGs after 2 h treatment with compounds. Bars represent mean values ± SD (n = 3). At least 500 cells were analyzed per compound and biological replicate. Statistical analysis was performed using a logistic regression model (ns = not significant; **p ≤ 0.01; ****p ≤ 0.0001). (E) Percentage of cells bearing aggregates after treatment with compounds and NM fibrils. Bars represent mean values ± SEM (n = 3). Experiment was performed three times in triplicates. At least 1100 cells were analyzed per compound and biological replicate. Statistical analysis was performed using a logistic regression model (****p ≤ 0.0001).

Treating cells with compounds and NM fibrils resulted in similar aggregate induction rates between NS and KD (Fig. 24E). The SG inducing compounds arsenite and MG132 showed a slightly increased number of cells with aggregates upon SG inhibition, whereas for NaCl, puromycin, and heat shock treated cells a reduction in aggregate induction was detectable. As shown before, SG inducing compounds were quite toxic to the cells (Fig. 20D), suggesting that the detected differences between NS and KD are not biologically relevant. However, there was a significant increase in aggregate induction upon G3BP knockdown for compounds not inducing SGs (Fig. 24E). Control treated cells (H_2O and DMSO) showed a 5-fold, salubrinal treated cells even a 12-fold increase in aggregate induction. Hence, knockdown of G3BP and the concomitant inhibition of SG assembly increased the aggregate induction rate upon treatment with non-SG inducing compounds. The effect seemed to be abolished upon activation of SG stress signaling.

To further investigate the effect of G3BP knockdown on the induction of NM aggregation, we had a closer look at autophagy. Autophagy is a degradative process that clears the cell of damaged organelles and aggregated proteins. In neurodegenerative diseases, autophagy plays a major role, especially as therapeutic target (Nixon, 2013). Moreover, autophagy has been implicated to

facilitate the clearance of SGs (Buchan et al., 2013). Hence, we tested whether the knockdown of G3BP had an effect on aggregate induction by altering autophagy. To examine the autophagic flux upon G3BP knockdown, we treated HeLa cells with chloroquine. Chloroquine inhibits the fusion of autophagosomes with lysosomes, leading to the accumulation of autophagy markers. Western blot analysis showed that upon chloroquine treatment, p62 and LC3-II were markedly increased (Fig. 25A). LC3-II serves as an autophagy marker as during autophagy the cytosolic form of LC3 (LC3-I) is conjugated to phosphatidylethanolamine (PE) to form LC3-PE (LC3-II), which is recruited to autophagosomal membranes (Tanida et al., 2008). P62 binds ubiquitinated proteins, and targets them to autophagosomes, thereby facilitating their clearance (Bjorkoy et al., 2009). Quantitative analysis of LC3-II and p62 signal showed that there was no significant difference between G3BP knockdown and non-silencing control (Fig. 25B, C). Hence, increased aggregate induction through G3BP knockdown is not facilitated by autophagy.

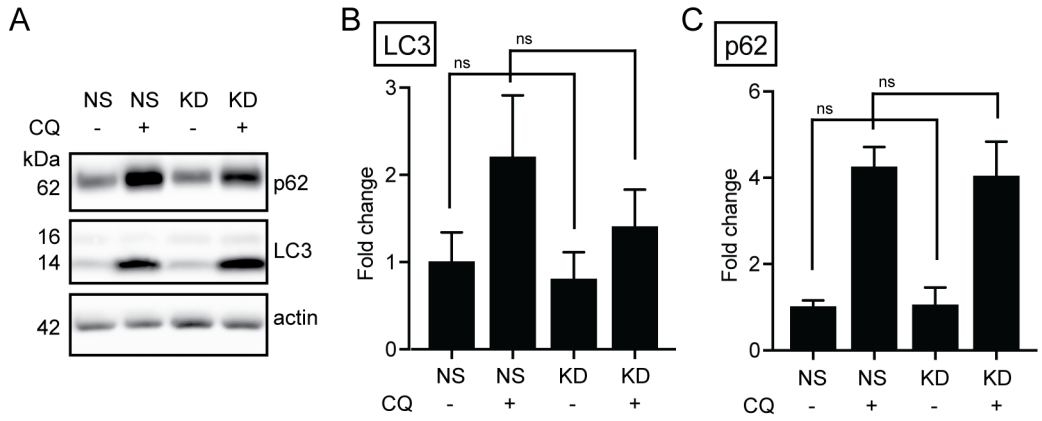

Figure 25. Knock down of G3BP does not induce autophagy. (A) HeLa NM-GFP cells were transfected with siRNA against G3BP (KD) or non-silencing (NS) siRNA. After 54 h, 10 µM chloroquine (CQ) or H_2O was added to cells for 16 h. Western blotting was performed using mAb anti-p62 and mAb-LC3A/B. Actin served as a loading control. (B-C) Quantification of LC3-II (B) and p62 (C) signals. Statistical analysis was performed using unpaired two-tailed Student's t-test (ns = not significant).

As inhibition of SGs by knockdown of G3BP causes additional effects by the depletion of G3BP, we tried to inhibit SG assembly in a different way.

Phosphorylation of eIF2α is an essential player in the upstream regulation of SG assembly. Four different kinases regulate the phosphorylation of eIF2α upon stress signals: PERK (ER stress), PKR (dsRNA, antiviral defense), GCN2 (amino acid starvation) and HRI (heme deficiency) (Jiang and Wek, 2005). Inhibition of PERK by the compound GSK2606414 has been shown to reduce arsenite and MG132 induced SG formation (Cheng et al., 2018). Hence, we used the PERK inhibitor GSK2606414 to inhibit SG assembly, followed by SG and aggregate induction (Fig. 26A).

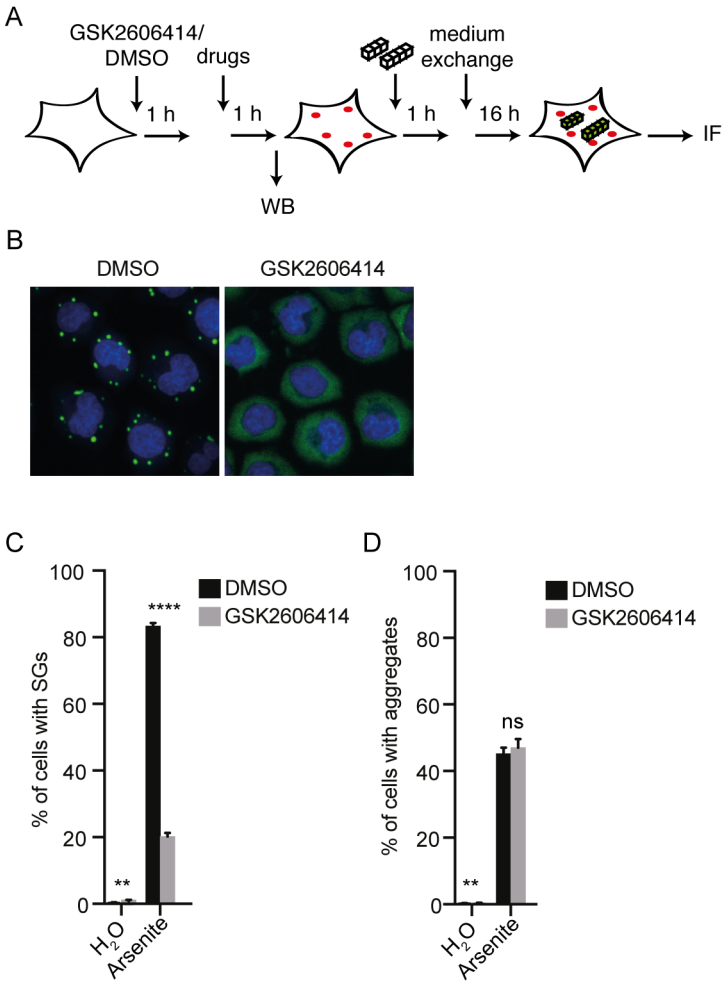

Figure 26. Inhibition of eIF2α phosphorylation and stress granule assembly has no effect on aggregate induction. (A) Schematic diagram of the experiment. HeLa NM-GFP cells were pre-treated with GSK2606414 or DMSO for 1 h. Arsenite was added and after 1 h, cells were exposed to 5 µM recombinant fibrillar NM (monomer concentration). The medium was exchanged after 1 h and cells were either fixed directly, to serve as the SG induction control, or further cultivated for 16 h. Immunofluorescence staining was performed using mAb anti-G3BP. (B) Immunofluorescence staining of HeLa cells pre-

treated with GSK2606414 or DMSO for 1 h and SG inducing treatment with 250 µM sodium arsenite for 2 h. SGs were stained using mAb anti-G3BP (green). Nuclei were stained with Hoechst (blue). (C) Percentage of cells with SGs after 2 h treatment with arsenite. Bars represent mean values ± SD (n = 3). At least 900 cells were analyzed per treatment and biological replicate. Statistical analysis was performed using a logistic regression model (**p ≤ 0.01; ****p ≤ 0.0001). (D) Percentage of cells bearing NM-GFP aggregates after treatment with arsenite and NM fibrils. Bars represent mean values ± SD (n = 3). At least 1200 cells were analyzed per treatment and biological replicate. Statistical analysis was performed using a logistic regression model (ns = not significant; **p ≤ 0.01).

We focused on arsenite as SG inducing agent since treatment with arsenite resulted in a robust SG induction that could be inhibited by G3BP knockdown (Fig. 24B, C). First, HeLa cells were tested for the ability of GSK2606414 to inhibit SG formation. HeLa cells were pre-treated with GSK2606414 or DMSO for 1 h, followed by addition of arsenite for 2 h (Fig. 26B, C). Immunofluorescence staining was performed and showed that GSK2606414 efficiently inhibited the assembly of SGs (Fig. 26B). Image analysis revealed that GSK2606414 significantly reduced SG positive cells to ~20 % (Fig. 26C). Interestingly, induction of NM aggregation with exogenous fibrils resulted in no significant difference between GSK2606414 and DMSO treated cells upon arsenite treatment (Fig. 26D). Thus, inhibition of SG assembly by inhibition of eIF2α phosphorylation has no effect on induction of NM aggregates. In conclusion, these findings show that neither the physical appearance of SGs nor eIF2α phosphorylation, or its downstream pathway are the reason for the increased aggregate induction upon treatment with SG inducing compounds.

4. Discussion

The cellular environment is shaped by numerous membrane-less compartments, which influence biological reactions through the condensation of proteins and nucleic acids. These compartments appear to assemble via intracellular phase transition, thereby forming a dense network of multiple weak interactions (Shin and Brangwynne, 2017). RBPs are a major component of membrane-less compartments, enabling phase transition by their LCDs or PrLDs. Interestingly, many RBPs are part of pathological inclusion that can be found in degenerative disorders. Especially RBPs harboring mutations in their PrLD have been implicated with disease (Johnson et al., 2009; Mackenzie et al., 2017; Patel et al., 2015). Several observations led to the hypothesis that these pathological protein inclusions are derived from membrane-less organelles. Here we investigated the correlation between stress granules, a cytosolic membrane-less compartment, and prion aggregates. Using the yeast prion domain NM of Sup35 as a model for cytosolic protein aggregation, we show that induction of persistent SGs is not sufficient to induce NM aggregates. The prolonged presence of SGs often resulted in cell death, indicating that SGs rather trigger cell death than evolve into pathological protein aggregates. However, chemical SG induction concomitant with NM aggregate induction by recombinant fibrils led to a severe increase in NM aggregate formation. Interestingly, this increase in aggregation was not abolished upon SG inhibition, arguing that other processes than the formation of SGs must be involved.

4.1 Stress granules and NM prions have a comparable interactome

SGs are involved in RNA metabolism by sequestering mRNA transcripts during stress situations, thus their proteome is enriched for proteins with RNA-binding activity. Furthermore, the SG proteome harbors many proteins that contain LCDs, especially PrLDs (Jain et al., 2016; Markmiller et al., 2018). Interestingly, the interactomes of SG proteins remain largely unchanged in non-stress and stress conditions (Youn et al., 2018). The interactomes of soluble and aggregated NM show a significant overlap with the SG proteome while also being enriched for

proteins involved in RNA metabolism and containing PrLDs (Fig. 8). The feature analysis of the NM and SG proteomes revealed enrichment for intrinsically disordered and nucleic acid binding proteins, further highlighting the similarities of these interactomes. Interestingly, the interactomes of soluble and aggregated NM appear very similar, although aggregated NM has almost 10 times more unique hits than soluble NM. In addition to proteins that are part of the RNA metabolism, aggregated NM recruited several proteins involved in protein degradation pathways, including proteins participating in degradation via autophagy and the ubiquitin-proteasome system (UPS). Autophagy and the UPS are the major proteolytic systems of eukaryotic cells. Ubiquitinated proteins are predominantly degraded via the UPS, whereas aggregated proteins are mostly directed to autophagic degradation. Aggregated proteins are targeted by autophagy adaptors, such as p62 and NBR1, which bind to misfolded proteins and deliver them to the autophagosome for lysosomal degradation (Cha-Molstad et al., 2015). P62 decorated NM prions, suggesting that they are recognized as misfolded proteins and targeted for degradation via autophagy. However, NM prions are faithfully transmitted to daughter cells and maintained over multiple passages, indicating that the cell is not able to fully degrade NM prions (Hofmann et al., 2013; Krammer et al., 2009). Similar to the interactome of aggregated NM, the SG proteome of neurons exhibits several proteins that function in autophagy (Markmiller et al., 2018). Autophagy has been suggested to play a role in SG clearance, indicating that SGs are monitored by autophagy factors (Buchan et al., 2013; Mateju et al., 2017). Hence, NM prions and SGs interact with similar proteins, which might be the first hint for a correlation between these two assemblies.

RNA is an important component of SGs, as their function is the sequestration and storage of mRNA transcripts. Analysis of the SG transcriptome revealed that SGs accumulate mostly diverse mRNAs and some noncoding RNAs (ncRNAs), with essentially every mRNA present to some extent (Khong et al., 2017). Interestingly, SGs contain only ~10% of total mRNA, leading to the suggestion that SGs may not have a large effect on global mRNA (Khong et al., 2017). However, RNA is important for SG assembly, as treatment with polysome

stabilizing drugs inhibits SG formation (Kedersha et al., 2000). We identified RNA as a component of NM prions, but did not further analyze the transcriptome or its role in aggregate formation. The sequestration of RNA to NM prions could occur by different mechanisms: RNA-binding might be a secondary effect by binding to recruited RBPs. Alternatively, RNA might bind directly to NM. Although NM does not harbor an RNA-binding motif, the intrinsically disordered PrD of NM could facilitate RNA-binding, as these domains were shown to bind RNA (Jarvelin et al., 2016). RNA has already been implicated in neurodegenerative diseases in different ways. *In vitro*, RNA has been shown to accelerate aggregation of a variety of proteins, including tau and PrP (Deleault et al., 2003; Kampers et al., 1996). Hence, the presence of free RNA might increase protein aggregation or decrease the threshold for this process in the cell or in SGs. Furthermore, the sequestration of RNA by protein aggregates might alter RNA processing that is required for normal cellular functions. Especially in neurodegenerative diseases where RBPs, such as TDP-43 and FUS, are accumulating, loss of RNA-dependent functions might contribute to pathology. Understanding the role of RNA in neurodegenerative disorders might help to elucidate the pathogenic mechanisms of RBP inclusions and other protein aggregates that sequester RNA.

4.2 Similar subdomains of N are required for binding to NM prions and SGs

SGs form by multiple weak interactions between proteins and RNAs. Thereby, RBPs bind to RNA through RRMs or other RNA-binding domains and further assemble into a dense network by engaging in protein-protein interactions through specific binding motifs or low complexity domains. Treatment with the aliphatic alcohol 1,6-hexanediol, which is hypothesized to disrupt weak hydrophobic interactions, disassembles SGs, indicating that hydrophobic interactions are a key component in the SG network (Kroschwald et al., 2015; Patel et al., 2007). Furthermore, SGs are dynamic structures, with their components being in a constant exchange with the surrounding cytosol. However, it is currently not known how specificity of SGs is generated and maintained. Direct protein-protein interactions may provide specificity, together with additional

features, such as number and spacing of binding motifs or post-translational modifications. In contrast to SGs, pathological protein inclusions often exhibit an amyloid structure, which is highly ordered and resistant to degradation. These inclusions contain mainly one protein that forms unbranched fibers consisting of β-strands. In mammalian cells, NM prions most likely have an amyloid structure as shown by SDD-AGE and seen by immuno electron microscopy, where staining of NM-HA in N2a NM-HA^{agg} cells revealed fibrillar structures (in collaboration with Al-Amoudi, unpublished). Interestingly, similar subdomains of N are involved in the binding of NM to the rather loose network of SGs and to highly ordered NM prions. Furthermore, the binding of NM to SGs is specific, as no recruitment of NM to P bodies, which is a closely to SGs related membrane-less organelle, was observed. For recruitment of NM to pre-existing NM prions, the carboxyterminal part of the N domain, comprising the last three repeats of the OPR and the CTN, were identified as the preferential binding sites in mammalian cells (Duernberger et al., 2018). The CTN was identified as the amyloid core and nucleation site, and being most important for *de novo* aggregate induction. Hence, in mammalian cells the last three repeats of the OPR and the CTN facilitate conversion into the aggregated form. Similar domains preferentially drove recruitment to SGs, namely the OPR and the CTN (Fig. 27).

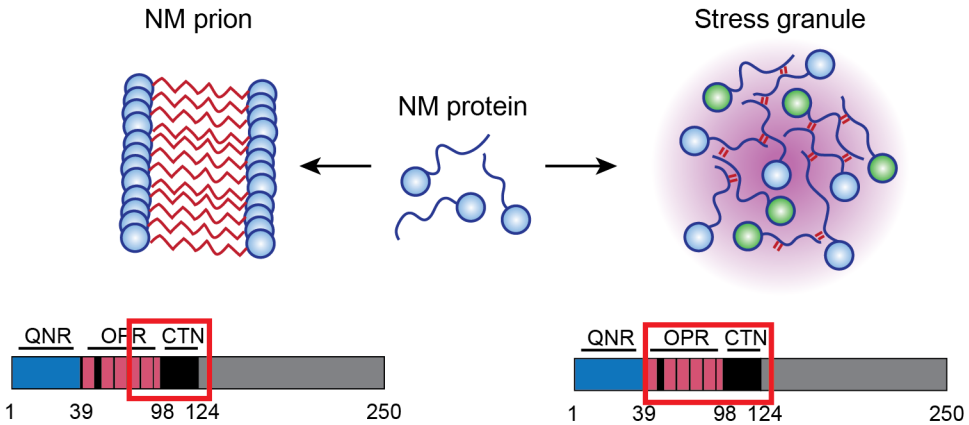

Figure 27. Similar domains drive recruitment of NM protein to NM prions and SGs. NM can be sequestered to NM prions and SGs. The subdomains of NM that are important for the recruitment to these assemblies are shown below, marked by a red rectangular. The position of regions and their lengths are shown in number of amino acids. QNR: Asparagine- and glutamine- rich region; OPR: Oligopeptide repeat region; CTN: Carboxyterminal N domain.

However, the size of the deletion had an effect on recruitment of NM to SGs, with larger deletions resulting in less efficient recruitment (Fig. 14). Furthermore, no deletion of any N subdomain totally abolished the recruitment of NM to SGs, suggesting that binding of NM to SGs is probably facilitated by multiple interactions with SG components and not by a single subdomain of N. Thereby, NM could bind to proteins through its PrD, as interactions between intrinsically disordered domains have been shown to contribute to SG assembly (Boeynaems et al., 2018; Gilks et al., 2004). The PrD of NM is enriched in glutamine and asparagine residues, which were shown to promote aggregation (Alberti et al., 2009; DePace et al., 1998; Michelitsch and Weissman, 2000). Furthermore, Q/N-rich PrLDs of SG proteins are important for recruitment to SGs, indicating that regions enriched in glutamine and asparagine can facilitate binding to SGs (Bentmann et al., 2012; Gilks et al., 2004). The QNR shows the highest Q/N content but its deletion only slightly affected recruitment to SGs (Fig. 28). However, also the carboxyterminal N domain displays a high Q/N content while being most important for binding to SGs. Hence, glutamine and asparagine residues could play a role in both, prion formation and the recruitment of NM to SGs. However, for binding to SGs additionally the OPR was important. Thus, other features than Q/N-rich regions seem to be relevant. A recent study suggested that interactions between tyrosine-rich and arginine-rich regions can facilitate phase separation, a process that is thought to describe SG formation (Wang et al., 2018). The N domain and especially the OPR are enriched for tyrosine residues, which could facilitate recruitment to SGs by binding to arginine-rich regions of other proteins. Furthermore, the OPR is enriched for glycine residues, which might act as a spacer and provide conformational flexibility as glycine residues have been suggested to maintain the liquid-like state of liquid droplets by increasing the flexibility of the molecules (Wang et al., 2018). Through the presence of spacers within the N domain, flexible binding of subdomains to multiple proteins might be facilitated. Hence, different interactions of N with SG components might play a role in recruitment of NM to SGs, facilitated by distinct residues or subdomains within the N domain. Additionally, intrinsically disordered regions have recently been identified to mediate RNA-binding, suggesting that NM might also be recruited to SGs by binding to RNA (Jarvelin et al., 2016). The

fact that similar subdomains, namely the carboxyterminal N domain, facilitate the binding of NM to preexisting NM prions and SGs, supports the hypothesis that there is a correlation between these two assemblies.

		QNR	OPR			OPR/CTN	CTN
	Region	1-39	39-57	39-74	75-97	75-123	98-123
	Length	39	19	36	23	49	26
polar	Q (Gln)	31.6	26.3	27.8	34.8	26.5	19.2
polar	N (Asn)	23.7	5.3	8.3	8.7	16.3	23.1
polar	Q+N	55.3	31.6	36.1	43.5	42.9	42.3
polar	S (Ser)	7.9	5.3	2.8	0	2	3.8
aromatic	Y (Tyr)	13.2	26.3	25	13	12.2	11.5
aromatic	F (Phe)	0	0	0	4.3	6.1	7.7
hydrophobic	A (Ala)	7.9	10.5	8.3	0	2	3.8
hydrophobic	G (Gly)	10.5	21.1	19.4	26.1	20.4	15.4
hydrophobic	L (Leu)	0	0	0	0	2	3.8
hydrophobic	P (Pro)	0	5.3	5.6	13	8.2	3.8
charged	R (Arg)	2.6	0	0	0	2	3.8
charged	D (Asp)	2.6	0	2.8	0	0	0
charged	K (Lys)	0	0	0	0	2	3.8

Figure 28. Amino acid composition of regions within the N domain of Sup35. The position of regions and their lengths are shown in number of amino acids. The abundance of single amino acids is depicted in percent.

4.3 NM prion induction is independent of eIF2α phosphorylation

Exposure of cells to stress conditions leads to an arrest of global translation to save energy. In many cases, translational inhibition is facilitated by phosphorylation of eIF2α as part of the integrated stress response. Phosphorylation of eIF2α reduces translation initiation and results in naked mRNAs, as ribosomes run off their transcripts. Free mRNA transcripts then bind to RBPs and are further assembled into SGs. Most SG inducing treatments require phosphorylation of eIF2α for SG formation, except for osmotic stress, where eIF2α phosphorylation is a secondary effect to mediate apoptosis (Bevilacqua et al., 2010). Hence, phosphorylation of eIF2α plays a major role in the cellular response to stress. Induction of NM aggregation by treatment with recombinant fibrils showed no phosphorylation of eIF2α, indicating that the stress

response is not triggered. Furthermore, inhibition of PERK, one of four kinases that is responsible for eIF2α phosphorylation, had no effect on NM aggregate induction. Hence, SGs and NM prions do not share this common pathway for their induction. This indicates that formation of NM prions by induction with an exogenous seed most likely does not involve the concomitant induction of SGs.

4.4 Stress granule dynamics are not altered by presence of NM

SGs are dynamic structures that have liquid-like properties. Upon exposure to stress, SGs rapidly assemble, merge over time to form larger structures and relax into spherical assemblies after fusion (Kroschwald et al., 2015). SG proteins, such as TIA-1 and G3BP, have a fast turnover inside SGs and with the surrounding cytosol (Kedersha et al., 2000; Kedersha et al., 2005; Kroschwald et al., 2015). The presence of misfolded proteins within SGs can alter the dynamic properties of SGs, as shown for SOD1 (Mateju et al., 2017). Furthermore, defective ribosomal products (DRiPs), prematurely terminated polypeptides, accumulate within SGs and change their dynamics and disassembly rate (Ganassi et al., 2016). However, cells have developed a surveillance system to remove misfolded proteins or DRiPs from SGs to ensure their liquid-like state. Chaperones constantly monitor SGs to target misfolded proteins for degradation, preventing the formation of aberrant SGs (Ganassi et al., 2016; Mateju et al., 2017). Hence, an active and efficient protein quality control (PQC) ensures SG dynamics. The presence of soluble or aggregated NM had no effect on SG dynamics as assessed by FRAP analysis of G3BP, indicating that NM does not alter the state of SGs. However, SG assembly and disassembly rates were slightly delayed in cells harboring NM prions and also soluble NM had an effect on SG disassembly. SG disassembly has been proposed to be a multi-step process, where first large SGs break into smaller foci, followed by their clearance (Wheeler et al., 2016). Chaperones, such as HSP70, and autophagy have been shown to play a role in dissolving SGs (Buchan et al., 2013; Mateju et al., 2017). Aberrant SGs are transported towards the aggresome, a perinuclear structure that sequesters misfolded proteins, for autophagic degradation (Fortun et al., 2003; Johnston et al., 1998; Mateju et al., 2017). The presence of NM in SGs might increase the workload of the SG clearance system as SGs need be transported towards the aggresome for

degradation, causing the delay. Furthermore, SG dynamics might be altered by the prolonged presence of NM within SGs and components could change over time. Though, it is not clear how long the remaining SGs persisted in the presence of NM and which effect persistent SGs have on the cell.

4.5 SG induction is not enough to induce aggregation of NM

Over the last years, the hypothesis that SGs contribute to disease pathology has been raised. It has been suggested that the persistence of SGs triggers the conversion of disease-associated proteins present in SGs into pathological protein aggregates. Evidence for this hypothesis mainly comes from *in vitro* studies, which showed that SG components can form liquid droplets, which in some cases adopt a gel-like or even fibrous state (Molliex et al., 2015; Patel et al., 2015). Many proteins can form liquid droplets above their saturation concentration *in vitro*, leading to a higher concentration of the protein within the droplet and a concomitant reduction in the surrounding cytosol (Shin and Brangwynne, 2017). Hence, by increasing the concentration of proteins in liquid compartments, their aggregation might be triggered. *In vivo* and *in vitro* studies already showed for FUS that increasing the concentration can cause a conversion of the protein into an aggregated state (Patel et al., 2015; Shelkovnikova et al., 2014; Sun et al., 2011). Hence, the local increase in concentration that occurs in membrane-less organelles might serve as nucleation site for the conversion of aggregation-prone proteins into pathological isoforms. Further evidence for a connection between SGs and protein aggregates came from patient biopsies of several degenerative diseases that harbored protein inclusions containing SG components, suggesting SGs as the starting point of aggregate formation (Hackman et al., 2013; Liu-Yesucevitz et al., 2010). In cell culture, disease-associated mutations in RBPs were shown to alter SG dynamics and to delay SG disassembly (Mackenzie et al., 2017; Mateju et al., 2017). However, SG disassembly was only monitored for a few hours and as long as SGs persisted. If SGs were eventually disassembled or how the cell responded was not stated. In our experiments, prolonged or severe treatment with SG inducing drugs could not induce NM aggregates, but rather led to cell death. Although some SGs were still present after 24 h, the conversion of NM into its prion isoform was not triggered or was prevented. Interestingly, a

recent study argued against a conversion of persistent SGs into protein aggregates by showing that the cytoplasmic translocation of FUS is independent of SG assembly and that FUS can escape persistent SGs (Hock et al., 2018). Furthermore, they suggested that the nuclear import receptor TNPO1 might function as a chaperone to prevent aberrant phase transition of FUS. Additionally, several other studies showed that nuclear import receptors can function as chaperones to counteract aggregation of RBPs (Guo et al., 2018; Hofweber et al., 2018; Qamar et al., 2018; Yoshizawa et al., 2018). Hence, the cell has developed efficient ways to combat protein misfolding in SGs by the surveillance with chaperones and degradation of aberrant SGs by autophagy (Mateju et al., 2017). As in SGs aggregation-prone proteins are abundant, cells will monitor this process closely to keep proteins from aggregating or to remove and degrade misfolded proteins. Maybe SGs even sequester aggregation-prone proteins to keep them from aggregating during times of stress by holding them in one place that is closely monitored. Posttranslational modification enzymes are part of SGs and might play a part in regulating aggregation-prone proteins. Protein phosphorylation, methylation and glycosylation were already shown to influence SG assembly (Goulet et al., 2008; Ohn et al., 2008; Tourriere et al., 2003). For TDP-43 it has been suggested that its localization to SGs prevents stress-induced phosphorylation and the concomitant aggregation of TDP-43 (McGurk et al., 2018). However, aging might be a risk factor for membrane-less organelles. Aging leads to reduced autophagic activity, as shown by downregulation of some proteins involved in autophagy in the human brain (Lipinski et al., 2010). Impaired autophagy has already been implicated with several neurodegenerative diseases, including Alzheimer's disease, Parkinson's disease, and Huntington disease (Menzies et al., 2017; Menzies et al., 2015). Also in ALS, mutations in a range of autophagy related proteins have been identified that cause autophagic dysregulation (Gal et al., 2009; Shen et al., 2015; Teyssou et al., 2013). In cultured cells, mutations in VCP or inhibition of HSP70 led to reduced clearance of SGs, suggesting that an impaired protein degradation system can cause the persistence of SGs (Buchan et al., 2013; Mateju et al., 2017). Furthermore, posttranslational modifications influence SG assembly and disassembly. SG dissolution is promoted by phosphorylation of the SG protein Grb7 and the

activation of DYRK3 kinase (Tsai et al., 2008; Wippich et al., 2013). The casein kinase 2 (CK2) was shown to regulate SG disassembly by phosphorylating the key SG component G3BP (Reineke et al., 2017). Posttranslational modifications represent an additional and important factor in the regulation of SG disassembly. Hence, SG disassembly represents a complex mechanism that is influenced by multiple factors. Numerous modulations can lead to persistence of SGs, but the influence of persistent SGs on cells is not known. Our data suggest that persistent SGs rather trigger cell death than protein misfolding. SG formation comes along with a global translational arrest and influences multiple cellular functions by the sequestration of proteins. Furthermore, it is not known whether SGs actually play a role *in vivo*. Using hyperthermia to induce stress in live mice, neurons were shown to exhibit cytoplasmic foci positive for TIAR and mRNA, most likely representing SGs (Shelkovnikova et al., 2017). However, neurons failed to assemble SGs upon elevated levels of phosphorylated eIF2α due to mutant tau, suggesting that chronic phosphorylation of eIF2α is deleterious to neurons due to impaired SG integrity. Only few studies were conducted using primary cells, including neurons, astrocytes, and glia cells, showing that the SG response is variable dependent on the cell type and stress conditions (Dewey et al., 2011; Khalfallah et al., 2018; Shelkovnikova et al., 2017). Neurons failed to assemble SGs upon osmotic stress and were more resistant to SG induction by arsenite, indicating that neurons are refractory to a certain extent to stress (Khalfallah et al., 2018). By contrast, another study using organotypic brain slices showed that SGs were triggered in neurons upon oxidative and osmotic stress (Hock et al., 2018). The SG response seems to be very different depending on the cell type, the stress conditions or experimental setup, indicating that the stress response is a complex mechanism. Whether the CNS reacts to stress by formation of SGs remains to be further investigated.

4.6 SG induction increases NM aggregation by exogenous seeds

Prolonged presence of SGs did not induce the aggregation of NM in our experimental setup. However, NM aggregate induction by recombinant fibrils was drastically increased in cell populations that contained chemically induced SGs. NM aggregate formation efficiency correlated to a certain degree with the number

of cells harboring SGs. during addition of fibrils. Stress inducing drugs that did not result in SG formation, such as the ER stress inducers tunicamycin or thapsigargin, had only minor effects on aggregate formation. Surprisingly, genetic or chemical inhibition of SG formation had no effect on the increased NM aggregate induction, arguing that the increased concentration of NM within SGs is not the reason for higher aggregate formation. Inhibition of SG formation was accomplished by two different mechanisms: genetically by siRNA knockdown of a SG component that is important for SG assembly, or pharmacologically by PERK inhibition, which abolishes phosphorylation of eIF2α. Both efficiently inhibited SG formation, demonstrating that the increased NM aggregate induction is not dependent on SG assembly downstream of eIF2α phosphorylation. Also superresolution microscopy did not reveal SGs as nucleation sites for aggregate induction by exogenous seeds. However, the presence of small, microscopically undetectable SGs or SG precursors upon SG inhibition, or small aggregates originating from SGs, cannot be ruled out. Youn and coworkers argue that submicroscopic SGs are already present in unstressed cells to serve as seeds for a rapid SG assembly upon stress conditions (Youn et al., 2018). These seeds most likely represent mRNP particles, which would also be present upon SG inhibition and could affect NM aggregation during stress conditions. As SG inhibition targeted two different steps of SG assembly, the signal responsible for the increased aggregate induction rate has to be further upstream in the SG induction pathway. SG induction might lead to the activation of the PQC and the subsequent recruitment of chaperones to mRNP particles to assist SG formation. Upon concomitant aggregate induction, chaperones would be occupied and could not combat aggregate formation. Treatment with SG inducing agents might activate chaperones in a stress-dependent manner, without the need of transcription. In bacteria several stress-inducible chaperones have already been identified, which use unfolding or oxidation for activation, but only few eukaryotic chaperones are known that can be directly activated by stress (Voth and Jakob, 2017). Under non-stress conditions, these proteins most likely have a different function and only exhibit chaperone-like activities upon stress. A chaperone function has already been attributed to several nuclear import receptors, which keep proteins containing a nuclear localization signal from aggregating in the

cytosol (Guo et al., 2018; Hofweber et al., 2018; Qamar et al., 2018; Yoshizawa et al., 2018). Further investigations are needed to identify unknown chaperones and to elucidate the role of chaperones in response to SG induction.

4.7 The correlation between stress granules and protein aggregates

Some studies found SG proteins as part of pathological protein inclusions in patient biopsies, suggesting that protein inclusions are derived from SGs (Liu-Yesucevitz et al., 2010; Vanderweyde et al., 2012). In our study, NM prions also exhibited a similar interactome than SGs, indicating that both assemblies are somehow related. However, we could not show that NM aggregates were induced by SG induction or evolved out of SGs. SGs were also not observed during aggregate induction by recombinant fibrils. Hence, there must be another explanation for the sequestration of SG proteins to NM prions. SG proteins might be recruited to NM prions by interactions between their LCDs and the PrD of NM, as the PrD mediates binding to SGs. This might also be the case for protein inclusions of TDP-43 and FUS, which can be found in some cases of ALS and FTLD. Furthermore, SG proteins could be sequestered to inclusions by binding to RNA, which is part of protein aggregates. Hence, the presence of SG proteins in protein inclusions can be explained in several ways. Although many *in vitro* studies over the last years suggest an involvement of persistent SGs in the formation of protein aggregates, only very few studies investigate this hypothesis in cell culture or even *in vivo*. The cell has developed an effective PQC system that combats protein misfolding and will especially monitor processes, which involve regulated protein aggregation such as the formation of SGs. Sequestering aggregation-prone proteins in SGs upon stressful conditions might be a way to actually keep proteins from misfolding by holding them together for surveillance. However, a defective or overwhelmed PQC might not be able to counteract protein misfolding and aggregation. The concomitant induction of SGs and NM aggregates by recombinant fibrils led to a drastically increased formation of NM aggregates. As treatment with other stress inducing drugs that did not result in SG formation, did not have such a drastic effect on NM aggregate induction, there has to be something special about SG inducing treatments. One explanation would be the redirection of the PQC system towards SG formation, while

disregarding and thereby enabling the aggregation of NM. For aggregation of NM to occur, recombinant NM fibrils need to be taken up and seed the aggregation of endogenous NM proteins. Once recombinant fibrils enter the cytoplasm they are most likely recognized as misfolded proteins by the PQC, which will initiate their degradation, and only fibrils that escape degradation can successfully induce NM aggregation. During stressful conditions the PQC would be busy assisting SG formation, neglecting the degradation of recombinant fibrils and permitting NM aggregation. Hence, the connection between SGs and protein aggregates might be different than hypothesized, in a way that rather the SG induction pathway than the presence of SGs is important.

4.8 Relevance

Several RBPs that harbor putative PrLDs and are part of SGs have already been implicated in degenerative disorders and recruitment of these RBPs to SGs has been hypothesized to facilitate their aggregation. However, the hypothesis that SGs are involved in disease pathology is mainly based on *in vitro* studies and evidence is still missing. Over the last years, research has focused on the idea that SGs evolve into pathological protein aggregates, but if SGs might be involved in the disease process in a different way was neglected. In our experimental setting, we were unable to turn NM sequestered by SGs into aggregates. Prolonged SG inducing treatment rather resulted in cell death, raising the question whether persistent SGs actually play a role in the disease process. The physical presence of SGs was not required for the increased aggregate induction by exogenous NM seeds, suggesting that the SG induction pathway and/or PQC could be involved in aggregate formation. Stress-inducible chaperones might be a key player in the first line of defense against protein misfolding upon stressful conditions. Sequestering aggregation-prone proteins in SGs could be a way of the cell to keep them under surveillance. However, exogenous triggers for protein misfolding, such as exogenous seeds, might overburden the PQC machinery under SG inducing conditions, facilitating protein aggregation. The spreading of protein aggregates from cell to cell, as it occurs in many neurodegenerative diseases, might benefit from the microenvironment during SG induction. The concomitant higher seeding efficiency would represent a risk factor for disease

pathology. Therefore, investigating the role of chaperones and the PQC in the SG induction pathway is crucial to understand a possible involvement of SGs in disease pathology.

Bibliography

Alberti, S., R. Halfmann, O. King, A. Kapila, and S. Lindquist. 2009. A systematic survey identifies prions and illuminates sequence features of prionogenic proteins. *Cell*. 137:146-158.

Anderson, P., and N. Kedersha. 2006. RNA granules. *J Cell Biol*. 172:803-808.

Anderson, P., and N. Kedersha. 2008. Stress granules: the Tao of RNA triage. *Trends Biochem Sci*. 33:141-150.

Arai, T., M. Hasegawa, H. Akiyama, K. Ikeda, T. Nonaka, H. Mori, D. Mann, K. Tsuchiya, M. Yoshida, Y. Hashizume, and T. Oda. 2006. TDP-43 is a component of ubiquitin-positive tau-negative inclusions in frontotemporal lobar degeneration and amyotrophic lateral sclerosis. *Biochem Biophys Res Commun*. 351:602-611.

Arimoto-Matsuzaki, K., H. Saito, and M. Takekawa. 2016. TIA1 oxidation inhibits stress granule assembly and sensitizes cells to stress-induced apoptosis. *Nat Commun*. 7:10252.

Aulas, A., M.M. Fay, S.M. Lyons, C.A. Achorn, N. Kedersha, P. Anderson, and P. Ivanov. 2017. Stress-specific differences in assembly and composition of stress granules and related foci. *J Cell Sci*. 130:927-937.

Aulas, A., and C. Vande Velde. 2015. Alterations in stress granule dynamics driven by TDP-43 and FUS: a link to pathological inclusions in ALS? *Front Cell Neurosci*. 9:423.

Bentmann, E., M. Neumann, S. Tahirovic, R. Rodde, D. Dormann, and C. Haass. 2012. Requirements for stress granule recruitment of fused in sarcoma (FUS) and TAR DNA-binding protein of 43 kDa (TDP-43). *J Biol Chem*. 287:23079-23094.

Bevilacqua, E., X. Wang, M. Majumder, F. Gaccioli, C.L. Yuan, C. Wang, X. Zhu, L.E. Jordan, D. Scheuner, R.J. Kaufman, A.E. Koromilas, M.D. Snider, M. Holcik, and M. Hatzoglou. 2010. eIF2alpha phosphorylation tips the balance to apoptosis during osmotic stress. *J Biol Chem*. 285:17098-17111.

Bjorkoy, G., T. Lamark, S. Pankiv, A. Overvatn, A. Brech, and T. Johansen. 2009. Monitoring autophagic degradation of p62/SQSTM1. *Methods Enzymol*. 452:181-197.

Bley, N., M. Lederer, B. Pfalz, C. Reinke, T. Fuchs, M. Glass, B. Moller, and S. Huttelmaier. 2015. Stress granules are dispensable for mRNA stabilization during cellular stress. *Nucleic Acids Res*. 43:e26.

Boeynaems, S., S. Alberti, N.L. Fawzi, T. Mittag, M. Polymenidou, F. Rousseau, J. Schymkowitz, J. Shorter, B. Wolozin, L. Van Den Bosch, P. Tompa, and M. Fuxreiter. 2018. Protein Phase Separation: A New Phase in Cell Biology. *Trends Cell Biol*. 28:420-435.

Bolton, D.C., M.P. McKinley, and S.B. Prusiner. 1982. Identification of a protein that purifies with the scrapie prion. *Science*. 218:1309-1311.

Bosco, D.A., N. Lemay, H.K. Ko, H. Zhou, C. Burke, T.J. Kwiatkowski, Jr., P. Sapp, D. McKenna-Yasek, R.H. Brown, Jr., and L.J. Hayward. 2010. Mutant FUS proteins that cause amyotrophic lateral sclerosis incorporate into stress granules. *Hum Mol Genet*. 19:4160-4175.

Bounedjah, O., B. Desforges, T.D. Wu, C. Pioche-Durieu, S. Marco, L. Hamon, P.A. Curmi, J.L. Guerquin-Kern, O. Pietrement, and D. Pastre. 2014. Free mRNA in excess upon polysome dissociation is a scaffold for protein multimerization to form stress granules. *Nucleic Acids Res*. 42:8678-8691.

Bounedjah, O., L. Hamon, P. Savarin, B. Desforges, P.A. Curmi, and D. Pastre. 2012. Macromolecular crowding regulates assembly of mRNA stress granules after osmotic stress: new role for compatible osmolytes. *J Biol Chem*. 287:2446-2458.

Brangwynne, C.P., C.R. Eckmann, D.S. Courson, A. Rybarska, C. Hoege, J. Gharakhani, F. Julicher, and A.A. Hyman. 2009. Germline P granules are liquid droplets that localize by controlled dissolution/condensation. *Science*. 324:1729-1732.

Brangwynne, C.P., T.J. Mitchison, and A.A. Hyman. 2011. Active liquid-like behavior of nucleoli determines their size and shape in Xenopus laevis oocytes. *Proc Natl Acad Sci U S A*. 108:4334-4339.

Brundin, P., R. Melki, and R. Kopito. 2010. Prion-like transmission of protein aggregates in neurodegenerative diseases. *Nat Rev Mol Cell Biol*. 11:301-307.

Buchan, J.R., R.M. Kolaitis, J.P. Taylor, and R. Parker. 2013. Eukaryotic stress granules are cleared by autophagy and Cdc48/VCP function. *Cell*. 153:1461-1474.

Buchan, J.R., and R. Parker. 2009. Eukaryotic stress granules: the ins and outs of translation. *Mol Cell*. 36:932-941.

Carpenter, A.E., T.R. Jones, M.R. Lamprecht, C. Clarke, I.H. Kang, O. Friman, D.A. Guertin, J.H. Chang, R.A. Lindquist, J. Moffat, P. Golland, and D.M. Sabatini. 2006. CellProfiler: image analysis software for identifying and quantifying cell phenotypes. *Genome Biol*. 7:R100.

Castello, A., B. Fischer, K. Eichelbaum, R. Horos, B.M. Beckmann, C. Strein, N.E. Davey, D.T. Humphreys, T. Preiss, L.M. Steinmetz, J. Krijgsveld, and M.W. Hentze. 2012. Insights into RNA biology from an atlas of mammalian mRNA-binding proteins. *Cell*. 149:1393-1406.

Caughey, B., D.A. Kocisko, G.J. Raymond, and P.T. Lansbury, Jr. 1995. Aggregates of scrapie-associated prion protein induce the cell-free conversion of protease-sensitive prion protein to the protease-resistant state. *Chem Biol*. 2:807-817.

Cha-Molstad, H., K.S. Sung, J. Hwang, K.A. Kim, J.E. Yu, Y.D. Yoo, J.M. Jang, D.H. Han, M. Molstad, J.G. Kim, Y.J. Lee, A. Zakrzewska, S.H. Kim, S.T. Kim, S.Y. Kim, H.G. Lee, N.K. Soung, J.S. Ahn, A. Ciechanover, B.Y. Kim, and Y.T. Kwon. 2015. Amino-terminal arginylation targets endoplasmic reticulum chaperone BiP for autophagy through p62 binding. *Nat Cell Biol*. 17:917-929.

Chen-Plotkin, A.S., V.M. Lee, and J.Q. Trojanowski. 2010. TAR DNA-binding protein 43 in neurodegenerative disease. *Nat Rev Neurol*. 6:211-220.

Cheng, W., S. Wang, A.A. Mestre, C. Fu, A. Makarem, F. Xian, L.R. Hayes, R. Lopez-Gonzalez, K. Drenner, J. Jiang, D.W. Cleveland, and S. Sun. 2018. C9ORF72 GGGGCC repeat-associated non-AUG translation is upregulated by stress through eIF2alpha phosphorylation. *Nat Commun*. 9:51.

Chernoff, Y.O., S.L. Lindquist, B. Ono, S.G. Inge-Vechtomov, and S.W. Liebman. 1995. Role of the chaperone protein Hsp104 in propagation of the yeast prion-like factor [psi+]. *Science*. 268:880-884.

Chiti, F., and C.M. Dobson. 2006. Protein misfolding, functional amyloid, and human disease. *Annu Rev Biochem*. 75:333-366.

Clemens, M.J. 2001. Initiation factor eIF2 alpha phosphorylation in stress responses and apoptosis. *Prog Mol Subcell Biol*. 27:57-89.

Come, J.H., P.E. Fraser, and P.T. Lansbury, Jr. 1993. A kinetic model for amyloid formation in the prion diseases: importance of seeding. *Proc Natl Acad Sci U S A*. 90:5959-5963.

Coustou, V., C. Deleu, S. Saupe, and J. Begueret. 1997. The protein product of the het-s heterokaryon incompatibility gene of the fungus Podospora anserina behaves as a prion analog. *Proc Natl Acad Sci U S A*. 94:9773-9778.

Couthouis, J., M.P. Hart, J. Shorter, M. DeJesus-Hernandez, R. Erion, R. Oristano, A.X. Liu, D. Ramos, N. Jethava, D. Hosangadi, J. Epstein, A. Chiang, Z. Diaz, T. Nakaya, F. Ibrahim, H.J. Kim, J.A. Solski, K.L. Williams, J. Mojsilovic-Petrovic, C. Ingre, K. Boylan, N.R. Graff-Radford, D.W. Dickson, D. Clay-Falcone, L. Elman, L. McCluskey, R. Greene, R.G. Kalb, V.M. Lee, J.Q. Trojanowski, A. Ludolph, W. Robberecht, P.M. Andersen, G.A. Nicholson, I.P. Blair, O.D. King, N.M. Bonini, V. Van Deerlin, R. Rademakers, Z. Mourelatos, and A.D. Gitler. 2011. A yeast

functional screen predicts new candidate ALS disease genes. *Proc Natl Acad Sci U S A*. 108:20881-20890.

Cox, B.S., M.F. Tuite, and C.S. McLaughlin. 1988. The psi factor of yeast: a problem in inheritance. *Yeast*. 4:159-178.

Cox, J., M.Y. Hein, C.A. Luber, I. Paron, N. Nagaraj, and M. Mann. 2014. Accurate proteome-wide label-free quantification by delayed normalization and maximal peptide ratio extraction, termed MaxLFQ. *Mol Cell Proteomics*. 13:2513-2526.

de Calignon, A., M. Polydoro, M. Suarez-Calvet, C. William, D.H. Adamowicz, K.J. Kopeikina, R. Pitstick, N. Sahara, K.H. Ashe, G.A. Carlson, T.L. Spires-Jones, and B.T. Hyman. 2012. Propagation of tau pathology in a model of early Alzheimer's disease. *Neuron*. 73:685-697.

Deleault, N.R., R.W. Lucassen, and S. Supattapone. 2003. RNA molecules stimulate prion protein conversion. *Nature*. 425:717-720.

DePace, A.H., A. Santoso, P. Hillner, and J.S. Weissman. 1998. A critical role for amino-terminal glutamine/asparagine repeats in the formation and propagation of a yeast prion. *Cell*. 93:1241-1252.

Derkatch, I.L., Y.O. Chernoff, V.V. Kushnirov, S.G. Inge-Vechtomov, and S.W. Liebman. 1996. Genesis and variability of [PSI] prion factors in Saccharomyces cerevisiae. *Genetics*. 144:1375-1386.

Dewey, C.M., B. Cenik, C.F. Sephton, D.R. Dries, P. Mayer, 3rd, S.K. Good, B.A. Johnson, J. Herz, and G. Yu. 2011. TDP-43 is directed to stress granules by sorbitol, a novel physiological osmotic and oxidative stressor. *Mol Cell Biol*. 31:1098-1108.

Doi, H., S. Koyano, Y. Suzuki, N. Nukina, and Y. Kuroiwa. 2010. The RNA-binding protein FUS/TLS is a common aggregate-interacting protein in polyglutamine diseases. *Neurosci Res*. 66:131-133.

Dormann, D., R. Rodde, D. Edbauer, E. Bentmann, I. Fischer, A. Hruscha, M.E. Than, I.R. Mackenzie, A. Capell, B. Schmid, M. Neumann, and C. Haass. 2010. ALS-associated fused in sarcoma (FUS) mutations disrupt Transportin-mediated nuclear import. *EMBO J*. 29:2841-2857.

Duernberger, Y., S. Liu, K. Riemschoss, L. Paulsen, R. Bester, P.H. Kuhn, M. Scholling, S.F. Lichtenthaler, and I. Vorberg. 2018. Prion replication in the mammalian cytosol: Functional regions within a prion domain driving induction, propagation and inheritance. *Mol Cell Biol*.

Fortun, J., W.A. Dunn, Jr., S. Joy, J. Li, and L. Notterpek. 2003. Emerging role for autophagy in the removal of aggresomes in Schwann cells. *J Neurosci*. 23:10672-10680.

Gal, J., A.L. Strom, D.M. Kwinter, R. Kilty, J. Zhang, P. Shi, W. Fu, M.W. Wooten, and H. Zhu. 2009. Sequestosome 1/p62 links familial ALS mutant SOD1 to LC3 via an ubiquitin-independent mechanism. *J Neurochem*. 111:1062-1073.

Ganassi, M., D. Mateju, I. Bigi, L. Mediani, I. Poser, H.O. Lee, S.J. Seguin, F.F. Morelli, J. Vinet, G. Leo, O. Pansarasa, C. Cereda, A. Poletti, S. Alberti, and S. Carra. 2016. A Surveillance Function of the HSPB8-BAG3-HSP70 Chaperone Complex Ensures Stress Granule Integrity and Dynamism. *Mol Cell*. 63:796-810.

Geser, F., M. Martinez-Lage, J. Robinson, K. Uryu, M. Neumann, N.J. Brandmeir, S.X. Xie, L.K. Kwong, L. Elman, L. McCluskey, C.M. Clark, J. Malunda, B.L. Miller, E.A. Zimmerman, J. Qian, V. Van Deerlin, M. Grossman, V.M. Lee, and J.Q. Trojanowski. 2009. Clinical and pathological continuum of multisystem TDP-43 proteinopathies. *Arch Neurol*. 66:180-189.

Gilks, N., N. Kedersha, M. Ayodele, L. Shen, G. Stoecklin, L.M. Dember, and P. Anderson. 2004. Stress granule assembly is mediated by prion-like aggregation of TIA-1. *Mol Biol Cell*. 15:5383-5398.

Goedert, M., F. Clavaguera, and M. Tolnay. 2010. The propagation of prion-like protein inclusions in neurodegenerative diseases. *Trends Neurosci*. 33:317-325.

Goulet, I., S. Boisvenue, S. Mokas, R. Mazroui, and J. Cote. 2008. TDRD3, a novel Tudor domain-containing protein, localizes to cytoplasmic stress granules. *Hum Mol Genet*. 17:3055-3074.

Gunawardana, C.G., M. Mehrabian, X. Wang, I. Mueller, I.B. Lubambo, J.E. Jonkman, H. Wang, and G. Schmitt-Ulms. 2015. The Human Tau Interactome: Binding to the Ribonucleoproteome, and Impaired Binding of the Proline-to-Leucine Mutant at Position 301 (P301L) to Chaperones and the Proteasome. *Mol Cell Proteomics*. 14:3000-3014.

Guo, L., H.J. Kim, H. Wang, J. Monaghan, F. Freyermuth, J.C. Sung, K. O'Donovan, C.M. Fare, Z. Diaz, N. Singh, Z.C. Zhang, M. Coughlin, E.A. Sweeny, M.E. DeSantis, M.E. Jackrel, C.B. Rodell, J.A. Burdick, O.D. King, A.D. Gitler, C. Lagier-Tourenne, U.B. Pandey, Y.M. Chook, J.P. Taylor, and J. Shorter. 2018. Nuclear-Import Receptors Reverse Aberrant Phase Transitions of RNA-Binding Proteins with Prion-like Domains. *Cell*. 173:677-692 e620.

Hackman, P., J. Sarparanta, S. Lehtinen, A. Vihola, A. Evila, P.H. Jonson, H. Luque, J. Kere, M. Screen, P.F. Chinnery, G. Ahlberg, L. Edstrom, and B. Udd. 2013. Welander distal myopathy is caused by a mutation in the RNA-binding protein TIA1. *Ann Neurol*. 73:500-509.

Hershey, J.W. 1991. Translational control in mammalian cells. *Annu Rev Biochem*. 60:717-755.

Hock, E.M., Z. Maniecka, M. Hruska-Plochan, S. Reber, F. Laferriere, M.K.S. Sahadevan, H. Ederle, L. Gittings, L. Pelkmans, L. Dupuis, T. Lashley, M.D. Ruepp, D. Dormann, and M. Polymenidou. 2018. Hypertonic Stress Causes Cytoplasmic Translocation of Neuronal, but Not Astrocytic, FUS due to Impaired Transportin Function. *Cell Rep*. 24:987-1000 e1007.

Hofmann, J.P., P. Denner, C. Nussbaum-Krammer, P.H. Kuhn, M.H. Suhre, T. Scheibel, S.F. Lichtenthaler, H.M. Schatzl, D. Bano, and I.M. Vorberg. 2013. Cell-to-cell propagation of infectious cytosolic protein aggregates. *Proc Natl Acad Sci U S A*. 110:5951-5956.

Hofweber, M., S. Hutten, B. Bourgeois, E. Spreitzer, A. Niedner-Boblenz, M. Schifferer, M.D. Ruepp, M. Simons, D. Niessing, T. Madl, and D. Dormann. 2018. Phase Separation of FUS Is Suppressed by Its Nuclear Import Receptor and Arginine Methylation. *Cell*. 173:706-719 e713.

Hyman, A.A., C.A. Weber, and F. Julicher. 2014. Liquid-liquid phase separation in biology. *Annu Rev Cell Dev Biol*. 30:39-58.

Iko, Y., T.S. Kodama, N. Kasai, T. Oyama, E.H. Morita, T. Muto, M. Okumura, R. Fujii, T. Takumi, S. Tate, and K. Morikawa. 2004. Domain architectures and characterization of an RNA-binding protein, TLS. *J Biol Chem*. 279:44834-44840.

Jain, S., J.R. Wheeler, R.W. Walters, A. Agrawal, A. Barsic, and R. Parker. 2016. ATPase-Modulated Stress Granules Contain a Diverse Proteome and Substructure. *Cell*. 164:487-498.

Jarrett, J.T., and P.T. Lansbury, Jr. 1993. Seeding "one-dimensional crystallization" of amyloid: a pathogenic mechanism in Alzheimer's disease and scrapie? *Cell*. 73:1055-1058.

Jarvelin, A.I., M. Noerenberg, I. Davis, and A. Castello. 2016. The new (dis)order in RNA regulation. *Cell Commun Signal*. 14:9.

Jiang, H.Y., and R.C. Wek. 2005. Phosphorylation of the alpha-subunit of the eukaryotic initiation factor-2 (eIF2alpha) reduces protein synthesis and enhances apoptosis in response to proteasome inhibition. *J Biol Chem*. 280:14189-14202.

Johnson, B.S., D. Snead, J.J. Lee, J.M. McCaffery, J. Shorter, and A.D. Gitler. 2009. TDP-43 is intrinsically aggregation-prone, and amyotrophic lateral sclerosis-linked mutations accelerate aggregation and increase toxicity. *J Biol Chem*. 284:20329-20339.

Johnston, J.A., C.L. Ward, and R.R. Kopito. 1998. Aggresomes: a cellular response to misfolded proteins. *J Cell Biol*. 143:1883-1898.

Kampers, T., P. Friedhoff, J. Biernat, E.M. Mandelkow, and E. Mandelkow. 1996. RNA stimulates aggregation of microtubule-associated protein tau into Alzheimer-like paired helical filaments. *FEBS Lett*. 399:344-349.

Kedersha, N., and P. Anderson. 2002. Stress granules: sites of mRNA triage that regulate mRNA stability and translatability. *Biochem Soc Trans*. 30:963-969.

Kedersha, N., and P. Anderson. 2007. Mammalian stress granules and processing bodies. *Methods Enzymol*. 431:61-81.

Kedersha, N., S. Chen, N. Gilks, W. Li, I.J. Miller, J. Stahl, and P. Anderson. 2002. Evidence that ternary complex (eIF2-GTP-tRNA(i)(Met))-deficient preinitiation complexes are core constituents of mammalian stress granules. *Mol Biol Cell*. 13:195-210.

Kedersha, N., M.R. Cho, W. Li, P.W. Yacono, S. Chen, N. Gilks, D.E. Golan, and P. Anderson. 2000. Dynamic shuttling of TIA-1 accompanies the recruitment of mRNA to mammalian stress granules. *J Cell Biol*. 151:1257-1268.

Kedersha, N., M.D. Panas, C.A. Achorn, S. Lyons, S. Tisdale, T. Hickman, M. Thomas, J. Lieberman, G.M. McInerney, P. Ivanov, and P. Anderson. 2016. G3BP-Caprin1-USP10 complexes mediate stress granule condensation and associate with 40S subunits. *J Cell Biol*. 212:845-860.

Kedersha, N., G. Stoecklin, M. Ayodele, P. Yacono, J. Lykke-Andersen, M.J. Fritzler, D. Scheuner, R.J. Kaufman, D.E. Golan, and P. Anderson. 2005. Stress granules and processing bodies are dynamically linked sites of mRNP remodeling. *J Cell Biol*. 169:871-884.

Kedersha, N.L., M. Gupta, W. Li, I. Miller, and P. Anderson. 1999. RNA-binding proteins TIA-1 and TIAR link the phosphorylation of eIF-2 alpha to the assembly of mammalian stress granules. *J Cell Biol*. 147:1431-1442.

Khalfallah, Y., R. Kuta, C. Grasmuck, A. Prat, H.D. Durham, and C. Vande Velde. 2018. TDP-43 regulation of stress granule dynamics in neurodegenerative disease-relevant cell types. *Sci Rep*. 8:7551.

Khong, A., T. Matheny, S. Jain, S.F. Mitchell, J.R. Wheeler, and R. Parker. 2017. The Stress Granule Transcriptome Reveals Principles of mRNA Accumulation in Stress Granules. *Mol Cell*. 68:808-820 e805.

Kim, H.J., N.C. Kim, Y.D. Wang, E.A. Scarborough, J. Moore, Z. Diaz, K.S. MacLea, B. Freibaum, S. Li, A. Molliex, A.P. Kanagaraj, R. Carter, K.B. Boylan, A.M. Wojtas, R. Rademakers, J.L. Pinkus, S.A. Greenberg, J.Q. Trojanowski, B.J. Traynor, B.N. Smith, S. Topp, A.S. Gkazi, J. Miller, C.E. Shaw, M. Kottlors, J. Kirschner, A. Pestronk, Y.R. Li, A.F. Ford, A.D. Gitler, M. Benatar, O.D. King, V.E. Kimonis, E.D. Ross, C.C. Weihl, J. Shorter, and J.P. Taylor. 2013. Mutations in prion-like domains in hnRNPA2B1 and hnRNPA1 cause multisystem proteinopathy and ALS. *Nature*. 495:467-473.

King, C.Y., and R. Diaz-Avalos. 2004. Protein-only transmission of three yeast prion strains. *Nature*. 428:319-323.

King, O.D., A.D. Gitler, and J. Shorter. 2012. The tip of the iceberg: RNA-binding proteins with prion-like domains in neurodegenerative disease. *Brain Res*. 1462:61-80.

Klus, P., B. Bolognesi, F. Agostini, D. Marchese, A. Zanzoni, and G.G. Tartaglia. 2014. The cleverSuite approach for protein characterization: predictions of structural properties, solubility, chaperone requirements and RNA-binding abilities. *Bioinformatics*. 30:1601-1608.

Knowles, T.P., C.A. Waudby, G.L. Devlin, S.I. Cohen, A. Aguzzi, M. Vendruscolo, E.M. Terentjev, M.E. Welland, and C.M. Dobson. 2009. An analytical solution to the kinetics of breakable filament assembly. *Science*. 326:1533-1537.

Krammer, C., D. Kryndushkin, M.H. Suhre, E. Kremmer, A. Hofmann, A. Pfeifer, T. Scheibel, R.B. Wickner, H.M. Schatzl, and I. Vorberg. 2009. The yeast Sup35NM

domain propagates as a prion in mammalian cells. *Proc Natl Acad Sci U S A*. 106:462-467.

Kroschwald, S., S. Maharana, D. Mateju, L. Malinovska, E. Nuske, I. Poser, D. Richter, and S. Alberti. 2015. Promiscuous interactions and protein disaggregases determine the material state of stress-inducible RNP granules. *Elife*. 4:e06807.

Kryndushkin, D.S., I.M. Alexandrov, M.D. Ter-Avanesyan, and V.V. Kushnirov. 2003. Yeast [PSI+] prion aggregates are formed by small Sup35 polymers fragmented by Hsp104. *J Biol Chem*. 278:49636-49643.

Kushnirov, V.V., D.S. Kryndushkin, M. Boguta, V.N. Smirnov, and M.D. Ter-Avanesyan. 2000. Chaperones that cure yeast artificial [PSI+] and their prion-specific effects. *Curr Biol*. 10:1443-1446.

Lee, K.H., P. Zhang, H.J. Kim, D.M. Mitrea, M. Sarkar, B.D. Freibaum, J. Cika, M. Coughlin, J. Messing, A. Molliex, B.A. Maxwell, N.C. Kim, J. Temirov, J. Moore, R.M. Kolaitis, T.I. Shaw, B. Bai, J. Peng, R.W. Kriwacki, and J.P. Taylor. 2016. C9orf72 Dipeptide Repeats Impair the Assembly, Dynamics, and Function of Membrane-Less Organelles. *Cell*. 167:774-788 e717.

Li, L., and S. Lindquist. 2000. Creating a protein-based element of inheritance. *Science*. 287:661-664.

Li, P., S. Banjade, H.C. Cheng, S. Kim, B. Chen, L. Guo, M. Llaguno, J.V. Hollingsworth, D.S. King, S.F. Banani, P.S. Russo, Q.X. Jiang, B.T. Nixon, and M.K. Rosen. 2012. Phase transitions in the assembly of multivalent signalling proteins. *Nature*. 483:336-340.

Li, Y.R., O.D. King, J. Shorter, and A.D. Gitler. 2013. Stress granules as crucibles of ALS pathogenesis. *J Cell Biol*. 201:361-372.

Lipinski, M.M., B. Zheng, T. Lu, Z. Yan, B.F. Py, A. Ng, R.J. Xavier, C. Li, B.A. Yankner, C.R. Scherzer, and J. Yuan. 2010. Genome-wide analysis reveals mechanisms modulating autophagy in normal brain aging and in Alzheimer's disease. *Proc Natl Acad Sci U S A*. 107:14164-14169.

Liu, J.J., N. Sondheimer, and S.L. Lindquist. 2002. Changes in the middle region of Sup35 profoundly alter the nature of epigenetic inheritance for the yeast prion [PSI+]. *Proc Natl Acad Sci U S A*. 99 Suppl 4:16446-16453.

Liu-Yesucevitz, L., A. Bilgutay, Y.J. Zhang, T. Vanderweyde, A. Citro, T. Mehta, N. Zaarur, A. McKee, R. Bowser, M. Sherman, L. Petrucelli, and B. Wolozin. 2010. Tar DNA binding protein-43 (TDP-43) associates with stress granules: analysis of cultured cells and pathological brain tissue. *PLoS One*. 5:e13250.

Mackenzie, I.R., A.M. Nicholson, M. Sarkar, J. Messing, M.D. Purice, C. Pottier, K. Annu, M. Baker, R.B. Perkerson, A. Kurti, B.J. Matchett, T. Mittag, J. Temirov, G.R. Hsiung, C. Krieger, M.E. Murray, M. Kato, J.D. Fryer, L. Petrucelli, L. Zinman, S. Weintraub, M. Mesulam, J. Keith, S.A. Zivkovic, V. Hirsch-Reinshagen, R.P. Roos, S. Zuchner, N.R. Graff-Radford, R.C. Petersen, R.J. Caselli, Z.K. Wszolek, E. Finger, C. Lippa, D. Lacomis, H. Stewart, D.W. Dickson, H.J. Kim, E. Rogaeva, E. Bigio, K.B. Boylan, J.P. Taylor, and R. Rademakers. 2017. TIA1 Mutations in Amyotrophic Lateral Sclerosis and Frontotemporal Dementia Promote Phase Separation and Alter Stress Granule Dynamics. *Neuron*. 95:808-816 e809.

Mackenzie, I.R., R. Rademakers, and M. Neumann. 2010. TDP-43 and FUS in amyotrophic lateral sclerosis and frontotemporal dementia. *Lancet Neurol*. 9:995-1007.

March, Z.M., O.D. King, and J. Shorter. 2016. Prion-like domains as epigenetic regulators, scaffolds for subcellular organization, and drivers of neurodegenerative disease. *Brain Res*. 1647:9-18.

Markmiller, S., S. Soltanieh, K.L. Server, R. Mak, W. Jin, M.Y. Fang, E.C. Luo, F. Krach, D. Yang, A. Sen, A. Fulzele, J.M. Wozniak, D.J. Gonzalez, M.W. Kankel, F.B. Gao, E.J. Bennett, E. Lecuyer, and G.W. Yeo. 2018. Context-Dependent and

Disease-Specific Diversity in Protein Interactions within Stress Granules. *Cell*. 172:590-604 e513.

Masuda-Suzukake, M., T. Nonaka, M. Hosokawa, T. Oikawa, T. Arai, H. Akiyama, D.M. Mann, and M. Hasegawa. 2013. Prion-like spreading of pathological alpha-synuclein in brain. *Brain*. 136:1128-1138.

Mateju, D., T.M. Franzmann, A. Patel, A. Kopach, E.E. Boczek, S. Maharana, H.O. Lee, S. Carra, A.A. Hyman, and S. Alberti. 2017. An aberrant phase transition of stress granules triggered by misfolded protein and prevented by chaperone function. *EMBO J*. 36:1669-1687.

Matsuki, H., M. Takahashi, M. Higuchi, G.N. Makokha, M. Oie, and M. Fujii. 2013. Both G3BP1 and G3BP2 contribute to stress granule formation. *Genes Cells*. 18:135-146.

Mazroui, R., S. Di Marco, R.J. Kaufman, and I.E. Gallouzi. 2007. Inhibition of the ubiquitin-proteasome system induces stress granule formation. *Mol Biol Cell*. 18:2603-2618.

McGlinchey, R.P., D. Kryndushkin, and R.B. Wickner. 2011. Suicidal [PSI+] is a lethal yeast prion. *Proc Natl Acad Sci U S A*. 108:5337-5341.

McGurk, L., E. Gomes, L. Guo, J. Mojsilovic-Petrovic, V. Tran, R.G. Kalb, J. Shorter, and N.M. Bonini. 2018. Poly(ADP-Ribose) Prevents Pathological Phase Separation of TDP-43 by Promoting Liquid Demixing and Stress Granule Localization. *Mol Cell*.

McInerney, G.M., N.L. Kedersha, R.J. Kaufman, P. Anderson, and P. Liljestrom. 2005. Importance of eIF2alpha phosphorylation and stress granule assembly in alphavirus translation regulation. *Mol Biol Cell*. 16:3753-3763.

Menzies, F.M., A. Fleming, A. Caricasole, C.F. Bento, S.P. Andrews, A. Ashkenazi, J. Fullgrabe, A. Jackson, M. Jimenez Sanchez, C. Karabiyik, F. Licitra, A. Lopez Ramirez, M. Pavel, C. Puri, M. Renna, T. Ricketts, L. Schlotawa, M. Vicinanza, H. Won, Y. Zhu, J. Skidmore, and D.C. Rubinsztein. 2017. Autophagy and Neurodegeneration: Pathogenic Mechanisms and Therapeutic Opportunities. *Neuron*. 93:1015-1034.

Menzies, F.M., A. Fleming, and D.C. Rubinsztein. 2015. Compromised autophagy and neurodegenerative diseases. *Nat Rev Neurosci*. 16:345-357.

Michelitsch, M.D., and J.S. Weissman. 2000. A census of glutamine/asparagine-rich regions: implications for their conserved function and the prediction of novel prions. *Proc Natl Acad Sci U S A*. 97:11910-11915.

Molliex, A., J. Temirov, J. Lee, M. Coughlin, A.P. Kanagaraj, H.J. Kim, T. Mittag, and J.P. Taylor. 2015. Phase separation by low complexity domains promotes stress granule assembly and drives pathological fibrillization. *Cell*. 163:123-133.

Neumann, M., S. Roeber, H.A. Kretzschmar, R. Rademakers, M. Baker, and I.R. Mackenzie. 2009. Abundant FUS-immunoreactive pathology in neuronal intermediate filament inclusion disease. *Acta Neuropathol*. 118:605-616.

Neumann, M., D.M. Sampathu, L.K. Kwong, A.C. Truax, M.C. Micsenyi, T.T. Chou, J. Bruce, T. Schuck, M. Grossman, C.M. Clark, L.F. McCluskey, B.L. Miller, E. Masliah, I.R. Mackenzie, H. Feldman, W. Feiden, H.A. Kretzschmar, J.Q. Trojanowski, and V.M. Lee. 2006. Ubiquitinated TDP-43 in frontotemporal lobar degeneration and amyotrophic lateral sclerosis. *Science*. 314:130-133.

Nixon, R.A. 2013. The role of autophagy in neurodegenerative disease. *Nat Med*. 19:983-997.

Nott, T.J., E. Petsalaki, P. Farber, D. Jervis, E. Fussner, A. Plochowietz, T.D. Craggs, D.P. Bazett-Jones, T. Pawson, J.D. Forman-Kay, and A.J. Baldwin. 2015. Phase transition of a disordered nuage protein generates environmentally responsive membraneless organelles. *Mol Cell*. 57:936-947.

O'Nuallain, B., A.D. Williams, P. Westermark, and R. Wetzel. 2004. Seeding specificity in amyloid growth induced by heterologous fibrils. *J Biol Chem*. 279:17490-17499.

Ohn, T., N. Kedersha, T. Hickman, S. Tisdale, and P. Anderson. 2008. A functional RNAi screen links O-GlcNAc modification of ribosomal proteins to stress granule and processing body assembly. *Nat Cell Biol*. 10:1224-1231.

Oldfield, C.J., and A.K. Dunker. 2014. Intrinsically disordered proteins and intrinsically disordered protein regions. *Annu Rev Biochem*. 83:553-584.

Orgel, L.E. 1996. Prion replication and secondary nucleation. *Chem Biol*. 3:413-414.

Osherovich, L.Z., B.S. Cox, M.F. Tuite, and J.S. Weissman. 2004. Dissection and design of yeast prions. *PLoS Biol*. 2:E86.

Parham, S.N., C.G. Resende, and M.F. Tuite. 2001. Oligopeptide repeats in the yeast protein Sup35p stabilize intermolecular prion interactions. *EMBO J*. 20:2111-2119.

Parker, R., and U. Sheth. 2007. P bodies and the control of mRNA translation and degradation. *Mol Cell*. 25:635-646.

Patel, A., H.O. Lee, L. Jawerth, S. Maharana, M. Jahnel, M.Y. Hein, S. Stoynov, J. Mahamid, S. Saha, T.M. Franzmann, A. Pozniakovski, I. Poser, N. Maghelli, L.A. Royer, M. Weigert, E.W. Myers, S. Grill, D. Drechsel, A.A. Hyman, and S. Alberti. 2015. A Liquid-to-Solid Phase Transition of the ALS Protein FUS Accelerated by Disease Mutation. *Cell*. 162:1066-1077.

Patel, S.S., B.J. Belmont, J.M. Sante, and M.F. Rexach. 2007. Natively unfolded nucleoporins gate protein diffusion across the nuclear pore complex. *Cell*. 129:83-96.

Paul, K.R., C.G. Hendrich, A. Waechter, M.R. Harman, and E.D. Ross. 2015. Generating new prions by targeted mutation or segment duplication. *Proc Natl Acad Sci U S A*. 112:8584-8589.

Poser, I., M. Sarov, J.R. Hutchins, J.K. Heriche, Y. Toyoda, A. Pozniakovsky, D. Weigl, A. Nitzsche, B. Hegemann, A.W. Bird, L. Pelletier, R. Kittler, S. Hua, R. Naumann, M. Augsburg, M.M. Sykora, H. Hofemeister, Y. Zhang, K. Nasmyth, K.P. White, S. Dietzel, K. Mechtler, R. Durbin, A.F. Stewart, J.M. Peters, F. Buchholz, and A.A. Hyman. 2008. BAC TransgeneOmics: a high-throughput method for exploration of protein function in mammals. *Nat Methods*. 5:409-415.

Protter, D.S., and R. Parker. 2016. Principles and Properties of Stress Granules. *Trends Cell Biol*. 26:668-679.

Prusiner, S.B. 1982. Novel proteinaceous infectious particles cause scrapie. *Science*. 216:136-144.

Qamar, S., G. Wang, S.J. Randle, F.S. Ruggeri, J.A. Varela, J.Q. Lin, E.C. Phillips, A. Miyashita, D. Williams, F. Strohl, W. Meadows, R. Ferry, V.J. Dardov, G.G. Tartaglia, L.A. Farrer, G.S. Kaminski Schierle, C.F. Kaminski, C.E. Holt, P.E. Fraser, G. Schmitt-Ulms, D. Klenerman, T. Knowles, M. Vendruscolo, and P. St George-Hyslop. 2018. FUS Phase Separation Is Modulated by a Molecular Chaperone and Methylation of Arginine Cation-pi Interactions. *Cell*. 173:720-734 e715.

Ramaswami, M., J.P. Taylor, and R. Parker. 2013. Altered ribostasis: RNA-protein granules in degenerative disorders. *Cell*. 154:727-736.

Reineke, L.C., W.C. Tsai, A. Jain, J.T. Kaelber, S.Y. Jung, and R.E. Lloyd. 2017. Casein Kinase 2 Is Linked to Stress Granule Dynamics through Phosphorylation of the Stress Granule Nucleating Protein G3BP1. *Mol Cell Biol*. 37.

Romero, P., Z. Obradovic, X. Li, E.C. Garner, C.J. Brown, and A.K. Dunker. 2001. Sequence complexity of disordered protein. *Proteins*. 42:38-48.

Ross, E.D., H.K. Edskes, M.J. Terry, and R.B. Wickner. 2005. Primary sequence independence for prion formation. *Proc Natl Acad Sci U S A*. 102:12825-12830.

Scadden, A.D. 2007. Inosine-containing dsRNA binds a stress-granule-like complex and downregulates gene expression in trans. *Mol Cell*. 28:491-500.

Serio, T.R., A.G. Cashikar, A.S. Kowal, G.J. Sawicki, J.J. Moslehi, L. Serpell, M.F. Arnsdorf, and S.L. Lindquist. 2000. Nucleated conformational conversion and the

replication of conformational information by a prion determinant. *Science*. 289:1317-1321.

Serpell, L.C. 2000. Alzheimer's amyloid fibrils: structure and assembly. *Biochim Biophys Acta*. 1502:16-30.

Serpell, L.C., M. Sunde, M.D. Benson, G.A. Tennent, M.B. Pepys, and P.E. Fraser. 2000. The protofilament substructure of amyloid fibrils. *J Mol Biol*. 300:1033-1039.

Shelkovnikova, T.A., P. Dimasi, M.S. Kukharsky, H. An, A. Quintiero, C. Schirmer, L. Buee, M.C. Galas, and V.L. Buchman. 2017. Chronically stressed or stress-preconditioned neurons fail to maintain stress granule assembly. *Cell Death Dis*. 8:e2788.

Shelkovnikova, T.A., H.K. Robinson, J.A. Southcombe, N. Ninkina, and V.L. Buchman. 2014. Multistep process of FUS aggregation in the cell cytoplasm involves RNA-dependent and RNA-independent mechanisms. *Hum Mol Genet*. 23:5211-5226.

Shen, W.C., H.Y. Li, G.C. Chen, Y. Chern, and P.H. Tu. 2015. Mutations in the ubiquitin-binding domain of OPTN/optineurin interfere with autophagy-mediated degradation of misfolded proteins by a dominant-negative mechanism. *Autophagy*. 11:685-700.

Shin, Y., and C.P. Brangwynne. 2017. Liquid phase condensation in cell physiology and disease. *Science*. 357.

Sondheimer, N., and S. Lindquist. 2000. Rnq1: an epigenetic modifier of protein function in yeast. *Mol Cell*. 5:163-172.

Stansfield, I., and M.F. Tuite. 1994. Polypeptide chain termination in Saccharomyces cerevisiae. *Curr Genet*. 25:385-395.

Sun, Z., Z. Diaz, X. Fang, M.P. Hart, A. Chesi, J. Shorter, and A.D. Gitler. 2011. Molecular determinants and genetic modifiers of aggregation and toxicity for the ALS disease protein FUS/TLS. *PLoS Biol*. 9:e1000614.

Tanaka, M., P. Chien, N. Naber, R. Cooke, and J.S. Weissman. 2004. Conformational variations in an infectious protein determine prion strain differences. *Nature*. 428:323-328.

Tanida, I., T. Ueno, and E. Kominami. 2008. LC3 and Autophagy. *Methods Mol Biol*. 445:77-88.

Ter-Avanesyan, M.D., V.V. Kushnirov, A.R. Dagkesamanskaya, S.A. Didichenko, Y.O. Chernoff, S.G. Inge-Vechtomov, and V.N. Smirnov. 1993. Deletion analysis of the SUP35 gene of the yeast Saccharomyces cerevisiae reveals two non-overlapping functional regions in the encoded protein. *Mol Microbiol*. 7:683-692.

Teyssou, E., T. Takeda, V. Lebon, S. Boillee, B. Doukoure, G. Bataillon, V. Sazdovitch, C. Cazeneuve, V. Meininger, E. LeGuern, F. Salachas, D. Seilhean, and S. Millecamps. 2013. Mutations in SQSTM1 encoding p62 in amyotrophic lateral sclerosis: genetics and neuropathology. *Acta Neuropathol*. 125:511-522.

Toombs, J.A., N.M. Liss, K.R. Cobble, Z. Ben-Musa, and E.D. Ross. 2011. [PSI+] maintenance is dependent on the composition, not primary sequence, of the oligopeptide repeat domain. *PLoS One*. 6:e21953.

Toombs, J.A., B.R. McCarty, and E.D. Ross. 2010. Compositional determinants of prion formation in yeast. *Mol Cell Biol*. 30:319-332.

Tourriere, H., K. Chebli, L. Zekri, B. Courselaud, J.M. Blanchard, E. Bertrand, and J. Tazi. 2003. The RasGAP-associated endoribonuclease G3BP assembles stress granules. *J Cell Biol*. 160:823-831.

True, H.L., and S.L. Lindquist. 2000. A yeast prion provides a mechanism for genetic variation and phenotypic diversity. *Nature*. 407:477-483.

Tsai, N.P., P.C. Ho, and L.N. Wei. 2008. Regulation of stress granule dynamics by Grb7 and FAK signalling pathway. *EMBO J*. 27:715-726.

Uptain, S.M., and S. Lindquist. 2002. Prions as protein-based genetic elements. *Annu Rev Microbiol*. 56:703-741.

Vanderweyde, T., H. Yu, M. Varnum, L. Liu-Yesucevitz, A. Citro, T. Ikezu, K. Duff, and B. Wolozin. 2012. Contrasting pathology of the stress granule proteins TIA-1 and G3BP in tauopathies. *J Neurosci*. 32:8270-8283.

Voth, W., and U. Jakob. 2017. Stress-Activated Chaperones: A First Line of Defense. *Trends Biochem Sci*. 42:899-913.

Wallace, E.W., J.L. Kear-Scott, E.V. Pilipenko, M.H. Schwartz, P.R. Laskowski, A.E. Rojek, C.D. Katanski, J.A. Riback, M.F. Dion, A.M. Franks, E.M. Airoldi, T. Pan, B.A. Budnik, and D.A. Drummond. 2015. Reversible, Specific, Active Aggregates of Endogenous Proteins Assemble upon Heat Stress. *Cell*. 162:1286-1298.

Wang, H.Y., I.F. Wang, J. Bose, and C.K. Shen. 2004. Structural diversity and functional implications of the eukaryotic TDP gene family. *Genomics*. 83:130-139.

Wang, J., J.M. Choi, A.S. Holehouse, H.O. Lee, X. Zhang, M. Jahnel, S. Maharana, R. Lemaitre, A. Pozniakovsky, D. Drechsel, I. Poser, R.V. Pappu, S. Alberti, and A.A. Hyman. 2018. A Molecular Grammar Governing the Driving Forces for Phase Separation of Prion-like RNA Binding Proteins. *Cell*.

Westermark, P., M.D. Benson, J.N. Buxbaum, A.S. Cohen, B. Frangione, S. Ikeda, C.L. Masters, G. Merlini, M.J. Saraiva, J.D. Sipe, and A. Nomenclature Committee of the International Society of. 2005. Amyloid: toward terminology clarification. Report from the Nomenclature Committee of the International Society of Amyloidosis. *Amyloid*. 12:1-4.

Wheeler, J.R., T. Matheny, S. Jain, R. Abrisch, and R. Parker. 2016. Distinct stages in stress granule assembly and disassembly. *Elife*. 5.

Wickner, R.B. 1994. [URE3] as an altered URE2 protein: evidence for a prion analog in Saccharomyces cerevisiae. *Science*. 264:566-569.

Wickner, R.B., K.L. Taylor, H.K. Edskes, M.L. Maddelein, H. Moriyama, and B.T. Roberts. 2001. Yeast prions act as genes composed of self-propagating protein amyloids. *Adv Protein Chem*. 57:313-334.

Wippich, F., B. Bodenmiller, M.G. Trajkovska, S. Wanka, R. Aebersold, and L. Pelkmans. 2013. Dual specificity kinase DYRK3 couples stress granule condensation/dissolution to mTORC1 signaling. *Cell*. 152:791-805.

Wolozin, B. 2012. Regulated protein aggregation: stress granules and neurodegeneration. *Mol Neurodegener*. 7:56.

Woulfe, J., D.A. Gray, and I.R. Mackenzie. 2010. FUS-immunoreactive intranuclear inclusions in neurodegenerative disease. *Brain Pathol*. 20:589-597.

Xiang, S., M. Kato, L.C. Wu, Y. Lin, M. Ding, Y. Zhang, Y. Yu, and S.L. McKnight. 2015. The LC Domain of hnRNPA2 Adopts Similar Conformations in Hydrogel Polymers, Liquid-like Droplets, and Nuclei. *Cell*. 163:829-839.

Yoshizawa, T., R. Ali, J. Jiou, H.Y.J. Fung, K.A. Burke, S.J. Kim, Y. Lin, W.B. Peeples, D. Saltzberg, M. Soniat, J.M. Baumhardt, R. Oldenbourg, A. Sali, N.L. Fawzi, M.K. Rosen, and Y.M. Chook. 2018. Nuclear Import Receptor Inhibits Phase Separation of FUS through Binding to Multiple Sites. *Cell*. 173:693-705 e622.

Youn, J.Y., W.H. Dunham, S.J. Hong, J.D.R. Knight, M. Bashkurov, G.I. Chen, H. Bagci, B. Rathod, G. MacLeod, S.W.M. Eng, S. Angers, Q. Morris, M. Fabian, J.F. Cote, and A.C. Gingras. 2018. High-Density Proximity Mapping Reveals the Subcellular Organization of mRNA-Associated Granules and Bodies. *Mol Cell*. 69:517-532 e511.

Zhang, P., Y. Li, J. Xia, J. He, J. Pu, J. Xie, S. Wu, L. Feng, X. Huang, and P. Zhang. 2014. IPS-1 plays an essential role in dsRNA-induced stress granule formation by interacting with PKR and promoting its activation. *J Cell Sci*. 127:2471-2482.

Abbreviations

%	Percent
°C	Degree Celsius
Δ	Deletion
aa	Amino acid
AD	Alzheimer’s disease
ALS	Amyotrophic lateral sclerosis
ATCC	American type culture selection
BSA	Bovine serum albumin
CNS	Central nervous system
conj.	Conjugated
CTN	Carboxyterminal N domain
DCP1a	Decapping protein 1a
DMEM	Dulbecco's modified eagle's medium
DMSO	Dimethyl sulfoxide
DNA	Deoxyribonucleic acid
E.coli	*Escherichia coli*
ECL	Enhanced chemiluminescence
EDTA	Ethylenediaminetetraacetic acid
eIF2α	Eukaryotic translation initiation factor 2 alpha
ER	Endoplasmic reticulum
et al.	And others (" et alia")
FCS	Fetal calf serum
Fig.	Figure
FRAP	Fluorescence recovery after photobleaching
FRMP	Fragile X mental retardation protein
FTLD	Frontotemporal lobar degeneration
FUS	Fused in sarcoma
g	Gram
G3BP	Ras GTPase-activating protein-binding protein
GCN2	general control non-depressible-2

GFP	Green fluorescent protein
h	Hour
H_2O_{bidest}	Bidistilled water
HA	Hemagglutinin
HMW	High molecular weight
HRI	Heme-regulated inhibitor
HRP	Horseradish peroxidase
Hsp	Heat shock protein
IDR	Intrinsically disordered region
IF	Immunofluorescence
Ig	Immunoglobulin
IPTG	Isopropyl-β-D-thiogalactopyranoside
kDa	Kilodalton
Keap1	Kelch-like ECH-associated protein 1
l	Litre
LB	Lysogeny *broth*
LC3 A/B	Light chain 3 alpha/beta
LCD	Low complexity domain
LMW	Low molecular weight
LLPS	Liquid-liquid phase separation
M	Molar concentration
mA	Milliampere (10^{-3})
mAb	Monoclonal antibody
min	Minute
ml	Milliliter (10^{-3})
mM	Millimolar concentration (10^{-3})
mRNA	Messanger ribonucleic acid
mRNP	Messanger ribonucleoprotein
N	Asparagine
N2a	Murine neuroblastoma cell line
ng	Nanogram (10^{-9})
nm	Nanometer (10^{-9})
NM	NM domain of Sup35

NM^{agg}	Aggregated NM protein
NM^{sol}	Soluble NM protein
ns	Not significant
OD	Optical density
OPR	Oligopeptide repeat region
pAb	Polyclonal antibody
PAGE	Polyacrylamide gel electrophoresis
PBS	Phosphate buffered saline
PERK	endoplasmatic reticulum-resident protein kinase
PKR	protein kinase R
PQC	Protein quality control
PrD	Prion domain
PrLD	Prion-like domain
PrP	Prion protein
PrP^{C}	Cellular isoform of the prion protein
PrP^{Sc}	Pathogenic isoform of the prion protein
PVDF	Polyvinylidene difluoride
Q	Glutamine
QNR	Asparagine- and glutamine- rich region
RBP	RNA-binding protein
RNA	Ribonucleic acid
RNP	Ribonucleoprotein
rpm	Revolutions per minute
RRM	RNA recognition motif
RT	Room temperature
S. cerevisiae	*Saccharomyces cerevisiae*
SD	Standard deviation
SDD-AGE	Semi-denaturing detergent - agarose gel electrophoresis
SDS	Sodium dodecyl sulfate
SDS-PAGE	sodium dodecyl sulfate polyacrylamide gel electrophoresis
sec	Second
SG	Stress granule
siRNA	Small silencing RNA

SOD1	Superoxide dismutase 1
TBS	Tris-buffered saline
TBST	Tris-bufferd saline, Tween-20
TDP-43	43 kDa, transactive response DNA binding protein
TIA-1	T-cell-restricted intracellular antigen-1
TIAR	TIA-1-related protein
Tris	Tris(hydroxymethyl)aminomethane
TSEs	Transmissible spongiform encephalopathies
UV	Ultraviolet
V	Volt
VCP	Valosin-containing protein
WB	Western blot
µg	Microgram (10^{-6})
µl	Microlitre (10^{-6})
µm	Micrometer (10^{-6})
µM	Micromolar concentration (10^{-6})